

https://dspace.org/

Effects of TiO2 and CS supports on hydrogen spillover in Co and Ru supported catalysts

Dlamini, Sthembile

2018

https://hdl.handle.net/10539/25736

Dlamini, Sthembile, (2018) Effects of Ti02 and CS supports on hydrogen spillover in Co and Ru supported catalysts, University of the Witwatersrand, Johannesburg, https://hdl.handle.net/10539/25736.

Downloaded from a DSpace repository. https://dspace.org/



Effects of TiO_2 and CS supports on hydrogen spillover in Co and Ru supported catalysts

Sthembile N. Dlamini

School of Chemical and Metallurgical Engineering, Faculty of Engineering and the Built Environment, University of the Witwatersrand, Johannesburg, South Africa

22nd of February, 2018

DECLARATION

I declare that this thesis is my own unaided work. It is being submitted for the Degree of Master of Science in Engineering to the University of the Witwatersrand, Johannesburg. It has not been submitted before for any degree or examination to any other University.

_____on this ***_22nd_ day of _February 2018__***

(Sthembile N. Dlamini)

ABSTRACT

Hydrogen spillover is the surface migration of activated hydrogen atoms from a metal catalyst particle, on which they are generated, onto the catalyst support. A lot of research work has been done on hydrogen spillover since its discovery in 1964, and its incidence on reducible supports such as titanium oxide is established, yet questions remain about the role of the support in hydrogen spillover in heterogeneous catalysis.

The aim of this research was to investigate the role of a support in hydrogen spillover, using cobalt and ruthenium supported on TiO_2 and CS catalysts. These two catalysts were prepared by deposition precipitation-urea, incipient wetness impregnation and polyol methods and characterized using TGA, TEM, BET, XRD and Raman spectroscopic analysis. The Fischer-Tropsch evaluation of the catalysts was done in a fixed bed reactor and the products were analyzed on offline gas chromatographs.

The results show a significant shift to lower reduction temperatures for the CoO to Co peak for the physical mixture of Co/TiO_2 and Ru/TiO_2. However, when Co/TiO_2 and Ru/TiO_2 catalysts were packed in a bed system separated by different amounts of TiO_2, no significant change was observed compared to the "hybrid" catalyst. The separation distance between the two catalysts had no effect in the reduction temperature. The improved reducibility of CoO to Co was attributed to the dissociation of H_2 on the Ru, which made the Ru/TiO_2 catalyst the donor phase causing the hydrogen to spillover to the acceptor phase which is the Co/TiO_2. The same finding was observed for the Ru and Co catalysts supported on the carbon spheres where the CoO to Co peak was shifted to lower reduction temperature compared to the monometallic Co/CS catalyst. The reducibility was attributed to the presence of Ru. For the Co and Ru catalysts supported on carbon spheres the physically mixed Co/CS and Ru/CS catalysts resulted in the increase of $C5^+$ selectivities compared to the monometallic catalysts of Co catalysts. Microwave irradiation had a positive effect on the dispersion and surface area on the catalyst prepared using the polyol and incipient wetness methods.

DEDICATION

I would like to dedicate this dissertation to the following people:

- My mother, Duduzile Maureen Dlamini and step-father David Knox
- My late grandparents, Edith Maureen and Antony Dlamini, I know you would be proud.
- My husband, Rudge Sitai, for all the support.

ACKNOWLEDGEMENTS

I would like to thank my supervisors, Doctor Diakanua Nkazi, Professor Neil Coville and Professor Linda Jewell for their patience and for supporting me and encouraging me to finish my MSc.

I am also grateful to Dr Joshua Gorimbo and Dr Adolph Anga for being my cheerleaders when the morale and motivation was low.

A big thank you to Mr Basil Chaussoulas for the assistance he provided with the Fischer Tropsch rig.

I would like to thank the School of Chemistry, the School of Chemical and Metallurgical Engineering and CATOMMAT (Catalysis and Materials) group for providing a lovely environment to work in.

I am grateful to the various research units for allowing me to use their instruments to conduct my research, especially the MMU (Microscopy and Microanalysis Unit) and the XRD(X-ray Diffraction) Unit led by Professor Alexander Ziegler and Professor Dave Billing.

I would like to thank DST-NRF Centre of Excellence in Catalysis for the financial support.

PRESENTATIONS AND PUBLICATIONS

Conference presentations

- Oral-S.N. Dlamini, L. Jewell, N.Coville, DST-NRF Centre of Excellence in Catalysis /CATSA conference, “Studies of hydrogen spillover effects in Co and Ru catalysts supported on carbon spheres and titania”, November 2012.
- Oral-S.N. Dlamini, L. Jewell, N.Coville, DST-NRF Centre of Excellence in Catalysis meeting, UCT, “Studies on Ru catalysts using conventional and microwave heating methods”, November 2013.

Contents

DECLARATION ii
ABSTRACT iii
DEDICATION iv
ACKNOWLEDGEMENTS v
PRESENTATIONS AND PUBLICATIONS vi
Conference presentations vi
Contents vii
List of Figures xii
List of Tables xiv
Nomenclature xv
CHAPTER 1 1
1. Introduction 1
1.1 Introduction 1
1.2 Aims and objectives 1
1.3 Dissertation outline 3
CHAPTER 2 4
LITERATURE REVIEW 4
2.1 Introduction 4
2.2 Spillover 7
2.2.1 History of spillover 7
2.2.2 Spillover onto reducible and non-reducible supports 10
2.2.3 Spillover between stacked beds 12
2.2.4 Spillover distances 14
2.2.5 Spillover in syngas reactions 15
2.2.6 Hydrogen spillover from metal onto oxides 18
2.3. Fischer-Tropsch synthesis 20
2.3.1. History and background information 20
2.3.2. The Fischer Tropsch chemistry 21
2.3.3. The Fischer Tropsch catalysts 23
2.3.4. Co-based Fischer- Tropsch catalysts 24
2.3.5. Promoters for Fischer- Tropsch catalysts 25
2.3.6. Ruthenium as Co-based catalyst promoter 25

2.3.7. FT catalyst supports 26
2.4. Microwave Chemistry 27
2.4.1. Discovery of the microwave chemistry 28
2.4.2. Microwave radiation 28
2.4.3. Dielectric heating 29
2.4.4. Materials and microwaves 30
2.4.5. The microwave oven 31
2.4.6. Microwave enhanced chemistry 32
References 36
CHAPTER 3 43
EXPERIMENTAL METHODS 43
3.1 Introduction 43
3.2 Preparation of Carbon Spheres 43
3.2.1Materials 43
3.2.2 Gases 43
3.2.3 Method for the preparation of carbon spheres 44
3.3 Catalyst preparation 45
3.3.1 Deposition precipitation-urea (DPU) method 46
3.3.2 Incipient wetness impregnation (IWI) method (conventional) 46
3.3.3 Incipient wetness impregnation (IWI) method (microwave) 47
3.3.4 Polyol method (conventional) 47
3.3.5 Polyol method (microwave) 47
3.4 Catalyst characterization instruments 48
3.4.1 Thermal Gravimetric Analysis 48
3.4.2 Transmission electron microscope (TEM) 49
3.4.3 Brunauer Emmett Teller (BET) analysis 50
3.4.4 Temperature programmed reduction (TPR) 51
3.4.5 Raman spectroscopy 52
3.4.6 Powder x-ray diffraction 52
3.5 Hydrogen spillover studies 53
3.6 Reaction studies 54
3.6.1 Gases 54
3.7 Catalyst evaluation 55
3.7.1 Equipment setup 55

3.7.2 Micro fixed bed reactor 57
3.8 Experimental procedure for FT reactions 58
3.9 Gas chromatogram (GC) calibration 59
3.10 Product analysis 61
3.11 Mass Balances 61
References 67
CHAPTER 4 69
EVALUATION OF COBALT AND RUTHENIUM SUPPORTED ON TITANIA AS CATALYSTS IN FISCHER TROPSCH SYNTHESIS 69
4.1 Characterization 69
4.1.1 Scanning electron microscopy and energy dispersive X-ray studies 69
4.1.2 TEM and EDX 71
4.1.3 XRD 73
4.1.4 BET 73
4.1.5 H_2-TPR studies 74
4.3 Catalyst testing 80
4.4 Product selectivity 82
4.5 Olefin to paraffin ratio 83
4.6 Conclusion 84
References 85
CHAPTER 5 88
EVALUATION OF CARBON SUPPORTED CATALYSTS IN FISCHER-TROPSCH SYNTHESIS 88
5.1 Characterization 88
5.1.1 TEM and particle size distribution 88
5.1.2 Raman spectroscopy 91
Figure 5.5: Raman spectra of as-synthesised CS 92
5.1.3 Brunauer Emmett Teller analysis 92
5.1.4 Thermogravimetric Analysis 93
5.1.5 X-Ray Diffraction data analysis 94
5.1.6 H_2-TPR studies 95
5.3 Catalytic activity 97
5.4 Product selectivity 98
5.5 Olefin to paraffin ratio 99
5.6 Conclusion 100

References 102
CHAPTER 6 105
CONCLUSIONS AND RECOMMENDATIONS 105
6.1 Conclusions 105
6.2 Recommendations 106

List of Figures

Figure 2.1: Schematic diagram of spillover of a gaseous diatomic molecule from an adsorbing species onto a non-adsorbing surface. An energy level diagram for the spillover process is also shown (Conner and Falconer, 1995). 5
Figure 2.2: Schematic diagram of spillover from a metal adsorbing surface onto a primary support and then onto the inert surface of the secondary support which is in direct contact with the primary support (Conner and Falconer, 1995).....6
Figure 2.3: Reaction chamber measuring hydrogen spillover. The reactor on the left has Ni/Al_2O_3 catalyst filled in a bucket, surrounded by Al_2O_3 support. On the right the bucket filled with Ni/Al_2O_3 is pulled up (Teichner, 1990; Prins, 2012). 10
Figure 2.4: Schematic diagram of the adsorption of H_2 on Pt and spillover of H atoms to the TiO2 support, which produces protons and Ti^{3+} cations (Huizinga and Prins, 1981). 11
Figure 2.5: Schematic diagrams of stacked bed reactor with sulfided Co/Al_2O_3 in the upper bed, Al_2O_3 in the separator bed, and sulfided Mo/Al_2O_3 in the lower bed.....13
Figure 2.6: Influence of different arrangements of 0.5 wt % Pt/Al_2O_3 catalyst (dark regions) and H-mordenite (cross-hatched regions) on n-butane hydroconversion at 633K (Roland, Winkler, and Steinberg, 1989).....14
Figure 2.7: Photos of a quartz glass reactor for catalyst arrangements shown in the top part of Figure 1.6 after 1.5 h hydroconversion of n-butane at 633K. Reactant flow was from top to bottom: (A) H-mordenite; (B) 0.5 wt % Pt/Al_2O_3 15
Figure 2.8: TPR profile of methane and CH3O hydrogenation.....16
Figure 2.9: Illustration of the mechanisms of reduction zone formation: (a) hydrogen spillover from Ni to PDC followed by surface diffusion of H atoms across PDC, (b) hydrogen spillover from Ni to PDC followed by surface oxygen diffusion to the triple phase boundary 19
Figure 2.10: Temperature gradient within samples heated by (a) conventional heating and (b) microwave dielectric heating. The circles represent the sample; the squares correspond to the cavity used in both heating systems.....30
Figure 2.11: SEM images of the Co/SiO_2 catalysts (20kV, x4,500): (a) Silica support, (b) conventional heating catalyst and (c) microwave irradiated catalyst 34
Figure 3.1: Vertical CVD setup for the synthesis of carbon spheres.....35
Figure 3.2: Soxhlet apparatus for the purification of as-grown carbon spheres 36

Figure 3.3: Image of Perkin Elmer thermo-gravimetric Analyzer 4000 40
Figure 3.4: Image of FEI G2 Spirit TEM instrument 41
Figure 1.5: ASAP-2000 Tristar analyser (BET) 42
Figure 3.6: Image of Micromeritics Autochem II TPR instrument 43
Figure 3.7: Brüker D2 Phaser X-ray diffractometer 44
Figure 3.8: Schematic diagram of the loading of stacked catalyst beds into the TPR sample holder 45
Figure 3.9: Flow sheet diagram of Fischer-Tropsch rig set-up 46
Figure 3.10: Fischer Tropsch rig set-up with FID and TCD 48
Figure 3.11: Schematic diagram of a Fischer Tropsch reactor 49
Figure 3.12: A chromatograph for the calibration gas using the GC-FID with nitrogen as the carrier gas 50
Figure 3.13: A chromatograph for the calibration gas using the GC-TCD with argon as the carrier gas 50
Figure 4.1: SEM images and EDX spectra of a) 10%Co/TiO_2 and b) 3%Ru/TiO_2 catalysts ... 61
Figure 4.2: TEM images of a) 10%Co/TiO_2 and b) EDX of 10%Co/TiO_2 c) TEM image of 3%Ru/TiO_2, and d) EDX of 3% Ru/TiO_2 63
Figure 4.3: XRD pattern of 3% Ru/TiO_2 and 10% Co/TiO_2 (*-Co_3O_4 and #-RuO_2) 64
Figure 4.42: TPR profiles of black-3% Ru/TiO_2; Red-10% Co/TiO2 and blue-bimetallic catalyst 66
Figure 4.5: TPR profile of hybrid catalyst (Ground mixture) 67
Figure 4.6: TPR profiles of 3% Ru/TiO_2 and 10% Co/TiO_2 separated by different amounts of Titania 67
Figure 4.7: TPR profiles of 3% Ru/TiO_2 and 10% Co/TiO_2 separated by different amounts of oxides 69
Figure 4.8: TPR profiles of 3% Ru/TiO_2 and 10% Co/TiO_2 separated by alumina 71
Figure 4.9: Conversion of the catalysts over 120 hours on stream a) 3% Ru/TiO_2 b) 10% Co/TiO2 and c) Ground mixture of 3%Ru/TiO_2 and 10%Co/TiO_2 72
Figure 4.10: Selectivity of the catalysts over 120 hours on stream a) 3% Ru/TiO_2, and b) 10%Co/TiO_2 c) Ground mixture (3%Ru/TiO_2 and 10%Co/TiO_2) 74
Figure 4.11: Olefin to paraffin ratio of Co catalysts supported on titania 75
Figure 5.1: TEM image of as-synthesised carbon spheres and particle size distribution histogram (the superimposed dashed line represents a Gaussian distribution) 79

Figure 5.2: TEM images of 3% Ru/CSs catalyst prepared by incipient wetness a) using conventional heating and b) using microwave heating during the calcination step 80
Figure 5.3: TEM images of 3% Ru/CSs catalyst prepared by deposition precipitation a) using conventional heating and b) microwave heating for the drying step 81
Figure 5.4: TEM images of 3% Ru/CSs catalyst prepared by polyol method a) using conventional and b) microwave heating for the drying step 82
Figure 5.5: Raman spectra of as-synthesised CS 83
Figure 5.6: TGA profiles run on air of 3% Ru/CSs catalyst prepared by polyol method a) using conventional heating and b) microwave heating for the drying step 85
Figure 5.7: XRD patterns for catalysts heated conventional using the a) Polyol b) DPU c) IWI preparation method 86
Figure 5.8: TPR profiles of black-3% Ru/CSs; Red-10% Co/CSs and blue-ground mixed catalysts 87
Figure 5.9: Conversion of the catalysts over 120 hours on stream a) 10% Co/CSs, b) for the ground mixture of 3% Ru/CS and 10% Co/CS and c) 3% Ru/CSs 89
Figure 5.10: Selectivity of the catalysts over 120 hours on stream a) 5% Co/CSs, b) for the ground mixture of 3% Ru/CS and 10% Co/CS and c) 3% Ru/CSs 90
Figure 5.11: Olefin to paraffin ratio of Co catalysts supported on carbon spheres 91

List of Tables

Table 2.1: Overview of some characteristics of Ni-, Fe-,Co- and Ru-based F-T catalysts.....24

Table 3.1: Molar response factors for hydrocarbons (Dietz 1967).....645

Table 4.1: Porosity measurements of catalysts.....775

Table 4.2: Peak reduction temperatures from TPR profiles with TiO_2.....77

Table 4.3: Peak reduction temperatures from TPR profiles with CeO_2.....79

Table 4.4: Peak reduction temperatures from TPR profiles with Al_2O_3.....80

Table 5.1: BET results of the functionalized and un-functionalized carbon spheres 83

Table 5.2: BET results of the catalysts prepared by different synthesis and heating methods……..92

Nomenclature

FTS	Fischer-Tropsch Synthesis
PXRD	Powder X-ray Diffraction
TPR	Temperature programmed reduction
TPD	Temperature Programmed Desorption
TGA	Thermo-Gravimetric Analysis
EDX	Energy-dispersive X-ray spectroscopy
CSs	Carbon spheres
GC	Gas chromatography
BET	Brunauer, Emmett and Teller
tan Δ	Dissipation factor
SEM	Scanning Electron Microscope
TEM	Transmission Electron Microscopy
CVD	Chemical Vapour Deposition
FID	Flame Ionization Detector
TCD	Thermal Conductivity Detector

WGS	Water Gas Shift
ESR	Electron Spin Resonance
DPU	Deposition Precipitation-Urea
IWI	Incipient Wetness Impregnation
CO	Carbon monoxide
CoO	Cobalt (I) oxide
H_2	Hydrogen
TiO_2	Titanium dioxide
CH_4	Methane

CHAPTER 1

1. Introduction

1.1 Introduction

The use of supported cobalt catalysts in Fischer-Tropsch Synthesis (FTS) is preferred over other supported catalysts because of their high activities, high selectivity to linear hydrocarbons and low activities for the competitive water-gas shift (WGS) reaction. Many promoters such as ruthenium (Ru), zirconium (Zr), lanthanum (La), rhodium (Rh), boron (B), and platinum (Pt) have been investigated for their use to increase the catalytic activity of the Co catalysts (Khangale, 2016). It has been reported that these promoters can increase the reducibility of Co, preserve the activity by preventing the formation of coke, exhibit cluster and ligand effects, and act as a source of hydrogen spillover and enhance dispersion.

Marin et al. (2013) stated that the ability of a supported Ru catalyst to aid in the reduction of a supported Co catalyst (as seen in the FT reaction) is due to a spill-over effect. In essence the Ru is more easily reduced by H_2 and the Ru, and then generates Ru-H species and this H then can transfer to Co, leading to Co reduction. It should be mentioned that the active form of Co catalysts is the reduced Co metal surface atom. The role of the support in this reaction is however not clear. There has been no previous study that has looked into the role of the support in the H transfer reaction for carbon based supports and hence this study will focus on the effect of a series of Ru/C, Co/C, Ru/TiO_2, Co/TiO_2 catalysts which will be synthesized, characterized and evaluated for the H transfer reactions.

1.2 Aims and objectives

The aims of this research work were to investigate the role of the support in hydrogen spillover using cobalt and ruthenium catalysts used in Fischer-Tropsch Synthesis and to evaluate the effect of microwave radiation in Ru supported catalysts. These supports

include titania and carbon spheres (CSs). These aims will be achieved through the following objectives:

- To synthesize Ru/TiO_2 and Co/TiO_2 catalysts using the deposition precipitation method with urea as a precipitation agent.

- Characterize the Ru/TiO_2 and Co/TiO_2 catalysts using TEM (for the morphology), SEM (morphology) and BET (surface area, pore volume and pore size) methods.

- Extensively characterize the Ru/TiO_2 and Co/TiO_2 catalysts using H_2-TPR, focusing specifically on the hydrogen spillover effect:

    - Varying the distance between the Ru/TiO_2 and Co/TiO_2 catalysts and Ru/CSs and Co/CSs

- To evaluate the catalysts in terms of their Fischer-Tropsch activity and selectivity in a fixed-bed micro reactor.

- To synthesize CSs using acetylene as a carbon source, with a narrow size distribution using a catalyst-free chemical vapour deposition method (CVD) by employing a swirled floating vertically positioned reactor.

    - To purify the synthesized CSs using toluene using a conventional Soxhlet extraction apparatus.

    - To functionalize the synthesized CSs using nitric acid (HNO_3).

- To characterize the synthesized, purified and functionalized CSs using Transmission Electron Microscopy (TEM) - morphology, size and structure; BET - specific surface area, pore diameter and pore volume; Thermogravimetric analysis (TGA) - purity, composition, thermal stability and Raman spectroscopy for the extent of carbon graphitization.

- To conventionally load Ru onto the CSs, by the deposition precipitation method with urea as the precipitating agent, incipient wetness and polyol methods.

- To characterize the catalysts using TEM, TGA, XRD and BET.

- To synthesize the ruthenium catalysts using the microwave method, and other synthesis methods: the deposition precipitation method with urea as the precipitating agent, incipient wetness and polyol method.

- To characterize the catalysts using TEM, TGA, XRD and BET.

1.3 Dissertation outline

Chapter 1 presents a brief history of hydrogen spillover and microwave studies and also gives a general literature review. In chapter 2 the aims and objectives are presented. Chapter 3 describes in detail the experimental procedures and instrumentation used for the project. Chapter 4 presents results and discussion of hydrogen spillover studies using the TPR technique. Chapter 4 is followed by chapter 5 where the results and discussion of the studies on Ru catalysts using conventional and microwave heating methods are presented. In chapter 6, the topic "Comparison of catalysts supported on titania and carbon spheres in Fischer Tropsch Synthesis" is discussed. Chapter 7 presents a summary of the overall conclusions from chapters 4, 5 and 6.

CHAPTER 2

LITERATURE REVIEW

2.1 Introduction

"Spillover is defined as the transport of active species sorbed or formed on a first surface onto another surface that does not *under the same conditions* ,sorb or form the active species" (Falconer and Conner, 1989). Spillover was found to play a part in many surface reactions and transport phenomena, which also included atoms like O, H and also molecules or molecular fragments like CO or NCO. The many species that are involved in spillover include single molecules and different fragments as mentioned above, and these can be charged, uncharged or radical in nature (Pajonk et al., 1983).

Spillover is not only involved in adsorption but also in the gasification of solids, in the formation of catalytic active sites, and reaction with adsorbed species (Emmett, 1940). Figure 2.1 shows the chemisorption and activation of a diatomic molecule onto a surface and diffusion onto a non-adsorbing surface. The term "spill" and "over" from the English words spill over, was coined by Benson et al. (1966) to describe the migration of H atoms from a metal particle to a support; the H atoms spillover from a hydrogen-rich region to a hydrogen-poor surface (Emmett, 1940).

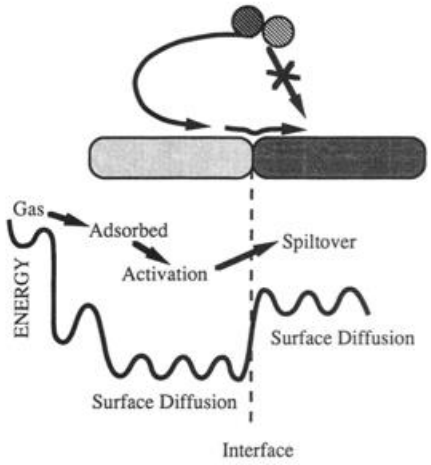

Figure 2.3: Schematic diagram of spillover of a gaseous diatomic molecule from an adsorbing species onto a non-adsorbing surface. An energy level diagram for the spillover process is also shown (Conner and Falconer, 1995).

In spillover, the phase which generates the active species is called the initiator or activator and the phase which adsorbs the active species is known as the acceptor. There are two types of spillover that can occur, "primary" or "secondary." In the former the two phases (initiator and acceptor) are in direct contact, whereas in the latter the two phases are separated by an additional inert carrier (Conner and Falconer, 1995). Figure 2.2 depicts secondary spillover events.

In spillover phenomena, the adsorbed active species can move across the surface to the interface with the second support surface as shown in Figure 2.2. The diatomic molecules cannot directly adsorb onto the second phase.

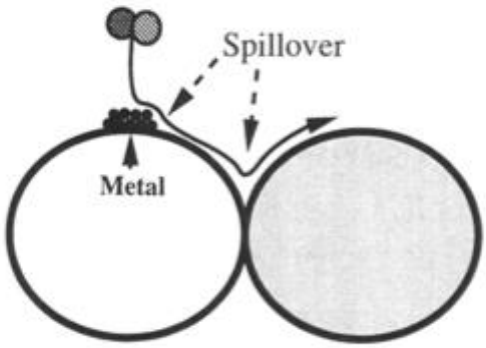

Figure 4.2: Schematic diagram of spillover from a metal adsorbing surface onto a primary support and then onto the inert surface of the secondary support which is in direct contact with the primary support(Conner and Falconer, 1995).

The spiltover species can however diffuse across the non-adsorbing surface. From initial studies of spillover, it was thought that the spiltover atoms are formed by dissociation of adsorbing molecules. However, more recent studies have shown that the adsorbing species need to only partially dissociate or even retain their molecular identity during spillover (Conner and Falconer, 1995). The movement of these spiltover species across the surfaces involves the formation and breakage of equivalent bonds with similar neighboring atoms. This exchange of bonds between the adsorbed species and the support surface allows for the adsorbed species to reach the interface between the activating support and the accepting support. Spillover can take place in different ways, from one oxide to another, from a metal to an oxide, from one metal to another, or from a metal oxide onto a metal (Conner and Falconer, 1995; Kuriacose, 1957; Taylor, 1961).

In Figure 2.1, the energetics of spillover is shown. The chemisorption of diatomic molecules onto the original surface is exothermic, and the surface diffusion that follows may have a small activation energy. The formation and breakage of bonds at the interface of the activating and accepting surfaces is endothermic, which is facilitated by an increase in the entropy for the spiltover species. If the spiltover species bind strongly to the accepting surface, the event can then be exothermic.

2.2 Spillover

2.2.1 History of spillover

The history of spillover dates back to 1940 (Sinfelt and Lucchessi, 1963), when Emmett (1940) discussed the possibility of spillover in his work on NH_3 synthesis and decomposition. It was observed that the rate of NH_3 decomposition or synthesis increased over a metallic catalyst, but only using a certain particle size. Below this particle size, the rate did not show any further increase. Emmett (1940) concluded that below this particle size, "either the entire surface or a portion of it is active…" and "some form of activated surface diffusion phenomena may easily constitute a major means by which gases reach the inner surface of metallic catalysts … this must await further experimental results."

Almost two decades later, Kuriacose (1957) found that a Pt wire accelerated the decomposition of GeH_4 on a Ge film. Taylor (1961) suggested that the Pt wire served as a "porthole" where H atoms recombined to form H_2. Sinfelt and Lucchessi (1963) reported that ethane could be hydrogenated and spilled over from Pt/SiO_2 to the surface of an inert Al_2O_3 support. However, it was later found that Sinfelt and Lucchessis' findings were due to impurities rather than spillover (Khoobiar, 1964). In the following year, Khoobiar (1964) reported that a blue colour tungsten bronze (WO_{3-x}) formed, through the reduction of yellow WO_3 by H_2 in the presence of a Pt catalyst at room temperature (Khoobiar, 1964). Khoobiar's work has since been known to represent the beginning of the spillover concept, as it was the first direct evidence of spillover (Rozanov and Krylov, 1997).

Tungsten trioxide is known to be reduced by hydrogen at temperatures above 200 °C forming blue coloured oxide W_4O_{11}. However, when H_2 is passed over a mechanical mixture of 0.5% Pt/Al_2O_3 + WO_3, the colour change is observed to occur at room temperature. This effect is not observed in the absence of the Pt when only Al_2O_3 + WO_3 are present (Rozanov and Krylov, 1997). This effect can be explained by a mechanism that requires that hydrogen dissociatively chemisorbs on the platinum and migrates via the Al_2O_3 onto the WO_3 in the form of atoms or H^+ ions. The reaction is shown below.

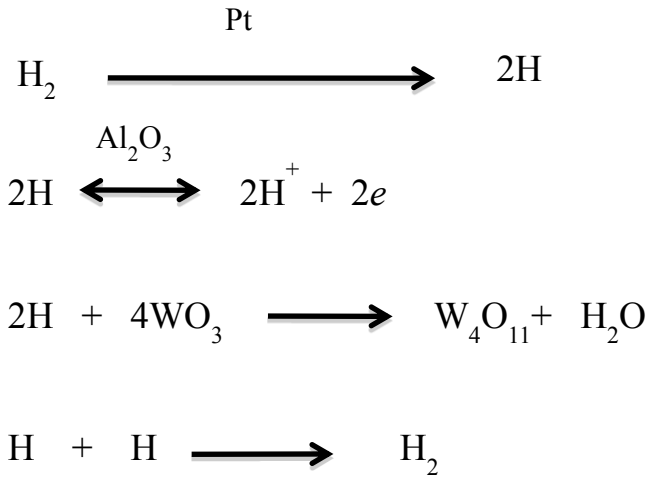

Further experiments have been done since Khoobiar's initial work, e.g. by measuring the amount of adsorbed hydrogen on a Pt/SiO_2 + WO_3 mechanical mixture. These measurements showed that the amount of H_2 adsorbed by the mechanical mixture of Pt/SiO_2 + WO_3 was several times more than what adsorbs on the same amount of Pt/SiO_2 without WO_3. The difference in adsorption measurements was attributed to a so-called structural sensitivity i.e. the dependence of the specific catalytic activity (calculated per unit surface or per active centre) on the particle size. This led to a difference between the specific activities of supported and unsupported catalysts. The cause of this was proposed to be due to the involvement in the reaction of the initially inactive support surface as a result of the movement of active adsorbed species onto the support via spillover (Rozanov and Krylov, 1997).

Pajonk et al. (1983) made the next discovery, which brought further understanding of the spillover phenomena (Bianchi et al., 1975; Conner and Pajonk, 1984). They discovered that a pure support such as Al_2O_3 or SiO_2 was able to hydrogenate ethene and benzene when exposed to H_2 for a number of hours at high temperatures by means of indirect contact with a metal-on-support catalyst. A pyrex bucket was filled with Ni/Al_2O_3 and then immersed in a pure Al_2O_3 support. Hydrogen was passed through the Ni/Al_2O_3 for several hours at 300 °C and the reaction chamber (Figure 2.3) was then cooled with flowing H_2. The Ni/Al_2O_3 was removed from the reaction chamber system by a winch mechanism and the valve was closed and only the "pure" Al_2O_3 and flowing H_2 was left in the chamber. When ethene was added to the chamber in the presence of only Al_2O_3 and hydrogen, the

formation of ethane was observed at 110 °C in the absence of the metal. This observation was ascribed to the spillover of hydrogen atoms, produced during the pre-reduction of the Ni/Al_2O_3 catalyst which spiltover over into the pyrex bucket and moved to the pure Al_2O_3, which was placed outside the bucket. These spilt over hydrogen atoms had remained on the alumina support, transforming the support into an unusual hydrogenation catalyst.

Teichner and co-workers (1990) found that the spiltover hydrogen itself was not very reactive. The true agent of hydrogenation was considered to be molecular hydrogen activated on the spillover-treated surface of the aluminium oxide. This observation was deduced from quantitative measurements of the ethane formed, which was much higher than the estimated amount of spilt over hydrogen (1.5 $cm^3\ g^{-1}$) (Teichner, 1990; Prins, 2012). On the other hand, formation of ethane in the absence of H_2 was not observed, nor was it observed when alumina was evacuated before the ethane hydrogenation reaction occurred. This was attributed to the removal of spiltover hydrogen, by removal of the alumina.

Other experiments were conducted in the same reactor chamber, with a Pt/Al_2O_3 catalyst and SiO_2 as the support surrounding the bucket. Hydrogen was passed through the chamber for 12 h at 430 °C similar to the previous experiment. The bucket filled with the catalyst was then removed after the pre-reduction step, and only SiO_2 was left. It was observed in this experiment that when ethene was added, neither SiO_2, which was in indirect contact with the bucket filled with Pt/Al_2O_3, nor the SiO_2 that had been treated with H_2 for 12 h at 430 °C showed any hydrogenation activity. The authors concluded that defect sites could be involved, because the number of sites accepting spilled over H atoms was estimated to be $10^{12}\ cm^{-2}$, which is 0.1 % of the surface of the Si or Al atoms. The possible explanation of the hydrogenation of ethene in the absence of a metal could be that the long exposure of hydrogen to the support at high temperatures led to the creation of defects in the alumina, which then accepted hydrogen atoms and that finally hydrogenated the ethane (Teichner, 1990; Prins, 2012).

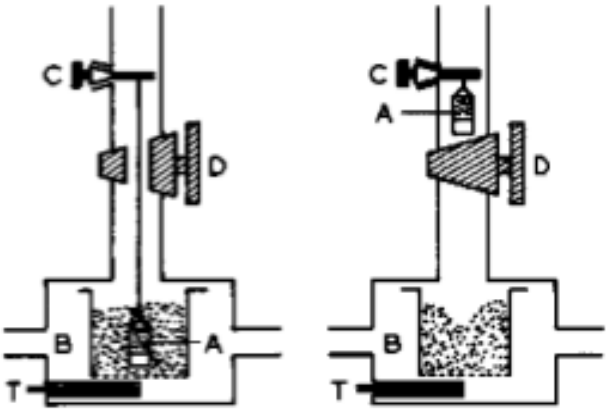

Figure 2.5: Reaction chamber measuring hydrogen spillover. The reactor on the left has Ni/Al_2O_3 catalyst filled in a bucket, surrounded by Al_2O_3 support. On the right the bucket filled with Ni/Al_2O_3 is pulled up (Teichner, 1990; Prins, 2012).

2.2.2 Spillover onto reducible and non-reducible supports

The reduction of WO_3 (which is a reducible support) by H_2 in the presence of the Pt/WO_3 catalyst occurs by the dissociative chemisorption of H_2 molecules on the Pt particles. The H atom species then migrate to the WO_3 particles and reduce them forming a blue coloured oxide (Benson et al., 1966).

Work done by Benson and co-workers (1966) showed that it is necessary that the metal be present for the dissociation of the hydrogen into atoms in order to reduce the WO_3 but that the presence of water or alcohol could also be of great importance (Benson et al., 1966). The explanation behind the need for water or alcohol to be present in spillover is ascribed to the fact that the H atoms can separate into protons and electrons when in contact with the WO_3 support. The formed electrons move across the WO_3 lattice by reducing W^{6+} to W^{5+} cations, while on the other hand the protons are solvated by the water and are able to move rapidly by hydrogen bonding procedures. This allows for the W^{6+} species, which are not in close proximity with the Pt surface to be reduced faster (Prins, 2012). Other work involving the use of Pt/MoO_3 and MoO_3 showed a similar effect to that observed by Khoobiar (Prins, 2012). Benson and co-workers (1966) performed DFT studies and the results were in agreement with the proposed mechanism (Teichner et al., 1990; Prins,

2012). The extent of reduction of the metal oxide is known to depend on the activation energy of the proton-electron migration. For metal oxides such as WO_3 and MoO_3, which have similar crystal lattices, the activation energies are low. However, for metal oxides with different crystal lattices the proton-electron migration may be difficult and, this would limit the migration to the immediate environment of the metal particles. This can be seen in the work done on Pt/TiO_2 (Huizinga and Prins, 1981). The work done on the Pt/TiO_2 catalyst showed that the number of reduced Ti ions was similar to the number of atoms present in the catalyst. This data was interpreted as showing that only the Ti ions, which were under, or surrounding the Pt particles, were reduced (Figure 2.4) (Huizinga and Prins, 1981).

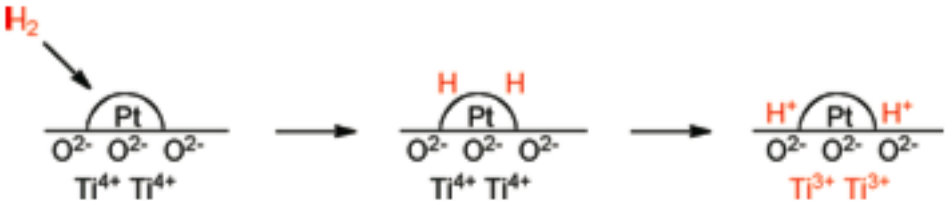

Figure 2.6: Schematic diagram of the adsorption of H_2 on Pt and spillover of H atoms to the TiO_2 support, which produces protons and Ti^{3+} cations (Huizinga and Prins, 1981).

Since evidence of the spillover of H atoms to reducible supports was observed, scientists assumed that the same would happen for non-reducible supports such as alumina, magnesia, silica and silica-alumina, but this has been difficult to prove. Spillover of H atoms onto reducible supports can transform the H atoms into protons and electrons; both these species can be detected. However, for defect free non-reducible supports this proton and electron formation cannot occur and only the presence of H atoms can be detected. This provides the only evidence for spillover. Even though no direct evidence of spillover onto non-reducible supports has been observed, Carley and co-workers claimed to have measured this effect indirectly (Carley et al., 1994). Pd/Al_2O_3 was exposed to H_2 at room temperature and a solution of *N*-benzylidene-*t*-butylamine-N-oxide was added. Since *N*-benzylidene-*t*-butylamine-N-oxide traps H atoms, any radicals formed can be detected by using Electron Spin Resonance (ESR) spectroscopy. The radical was only detected when the Pt/Al_2O_3 and H_2 were present and this was considered proof of hydrogen spillover. The

hydrogen atoms migrated from the metal particles over the support, to the organic molecules. When *N*-benzylidene-*t*-butylamine-N-oxide was placed in contact with a hydrogen covered Pt/Al_2O_3 catalyst, the organic molecules reacted with the H-atoms on the surface of the Pt particles on the alumina. Other authors have also claimed to have evidence of spillover of H atoms onto non-reducible supports using an H-D exchange method (Prins, 2012).

The theoretical and experimental results of hydrogen adsorption on graphitic structures are of interest not only for hydrogen storage, but also for catalysis. While it was shown in section 3 that hydrogen spillover does not occur from a metal to a defect-free non-reducible support, the discussion in this section shows that spillover to a carbon support may be possible, when a graphitic type of carbonaceous material covers the support. Carbonaceous deposits are easily produced in reactions of unsaturated hydrocarbons and organic molecules. Fragments of such deposits may function as transfer agents in hydrogen spillover from the metal particles to molecules adsorbed on the support. The temperatures applied in catalysis are higher than in hydrogen storage and desorption. Thus, relatively strong C-H bonds are less of a problem in H-transfer catalysis than in hydrogen storage (Prins, 2012).

2.2.3 Spillover between stacked beds

Baeza and co-workers have published a series of papers reporting on the spillover that occurred between beds of catalysts that were stacked on top of each other, separated by pure supports (Ojeda et al., 2003; Baeza et al., 2004; Baeza et al., 2006; Escalona et al., 2006; Valdevenito et al., 2010; Villarroel et al., 2008a; Villarroel et al., 2008b). These experiments used a CoS/support or a NiS/support above or under a bed of MoS/support separated by a bed containing 5 mm γ-Al_2O_3, SiO_2 or SiC. The beds were used to study hydrodesulfurization (HDS) as well as hydrodenitrogenation (HDN) reactions. The separating beds make it difficult to form Co-Mo-S or Ni-Mo-S phases. The stacked bed configuration was made of MS/support//separator//MoS_2/support or MoS_2/support//separator//MS/support (M=Co or Ni) (Figure 2.5) (Ojeda et al., 2003; Baeza et al., 2004; Baeza et al., 2006; Escalona et al., 2006; Valdevenito et al., 2010; Villarroel et al., 2008a; Villarroel et al., 2008b).

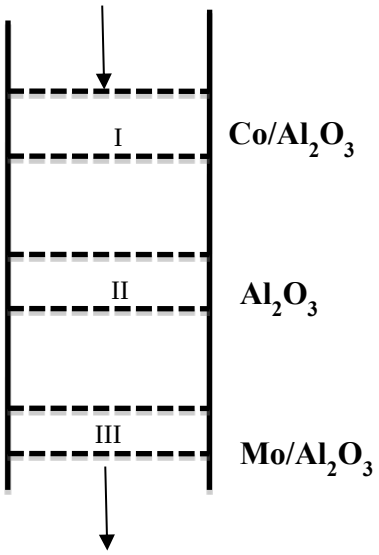

Figure 2.7: Schematic diagrams of stacked bed reactor with sulfided Co/Al_2O_3 in the upper bed, Al_2O_3 in the separator bed, and sulfided Mo/Al_2O_3 in the lower bed (Baeza et. al, 2004).

The feed used for these experiments was industrial oil and the HDS was carried out using similar conditions to those used in industry, (3 MPa and 325-375 °C). Combined catalysts such as MS/support//separator//MoS_2/support beds with SiO_2 or Al_2O_3 as the supports showed HDS activity, whereas separate CoS/support and NiS/support catalysts showed no HDS activity. The combined catalysts showed an increase in the conversion of the gas oil above that of the MoS_2/support. For the three different supports used as a separator, the SiO_2 showed higher synergy than when Al_2O_3 was used; no synergism with the SiC was detected. However, when the stacking of the beds was reversed (MoS_2/support//separator//MS/support) synergism was not observed at all for any of the three-separator supports. This could be explained by a remote control model, where spillover H atoms migrate from donor to the acceptor phase, and therefore influence the HDS activity. In this case, Co and Ni sulfides are the donors and Mo and W sulfides are the acceptor phases of the H atoms. The H atoms migrate downstream from the MS/support to the MoS_2/support bed.

2.2.4 Spillover distances

Roland et al. (1989) reported on spillover over long distances at room temperature for a two-component mixture of Pt/Al_2O_3 and H-NaY. The two components were studied either as physical mixtures or on packed beds in which a donor phase is placed on top of an acceptor phase (see Figure 2.6) to determine the distance over which spillover can happen. Occurrence of spillover over long distances is unlikely to be of any significance in steady-state catalytic reactions, but these measurements show how readily spillover can happen, and allow the processes that occur in spillover to be studied with accuracy.

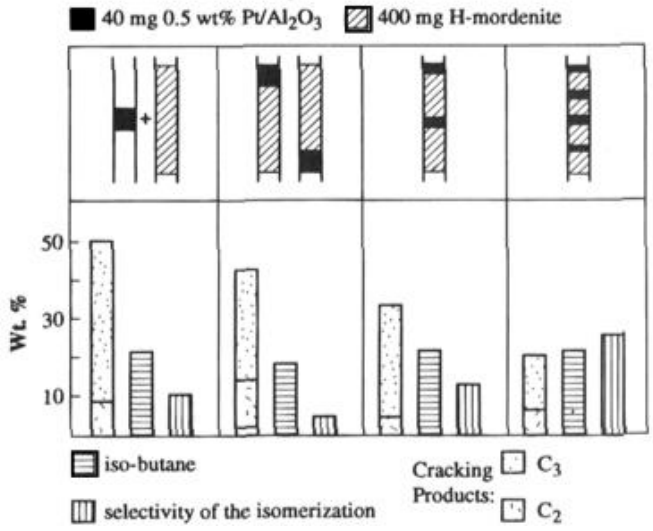

Figure 2.8: Influence of different arrangements of 0.5 wt % Pt/Al_2O_3 catalyst (dark regions) and H-mordenite (cross-hatched regions) on n-butane hydroconversion at 633K (Roland, Winkler, and Steinberg, 1989).

Figure 2.7 shows carbon which was removed from the zeolites as the dark regions in A, over a distance of 1 cm. This was done to demonstrate how readily spillover can occur.

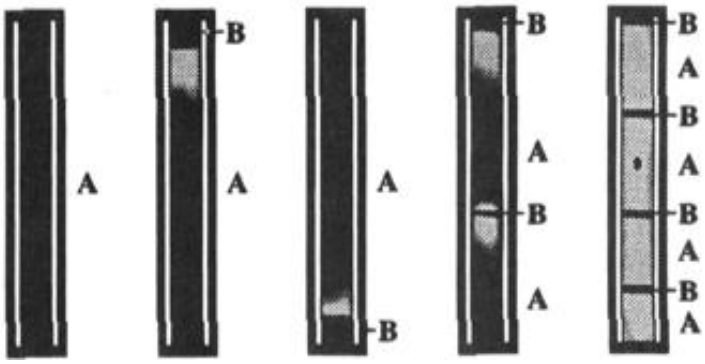

Figure 2.9: Photos of a quartz glass reactor for catalyst arrangements shown in the top part of Figure 1.6 after 1.5 h hydroconversion of n-butane at 633K. Reactant flow was from top to bottom: (A) H-mordenite; (B) 0.5 wt % Pt/Al_2O_3 (Roland et al., 1989).

2.2.5 Spillover in syngas reactions

Spillover work in syngas reactions was mostly done in the late 80's and early 90's, making use of Temperature Programmed Reduction (TPR) reactions and Temperature Programmed Desorption (TPD) studies to demonstrate directly the location and stoichiometry of the spiltover species. TPR studies have detected the presence of CH_3O spiltover species and verified their presence on supports such as SiO_2 and Al_2O_3 in an H_2 flow. CO that readily adsorbs on the metal surface at room temperatures reacts with H_2 when the temperature is raised to form CH_4. For a Ni/SiO_2 catalyst a CH_4 peak is observed in the hydrogenation of CO during the hydrogen TPR studies. For Ni/Al_2O_3, two distinct CH_4 peaks can be observed in the same experiment. Further experiments have shown that one of the peaks is the result of spillover that forms CH_3O on the Al_2O_3 (Figure 2.8) (Glugla et al. 1988; Glugla, 1989)

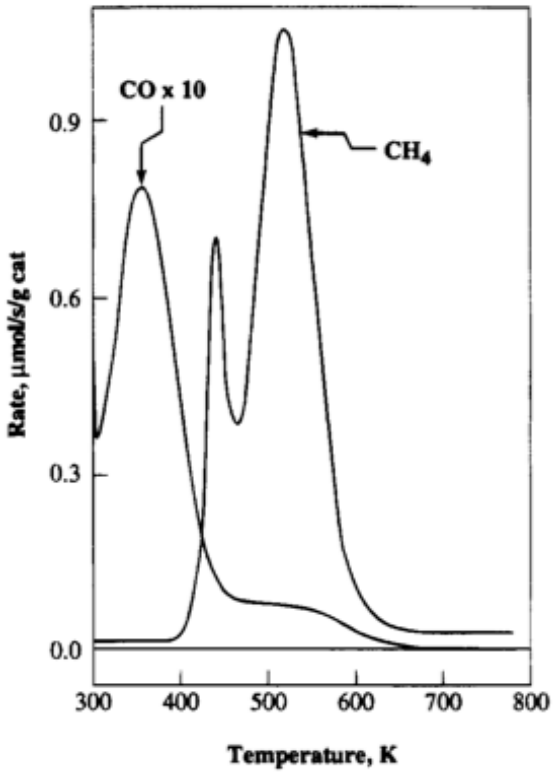

Figure 2.10: TPR profile of methane and CH3O hydrogenation (Glugla et al., 1988; Glugla, 1989).

Furthermore, because of the interest in methanation and Fischer-Tropsch synthesis, reactions of CO and H_2 to form adsorbed species have been extensively studied on supported metal catalysis. Although, temperature-programmed desorption (TPD) and reaction (TPR) have been particularly effective at demonstrating directly the location and stoichiometry of these spillover species, and thus the formation and reactivity of CH_3O (Conner and Falconer, 1995). Robbins (1989) clearly elucidated the spillover and hydrogenation steps on Pt/Al_2O_3 by combining TPR and IR spectroscopy. They observed the conversion of Pt-CO to Al-OCH_3 with FTIR spectroscopy as their Pt/Al_2O_3 was heated in a H_2 flow. Two distinct CH_4 peaks were seen during TPR studies, and they showed with IR spectra that in contrast to Ni/Al_2O_3, the spillover CH_3O species were more reactive in H_2 than the CO on Pt.

Several experiments indicated that CO and H_2 formation were due to CH_3O decomposition. Methanol TPD showed that the additional adsorption on the mixtures

showed that the spillover species could travel onto the Al_2O_3 surfaces across the SiO_2 or Al_2O_3 surface of the catalyst. This transport took place across the SiO_2 surface even though spillover did not produce measurable coverage's of CH_3O on the SiO_2 support of Ni/SiO_2. Co-adsorption of CO and H_2 also formed CH_3O on Ni/TiO_2, but the rate of spillover was much slower than on Ni/Al_2O_3 (Conner and Falconer, 1995). Studies of benzene hydrogenation on mechanical mixtures of catalyst and support have further demonstrated directly that hydrogen spillover can hydrogenate benzene adsorbed on the support (Conner and Falconer, 1995).

On supported Rh catalysts, however, the results were quite different. For all Rh catalysts, exposure to H_2, even at 298K, resulted in hydrogenation of the weakly adsorbed benzene to form cyclohexane. That is, H_2 dissociated on the Rh, spilled over onto the support, and hydrogenated the benzene on the support (Conner and Falconer, 1995).

Lewis (2013) examined the co-adsorption of CO and H_2, in the industrially important Fischer-Tropsch synthesis, on Co nanoparticles to investigate the effect of two-dimensional pressure. They found that CO adsorbed on the Co nanoparticles via spillover from a Cu (111) support, and when deposited onto preadsorbed adlayers of H, CO exerted two-dimensional pressure on H, compressing it into a higher–density, energetically less-preferred structure. When they deposited excess CO, Lewis (2013) found that H on the Co surface was forced to spillover onto the Cu (111) support. Thus, spillover of H from Co onto Cu, where it would not normally reside due to the high activation barrier, is preferred over desorption. They corroborated the mechanism of this spillover-induced displacement by calculating the relevant energetics using density functional theory, which showed that the displacement of H from Co is compensated for by the formation of strong Co-CO bonds. These results may have significant ramifications for Fischer-Tropsch synthesis kinetics on Co, as the segregation of CO and H, as well as the displacement of H by CO, limits the interface between the two molecules. Lewis (2013) and Nabaho (2015) reported that spillover can generate a hydrogen–rich microenvironment around the cobalt crystallites and thus have effects similar to those obtained at high H_2/CO ratios. The basis for the higher apparent STY in (Pt or Au)-Co/Al_2O_3 compared to the corresponding hybrid samples was conceived to lie in the physicochemical dissimilarities, and more specifically, in the great separation that had been introduced between the promoter and cobalt. Iglesias

(1993) stated that intimate interaction in a 0.14%Ru-11%Co/TiO_2 sample was attained during calcination. Conner and Falconer (1995) proposed that although current reaction mechanisms do not account for spillover species, it is likely that their effect is already incorporated in the proposed reaction kinetics so that spillover can be harnessed during future catalyst design.

Nabaho (2015) reported that direct hydrogen spillover from promoters occurred more competitively than hydrogen activation by the cobalt oxides, which allowed Au and Pt promoters to catalyse the reduction of the cobalt oxides. During the TPR analyses, Nahabo observed that the high temperature peak assigned to the reduction of non-stoichiometric cobalt aluminate species completely disappeared with use of a hybrid Pt-Co catalyst (Nabaho, 2015).

The role of spillover hydrogen was again invoked during the Fischer Tropsch reaction, this time providing a 'cleaning' effect on the cobalt surface via the removal of near surface or even subsurface oxygen/oxides that accumulate on the cobalt surface following C-O bond breaking. Despite the improved reducibility, the effects of spillover hydrogen under reactive conditions were significantly diminished in Hybrid Pt-Co.

Hydrogen spillover was corroborated by the enhanced selectivity towards hydrogenated products when compared at a similar level of conversion. The presence of Au and Pt promoters had a distinct effect on the apparent hydrogen (versus CO) availability under reaction conditions, which was characterised by higher CH_4 selectivity, lower C_{5+} selectivity, lower olefin selectivity, lower values of the chain growth probability (α) and higher extent of double-bond isomerisation (Nabaho, 2015).

2.2.6 Hydrogen spillover from metal onto oxides

In the literature, it has been found that catalytically active metals like Pt, Pd, Ru, Rh, and Ni can significantly lower the reduction temperature at which the reduction of oxide supports, like ceria, takes place. Research done by Sharma and co-workers, which looked at the spillover of hydrogen in Ni-loaded Pr-doped ceria, showed that nickel dissociatively adsorbeds hydrogen on its surface resulting in atomic hydrogen which could then be

transported to the oxide support via hydrogen spillover. They attributed their findings to two possible mechanisms for the reduction of an oxide support such as ceria. These two processes contributed to the formation of the surface reduction zone around the Ni particles; these are illustrated in Figure 2.9.

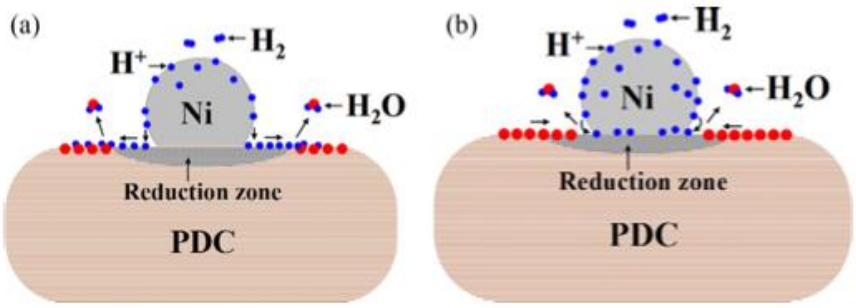

Figure 2.11: Illustration of the mechanisms of reduction zone formation: (a) hydrogen spillover from Ni to PDC followed by surface diffusion of H atoms across PDC, (b) hydrogen spillover from Ni to PDC followed by surface oxygen diffusion to the triple phase boundary (Fini and Breccia, 1999). (PDC= Praseodymium -doped ceria).

The first process involves the dissociative adsorption of hydrogen on the Ni metal particles followed by spillover of atomic hydrogen onto the oxide support with the reduction of the oxide at the interface. The second process involves the migration of oxygen ions towards the interface and the reaction with the spiltover hydrogen at the interface. In Figure 2.9a) the spiltover hydrogen diffuses from the nickel across the surface of the PDC away from the Ni-PDC interface in all directions. Since the surface oxygen atoms are bonded by fewer nearest neighbours (lower coordination number) than bulk oxygen atoms, they will initially combine with the highly reactive atomic hydrogen and form OH^- species. The surface OH^- species are known to "facilitate" the surface diffusion of spillover hydrogen. On combination with a second H atom, formation of H_2O occurs on the PDC surface. The H_2O is readily desorbed from the surface and the surface oxygen is lost, which forms an oxygen

vacancy at the surface. This surface vacancy readily diffuses into the bulk of PDC and the local stoichiometry is changed with a concomitant change in the Ce oxidation state. If more oxygen is lost from the surface, a reduction zone is formed around the Ni particle, which spreads in all directions. Figure 2.9b) mainly involves the diffusion of oxygen ions to the Ni/PDC interface. Initially the oxygen at the interface will be removed via reaction with spiltover hydrogen creating a narrow zone of oxygen vacancies around the Ni particles. At high temperatures, the surface oxygen atoms can rapidly migrate via vacancy hopping across the surface to fill the vacancies of the Ni/PDC interface. With a continuous loss of oxygen ions at the interface via H_2O formation, the surface concentration of oxygen vacancies increases and these are backfilled by bulk oxygen ions. The average oxidation state of Ce is thus locally changed in the PDC around the Ni particle. A reduction zone is thus formed around the nickel particle, which then spreads spatially in all directions. Which one of these two processes dominates is governed by the kinetics of the surface diffusion on the oxide.

2.3. Fischer-Tropsch synthesis

2.3.1. History and background information

The Fischer-Tropsch (FT) process was invented in petroleum-poor but coal-rich Germany in the 1920s, to produce liquid fuels. This process was originally developed by German researchers Franz Fischer, head of Max-Planck Institut für Kohlenforschung in Mülheim and Hans Tropsch a co-worker of Fischer and professor of chemistry in Prague (Czech Republic) in 1922. The process was a catalytic reaction between CO and H2, which yields mixtures of higher alkanes and alkenes. Germany and Japan during the World War II used this process to produce alternative fuels. In 1944, Germany's annual synthetic fuel production reached more than 124,000 barrels per day from 25 plants (Office of Fossil Energy, USA. 2017). These F-T plants were in operation making use of e.g. cobalt based F-T catalysts.

Even though the F-T process was a major scientific as well as a technical success, it could not compete economically with the refining process of crude oil, which was becoming

important starting from the 1950s (Morales, 2006). All of this coincided with the discovery of oil fields in the Middle East and consequently the dropping of crude oil prices. Regardless of economic situation, a F-T plant was built in Brownsville (Texas, USA), but due to the sharp price increase of methane, this led to the plant shutting down. After World War II due to the bad economics, the F-T technology became of little importance for the industrial world and no F-T plants were further constructed.However, in South Africa due to embargoes initiated by the apartheid government and its policies, they started making fuels and chemicals from gasified coal on a F-T process over half a century ago. The first commercial F-T plant was built by South African Coal, Oil and Gas Corporation, Ltd, SASOL in 1955. SASOL is still considered a major player in the F-T technology space until today. There are few reasons mentioned below that have renewed the interest in F-T technology today:

- Rising costs of crude oil, which is well above $50 per barrel
- Drive to supply environmentally friendly automotive fuels
- Commercialisation of unmarketable natural gas at remote locations

All of this has led to major investments by big petrochemical companies, such as Shell (Shell press release, 2004) and ExxonMobil (ExxonMobil press release 2004), to build large scale F-T plants in Qatar.

2.3.2. The Fischer Tropsch chemistry

The stoichiometry of the F-T process can be derived from the following two reactions, the polymerization reaction to produce hydrocarbon chains (1) and the water-gas shift reaction (2):

$$CO + 2H_2 \rightarrow -(CH2) - + H_2O \quad (1)$$

$$CO + H_2O \leftrightarrow H_2 + CO_2 \quad (2)$$

The overall stoichiometry in case reaction (2) is completely driven to the right is:

$$2CO + H_2 \rightarrow -(CH_2) - + CO_2 \quad (3)$$

The CO/H2 is usually called synthesis gas, or in short syngas. Syngas can either be produced, by partial oxidation or steam reforming. The F-T reaction involves the following main steps at the catalyst surface:

1. Adsorption and maybe dissociation of CO
2. The adsorption and dissociation of H_2;
3. Surface reactions leading to alkyl chains, which may terminate by the addition or elimination of hydrogen, giving rise to either paraffin or olefin formation.
4. Desorption of the final hydrocarbon products, which can be considered as the primary products of the F-T process.
5. Secondary reactions taking place on the primary hydrocarbon products formed due to e.g. olefin readsorption followed by hydrogenation or chain growth reinitiation.

Although the mechanism of the FT reaction is controversial, there is a general consensus that a stepwise chain growth process as explained above which involves similar to monomer polymerisation with CH_2 units as the building blocks. The CH_2 units are formed by hydrogenation of adsorbed CO on the metal catalyst surface (Schulz, 1999). FTS is therefore characterised by non-selectivity towards products. A typical product spectrum consists of a complex multicomponent mixture of linear and branched hydrocarbons and oxygenated products. The polymerization rates, and therefore the kinetics, are independent of the products formed (Dlamini, 2012). The probability of chain growth and chain termination are also independent of chain length. The probability of chain growth determines the distribution of the hydrocarbon products (Dry 1996; Dry 2001). The Anderson, Schulz and Flory (ASF) model gives an expression of the probability of chain growth. The ASF model is given by:

$$\frac{W_n}{n} = (1-n)^2 \alpha^{n-1} \quad (1)$$

The F-T reaction is a surface polymerisation which follows the principles of the Schulz-Flory kinetics, which mathematically expresses the weight content of the products of a certain carbon number as a function of carbon number and can be written as a linear expression by taking the logarithms of the appropriate terms.

$$\log(\frac{W_n}{n}) = n\log(\alpha) + \log\left(\frac{(1-\alpha)^2}{\alpha}\right) \quad (2)$$

Where:

W= weight fraction of product containing *n* number of atoms
α= probability of chain growth

The value of α can be determined from a plot $\frac{w_n}{n}$ against the carbon number *n*. The slope of the straight line is the chain growth probability.

However, this ideal case is often not observed in experimental data. For instance, the methane content is usually relatively high, particularly when using cobalt, nickel and ruthenium catalysts (Claeys and van Steen, 2002). The chain growth probabilty, α, can show apparent chain length dependency, which leads to a curved ASF distribution plot with preferred formation of long chain hydrocarbons. Syngas ratio, temperature, pressure and residence time are factors that can affect the FT product selectivity (Schulz and Cronje, 1977), Claeys and van Steen.

2.3.3. The Fischer Tropsch catalysts

Group VII transition metals are active for F-T synthesis, however, the only F-T catalysts, which have sufficient CO hydrogenation activity for commercial application, are composed of Ni, Co, Fe or Ru as the active metal phase. The metals mentioned are orders-of-magnitude more active than the other Group VII metals and some characteristics of these metals are summarized in Table 1. Choice of catalyst is important in FTS because the product distribution is dependent on the properties of the catalyst being used. The exact choice of the active F-T metal to be used in a particular catalyst formulation depends on a number of factors, which include the source of carbon for making the syngas, the price of the active element and the end product wanted. The Fe based catalyst is used to convert syngas made from a carbon-rich source such as coal, this is due to the high Water Gas Shift (WGS) activity of Fe, as given in reaction (2), which requires less hydrogen and oxygen exits the reactor in the form of carbon monoxide. The problem with using Fe based catalyst

is its high WGS activity, which will lead to an environmental issue such as the greenhouse effect, which will prohibit its use in the future. Nickel F-T catalysts are a problem, due to an easy dissociation of CO, and they possess too much hydrogenation activity, unfortunately, resulting in high yields of methane. The Ru based catalyst is the most active F-T element which can work at lowest reaction temperature of e.g. only 150 °C, and can produce very high molecular weight products. However, the problem with Ru is the very low availability and high cost, making it difficult to use in large-scale industrial F-T applications.

Table 2.1: Overview of some characteristics of Ni-, Fe-,Co- and Ru-based F-T catalysts

Active metal	Price	F-T activity	WGS activity	Hydrogenation activity
Ni	++++	+	+/-	+++++
Fe	+	+	+++	+
Co	+++	+++	+/-	+++
Ru	+++++	+++++	+/-	+++

2.3.4. Co-based Fischer- Tropsch catalysts

Interests in Co-based catalysts in the last three decades have been due to make more active catalysts with high wax selectivities. Co-based F-T catalyst composition contains the following components:

- Co as primary F-T metal
- Promoter metal, possessing noble metal behavior
- Oxidic promoter elements e.g. ceria, titania and manganese oxide
- High surface area oxide support e.g. alumina, titania and silica

Co-based catalysts are preferred choice for cases where syngas production occurs from hydrogen-rich carbon sources, such as natural gas and their lower WGS activities is also an advantage. Co is 3 times more active than Fe in F-T, while the price is much more

expensive. Co-based catalyst are preferred for the production of paraffins, as they give the highest yields for high molecular weight hydrocarbons from a relatively clean feedstock and produces less oxygenates than the Fe-based catalysts.

2.3.5. Promoters for Fischer- Tropsch catalysts

The surface of the catalyst often contains substances called promoters that are added deliberately to modify the turnover rate for a given catalytic reaction. A promoter is a doping agent added to a catalyst material in small quantities to improve the activity, selectivity and/or stability of the catalyst (Cornils et. al. 2000). There are different types of promoters: structural or structure promoters, electronic promoters, textural promoters, stabilizers and catalyst-poison-resistant promoters, but there are two main classes according to their intended functions. The structural promoters, which affect the formation and stability of the active phase of the catalyst and electronic promoters which directly affect the elementary steps involved in each turnover on the catalyst. The electronic promoter directly affects the local electronic structure of an active metal which results in the modification of the chemisorption properties of the active metal. This involves the adding and withdrawing of electron density near the Fermi level in the valence band of the metal. The above-mentioned promoters have overlapping effects, it sometimes difficult to precisely define the observed function of promoter. There are a few factors which affect the behavior in which the promoter modifies a catalysts activity in a positive or negative manner such as: the amount of the additives, the support oxide under consideration and the exact preparation method, which can cause it to either have a promoting effect or as poison.

2.3.6. Ruthenium as Co-based catalyst promoter

Ru has shown to play both roles as a structural and electronic promoter (Iglesia et. al. 1993 and Lapidus et. al. 1993). Research done by Turney and co-workers observed that the addition of Ru to Co/CeO_2 catalysts drastically increased the Co F-T activity without modifying the catalyst selectivity (Hoang et al., 1993 and Bruce et al., 1993). Data from XPS and TPR indicated that Ru caused a decrease of the reduction temperature of the supported Co_3O_4 nanoparticles. The authors proposed that Ru facilitated the reduction of cobalt via hydrogen spillover from Ru to Co, thereby leading to an increase of the number

of exposed Co° sites and consequently, to an increase in the CO hydrogenation rate. Further studies have shown that structural promotion of Ru has been to take place independently of the support material i.e. the addition of ru to Co/Al_2O_3 (Kogelbauer et al., 1996), Co/SiO_2 (Okabe K, et al., 1999), and Co/TiO_2 (Iglesia et al., 1994) catalysts decrease the reduction temperature of CoO_x to Co° during activation, which results in the catalysts with improved cobalt dispersions. Ru as an electronic promoter has been extensively studied the Co-Ru catalyst exhibit exceptionally high selectivities to C_{5+} products and higher turnover rates compared to unpromoted Co-based catalysts. Iglesia and co-workers (Iglesia 1994 and 1999) have done extensive work on Ru promotion, they observed that at reaction conditions that favor the formation of higher hydrocarbons, the apparent turnover numbers on cobalt catalysts are independent of the support material, but are markedly increased by small amounts of Ru added. Experimental data obtained by the Iglesia's group found that Ru inhibits the deactivation of the catalysts by keeping the Co surface "clean" and hence, preventing a carbon deposition on the Co particles. Intimate contact between Co and Ru atoms was required for this type of promotion to occur, since bimetallic nature of the active sites was found to exist and this nature was enhanced by oxidation treatments at high temperatures (>573 K).

2.3.7. FT catalyst supports

The role of the support in Fischer Tropsch synthesis has shown to be of significance importance because of the effect it has on the activity, selectivity and chemical nature of the supported catalyst. The support offers a large surface area which assists in metal dispersion which affects the performance of the catalyst (Chiwaye, 2012). The dispersion of the metal on a support increases the lifetime of the catalyst by slowing down the rate in which sintering occurs, this helps in maintaining the catalysts mechanical strength and to facilitate mass or heat transfer in a diffusion-limited or an exothermic reaction(Motchelaho, 2011) The catalyst support increases the resistance to poisoning. For industrial catalysts, they are often made of a metal or metal compounds supported on a suitable support. Further interest in support originates from the conclusion that transition metal-support interfaces influence catalytic activity which then generates improved catalysts than unsupported metals (Motchelaho, 2011). Supported catalysts are preferred in industry for the following reasons (Hagen, 2006): Costs, activity, selectivity and

regenerability. The costs of the active phase of the catalyst are usually an expensive metal. The dispersed active phase plays a role in achieving a higher activity per unit mass of metal, even though it makes up a small fraction of the total catalyst mass. For activity, the supported catalysts have a high activity which leads to faster reaction rates, shorter reaction time leading to maximum output. Selectivity is the most important parameter for catalyst design because of the crucial role it plays facilitating maximum yield of the desired products, elimination of side products and lowering of purification costs. Lastly the regenerability, by regenerating the supported catalyst this reduces process costs. It is important to note that active phase and the support can significantly affect the catalytic performance, therefore the choice of the appropriate catalyst support for a particular active metal since the support is not just a carrier. Reuel and Bartholomew reported on the effect that supports such as alumina, titania, silica, carbon nano-materials and magnesia have on the specific activity and selectivity properties of cobalt in CO hydrogenation. These researchers found that a decrease in hydrogenation activity (1 atm and 225 °C) in the following order Co/TiO_2 > Co/SiO_2 > Co/Al_2O_3 > Co/C > Co/MgO. Co/TiO_2 showed higher activity, this was considered to be a result of strong metal-support interactions (SMSI). Optimization of the support and metal interaction strength is of crucial importance, so that it is strong enough to obtain a good dispersion but not so strong as to inhibit low temperature reduction (Reuel and Bartholomew, 1991).

2.4. Microwave Chemistry

Chemists traditionally heat reactions using flames, hotplates, heating mantles, ovens and heating blocks, but since the accidental discovery of microwaves in the 1940's by Percy Spencer, research on microwave heating has continued unabated. The increase in the application of microwave technology across a number of fields, may lead to significant savings of both energy consumption and processing time (Neas and Coolins, 1998). The unique internal heating phenomenon associated with microwave energy, can enhance the overall production quality, which would allow for the development of new end-products and processes that cannot be realized using conventional methods.

2.4.1. Discovery of the microwave chemistry

The discovery of the microwave oven did not come about as result of someone trying to find a way to cook food faster. It was Percy Spencer of Raytheon Company who discovered accidentally that microwaves could be used to cook food, when he realized that a chocolate bar had melted in his pocket when he was standing in front of an open magnetron (Neas and Coolins, 1998). Magnetrons were used during the Second World War to spot Nazi warplanes on their way to bomb the British Isles. A magnetron is a tube, which produces microwaves. Two scientists Randall and Booth from the University of Birmingham in England designed them, and these magnetrons were installed in the RADAR system, to detect enemy planes during the Second World War (Neas and Coolins, 1998). After numerous experiments, using the microwaves to cook food, it was realized that microwave heating could increase the internal temperature of many different foods, much quicker than conventional heating. In the year 1967, a division of Raytheon introduced their first microwave oven called the "Radarange microwave oven" and this marked the beginning of the use of the microwave oven in home kitchens. Later on scientists took interest in the microwave effect. The use of microwaves has many advantages such as: reactions occur more rapidly, cleaner and easier and workup of the final material and microwave heating saves a great deal of time (Neas and Coolins, 1998). Interest grew among scientists because of the advantages microwave heating had in chemical systems. These included volumetric heating rather than surface heating via convection and radiation followed by conduction from the surface into the bulk, very high heating rates, and their good interaction with many insulating materials (Neas and Coolins, 1998).

2.4.2. Microwave radiation

Microwaves are based on electromagnetic radiation. The energy of a microwave is similar to that transported by infrared, visible or ultraviolet waves and they all follow similar laws. The frequency range of microwaves is from 300 MHz to 30 GHz (1-0.01 m wavelength). A frequency of 2.45 GHz (12.3 cm wavelength) was allotted by the International Commission for domestic and industrial ovens (Mingos and Baghurst, 1991). Microwaves represent a nonionizing radiation, which does not alter the molecular structure, but

influences molecular motions such as ion migration or dipole rotations. For 2.45 GHz microwaves, the oscillation of the electric field of the radiation occurs 4.9 x 10^9 times per second; the timescale in which the field changes is about the same as the response time (also known as relaxation time) of permanent dipoles present in most inorganic or organic molecules (Buchachenko and Frankevich, 1994). This allows for an efficient interaction between the electromagnetic field of microwaves and a chemical system. The absorption of microwaves causes a very fast increase to the temperature of reagents, solvents and products.

2.4.3. Dielectric heating

The ability of some liquids and solids to transform the absorbed electromagnetic energy into heat is what allows microwave heating to occur. The heating effect originates from the microwave electric field, which forces the dipoles to rotate and ions to migrate and to follow the rapid reversal of the electric field. The term "dissipation factor" (tan Δ) is the ability of a material to increase its temperature under microwave irradiation at a given frequency and temperature, which is defined as the:

$$\text{Tan}\,\Delta = \varepsilon'' / \varepsilon'$$

where, ε'' is the dielectric loss factor, which is related to the efficiency of a medium to convert microwave energy into heat, while ε' is the dielectric constant and measures the ability of a molecule to be polarized by an electric field. If water is taken as an example, the ε' of water is relatively high at low frequency but rapidly drops to zero above 30 GHz, while ε'' shows a parabolic profile reaching a maximum at around 20 GHz. The 2.45 GHz frequency which was chosen for practical purposes represents a compromise both to minimize the drop of the dielectric constant with increasing frequency and to maximize the penetration depth of the radiation (Mingos and Baghurst, 1991; Buchachenko and Frankevich, 1994; Galema, 1997).

Conventional and microwave heating differ in the temperature distribution, which is found in both heating systems. Conventional heating can be described as the heat transferred from the surface towards the center of the material by convection, conduction and

radiation. Microwave heating is the conversion of electromagnetic energy to thermal energy. Microwaves are able to penetrate through materials and deposit energy inside an object. Because of this ability, heat is generated throughout the volume of the material (volumetric heating), rather than from an external source. Microwave energy can therefore be seen as energy conversion rather than heat transfer. Thus, opposite thermal gradients are observed for both heating systems (see Figure 2.10).

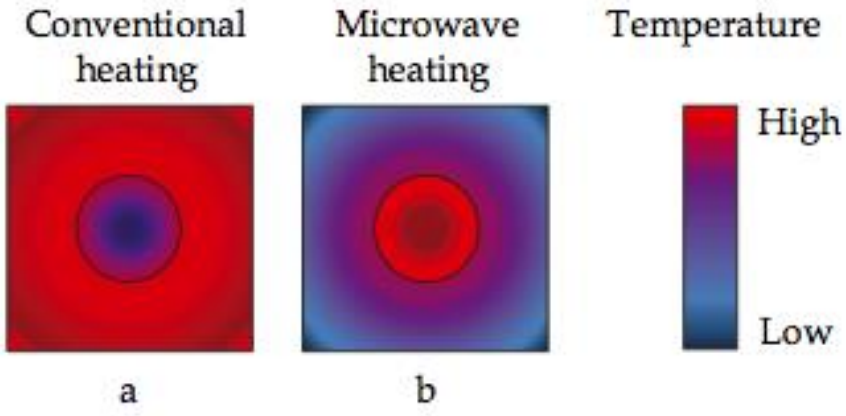

Figure 2.12: Temperature gradient within samples heated by (a) conventional heating and (b) microwave dielectric heating. The circles represent the sample; the squares correspond to the cavity used in both heating systems (Grundas, 2011; Majetich and Hicks,1995).

In conventional heating, the furnace cavity has to reach the operating temperature to begin heating, whereas in microwave heating, the material is at a higher temperature than the surrounding area. These heating systems favor different chemical reactions. A conventional heating system improves reactions that take place in the surroundings such as homogeneous reactions in the gas-phase, while a microwave heating systems favors reactions involving solid materials, e.g. heterogeneous reactions (Zhang and Hayward, 2006).

2.4.4. Materials and microwaves

The nature of the solid materials present in different modes inside a system subjected to radiation plays an important role in microwave applications to chemical reactions.

In the microwave process, materials can be divided into three categories: (1) conductors, which can reflect microwaves; (2) insulators, which are crossed by the microwaves, without being adsorbed; (3) absorbers, which absorb the radiation and therefore are able to start heating or activate a chemical reaction. Most materials such as teflon are found to be transparent; these materials can be penetrated by radiation without absorbing radiation (Breccia et al., 1995; Fini and Breccia, 1999). Some other materials, such as metals, reflect radiation. Materials such as dielectrics interact with microwaves to different extents. Containers which hold the reagents for a particular reaction have to be transparent to the microwaves and are therefore made of Teflon or polyethylene; glass is also suitable for high temperature reactions, but the problem with glass is that it is not completely transparent to microwaves (Breccia et al., 1995; Fini and Breccia, 1999).

The measuring of temperature during a chemical reaction in a microwave oven can prove to be a problem. The temperature cannot be measured using conventional instruments, such as mercury thermometers or metal thermocouples. The temperature can be measured by thermal indicators or indirectly by the heating of suitable probes such as glass fiber thermocouples (Breccia et al., 1995; Fini and Breccia, 1999).

Microwave heating gives a uniform heating distribution, therefore stirring is not necessary to homogenize the distribution of the heat, however when stirring is required in a reaction, mechanical stirrers made of Teflon and glass are preferred to magnetic stirrers (Fini and Breccia, 1999).

Solid materials that absorb microwaves can display different rates of heating, according to their composition and the dimension of their particles (Breccia et al., 1995). When such materials are in the form of a powder or fibers and placed within a polymer the microwave absorption can be improved and locally increase the temperature. This increases the hardening or the compaction of the polymeric materials.

2.4.5. The microwave oven

The most important part of an oven is the magnetron, which is an oscillator that converts a high voltage pulse into a pulse of microwave power. The microwave oven operates as

follows: the microwave enters a waveguide, whose reflective walls allow the transmission of the radiation from the magnetron into the cavity. A cavity is a box that is part of the oven where microwaves interact with the chemical system. The microwave oven is a setup to deliver in most cases a preset frequency of 2.45 GHz and power. A control unit regulates the power value introduced into the cavity in each run through an automatic on/off cycle of the magnetron (Fini and Breccia, 1999; Neas and Coolins, 1998; Mingos and Baghurst, 1991; Buchachenko and Frankevich, 1994; Galema, 1997; Majetich and Hicks, 1995; Zhang and Hayward, 2006).

There are two problems which arise under microwave irradiation: (1) the uniformity of the absorption and (2) the reflection of the waves. Microwave energy travels in a beam, and a guide is used to deviate the wave into the cavity by means of a circulator. The cavity walls reflect the beam, until it hits the sample and is absorbed. In order to increase the probability of the interaction between the sample and the wave, the sample is placed in a rotating glass disk.

The advantage of using microwaves in chemical reactions is generally evaluated by comparing the time needed to obtain a given yield of the final product with respect to traditional heating (Fini and Breccia, 1999).

Generally the time taken using microwaves is less than required by conventional heating. Reactions, which benefit more from the presence of microwaves, are obviously those reactions that have low rates under conventional heating conditions. These reactions include those found in organic synthesis such as the hydrolysis of nitriles, amides, and esters, as well as reactions involving formation of esters and ethers, oxidation and hydrogenations, rearrangements and polymerizations, to catalysis reactions.

2.4.6. Microwave enhanced chemistry

The hydrolysis of esters, amides and nitriles occur very slowly either in basic or acidic medium under traditional heating conditions. In the presence of strong acids and bases, an increase of heating rate is observed under microwave heating (Fini and Breccia, 1999).

In the Diels-Alder reaction the carbonyl group acts as a sort of antenna towards radiation. The reaction is initially rapid, when the starting diene is electron-rich and the dienophile is electron poor; but when the dienophile lacks an activating group the reactions require high temperatures (>300°C), using traditional heating. However, under microwave heating, the rate is strongly accelerated (Fini and Breccia, 1999).

In polymer chemistry, the use of microwaves has a positive effect, because the presence of polar groups in the starting materials particularly favors the adsorption of microwaves. This allows rapid and controlled synthesis and hardening and curing of the final products.

Work done by Reubroycharoen and co-workers has shown the effect of microwave irradiation in Fischer Tropsch Synthesis (Reubroycharoen et al., 2007). A study done used microwave irradiation to prepare a highly active Co/SiO_2 catalyst, showed more uniform and better dispersion of the Co particles within catalyst pellets, in comparison to the catalyst prepared by a traditional heating method (Figure 2.11). The activity of the microwave irradiated catalyst was greater than the traditional heated one. The longer the catalyst was irradiated, the greater the increase in activity of the catalyst; this was attributed to the particle distribution. The conventional catalyst was found to have large agglomerated Co particles at the surface which led to low catalytic activity, whereas the microwave irradiated catalyst provided more uniform dispersion, which led to higher activity which was solely dependent on the irradiation time, the optimum time being 14 min.

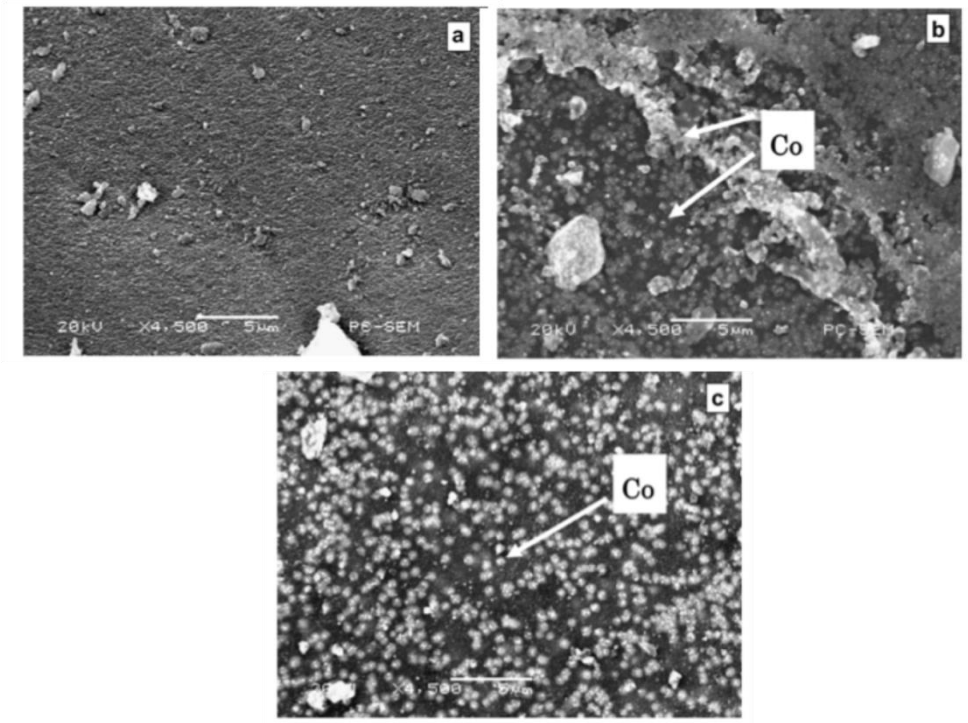

Figure 2.13: SEM images of the Co/SiO_2 catalysts (20kV, x4,500): (a) Silica support, (b) conventional heating catalyst and (c) microwave irradiated catalyst (Reubroycharoen et al., 2007).

Other work that has been reported using microwave irradiation in the area of Fischer Tropsch Synthesis has been accomplished by graduate students at the University of the Witwatersrand viz. Linganiso (Linganiso, 2010) and Dlamini (Dlamini, 2012). Linganiso's work focused on highly surface sensitive techniques such as temperature programmed surface reaction-mass spectrometry (TPSR) and Secondary Ion Mass Spectrometry (SIMS). These techniques gave details of reactions happening on the surface of a supported iron catalyst. After the microwave pre-treatment, SIMS measurements showed that the ratio of Fe:K increased from 0.055 to 0.095; this showed that the microwaves altered the surface of the iron catalyst (Linganiso, 2010). A TPSR study also showed an increase in the number and type of active sites present on the surface of the catalyst. Observations made by Linganiso during the Fischer Tropsch Synthesis study revealed that the microwave treatment gave an increase in carbon dioxide selectivity and olefin formation.

This increase was concluded to be due to the promoting effects that the microwaves had on the iron and potassium interaction (Linganiso, 2010; Dlamini, 2012).

Work done by Dlamini was a continuation from the research done by Linganiso. Microwave irradiated and non-microwaved samples were compared using TPSR as a function of potassium loading (0-1.5 wt% K range), and showed differences in CO adsorption for the K/Fe and K/Fe/SiO_2 catalysts. Observations made by Dlamini showed that for the non-supported catalysts, K/Fe at 0.2 wt % K loading, the total CH_4 evolved was 6 %. The CH_4 evolution increased as the K loading was increased, but at 0.7 wt % K loading, maximum total CH4 evolutions was observed at 35 % and post this K loading a drop in the CH_4 evolution to 14% was observed for the 1.0 and 1.5 wt % K loadings. For the supported catalysts, K/Fe/SiO_2, the total CH_4 evolved increased from 13 % for the 0.2 wt % K and rose until a maximum was reached of 66 % for the 0.7 wt % K catalyst. Dlamini concluded that the microwave irradiated K/Fe/SiO_2 catalysts showed a higher % CH_4 evolution than their non-supported K/Fe counterparts (Dlamini, 2012). The increase in % CH_4 evolved was attributed to the increase in K promoter loading and the microwave effect (Dlamini, 2012).

References

Baeza, P., Ureta-Zañartu, M.S., Escalona, N., Ojeda, J., Gil-Llambías, F.J. and Delmon, B. (2004) 'Migration of surface species on supports: A proof of their role on the synergism between CoSx or NiSx and moS2 in HDS', *Applied Catalysis A: General*, 274(1-2), pp. 303–309.

Baeza, P., Villarroel, M., Ávila, P., López Agudo, A., Delmon, B. and Gil-Llambías, F.J. (2006) 'Spillover hydrogen mobility during Co–Mo catalyzed HDS in industrial-like conditions', *Applied Catalysis A: General*, 304, pp. 109–115.

Benson, J., Kohn, H. and Boudart, M. (1966) 'On the reduction of tungsten trioxide accelerated by platinum and water', *Journal of Catalysis*, 5(2), pp. 307–313.

Bianchi, D., Gardes, G.E.E., Pajonk, G.M. and Teichner, S.J. (1975) 'ChemInform abstract: Hydrogenation of ethylene on alumina after hydrogen spillover', *Chemischer Informationsdienst*, 6(38),

Breccia, A., Fini, A., Feroci, G., Grassi, A.M., Dellonte, S. and Mongiorgi, R. (1995) *Journal of Microwave Power Electromagnetic Energy*, 30, p. 3.

Bruce L.A., Hoang M, Hughes., A.E. and Turney T.W., (1993) Applied Catalysis. A: General, 100, 51

Buchachenko, A.L. and Frankevich, E.L. (1994) *Chemical Generation and Reception of Radio and Microwaves*. New York: VCH Publisher.

Carley, A.F., Edwards, H.A., Mile, B., Roberts, M.W., Rowlands, C.C., Jackson, S.D. and Hancock, F.E. (1994) 'An EPR study of a palladium catalyst using a PBN (N-benzylidene-tert-butylamine n-oxide) spin trap: Direct demonstration of hydrogen spillover', *Journal of the Chemical Society, Chemical Communications*, (12), p. 1407.

Claeys, M. and E. van Steen: (2002), 'On the Effect of Water during Fischer-Tropsch Synthesis with a Ruthenium Catalyst'. Catalysis Today 71(3-4), 419-427.

Claeys, M. and H. Schulz: (2004), 'Effects of internal Mass Transfer on Activity and Selectivity in Iron based Fischer-Tropsch Synthesis'. American Chemical. Society., Div. Petro. Chem. 49(2), 195-199

Conner, C.Wm, (1995) 'New aspects of spillover effect in Catalysis. Edited by T. Inui, K. Fujimoto, T. Uchijima, and M. Masai. Studies in surface and Catalysis, Vol. 77. Elsevier, Amsterdam, 1993. 435 pp', *Journal of Catalysis*, 152(2), p. 421.

Conner, W.C. and Falconer, J.L. (1995) 'Spillover in heterogeneous Catalysis', *Chemical Reviews*, 95(3), pp. 759–788.

Conner, W.C. and Pajonk, G.M. (1984) *Discussion*. Villeurbarne, France: University of Claude Bernand, Lyons-1.

Cornils B., Herrmann W.A., Schlogl R.and Wong C.H., (2000) Catalysis from A to Z, A concise encyclopedia, Wiley-VCH, Weinheim.

Dlamini, M.W. (2012) *The effect of microwave treatment on potassium promoted iron Fischer-Tropsch catalysts* MSc dissertation, University of the Witwatersrand

Emmett, P.H. (1940) 'The Role of Ions in Surface Catalysis', Twelfth Report of the Committee on Catalysis, National Research Council: John Wiley & Sons, Inc. pp. 68–81.

Escalona, N., Garcia, R., Lagos, G., Navarrete, C., Baeza, P. and Gil-Llambias, F.J. (2006) 'Effect of the hydrogen spillover on the selectivity of dibenzothiophene hydrodesulfurization over CoSx/γ-al2O3, NiSx/γ-al2O3 and moS2/γ-al2O3 catalysts', *Catalysis Communications*, 7(12), pp. 1053–1056.

ExxonMobil press release on July, 14, 2014 (http://exxonmobil.com)

Falconer, J.L. and Conner, W.C. (1989) 'Second international conference on spillover', *Applied Catalysis*, 56(2), pp. N28–N29.

Fernandez, Y., Arenillas, A. and Menéndez, Á. (2011) *Advances in induction and microwave heating of mineral and organic materials*.

Flory, P., (1936), 'Molecular Size Distribution in linear Condensation Products'. Journal American Chemical Society. 58(10), 1877-1885.

Fini, A. and Breccia, A. (1999) 'Chemistry by microwaves', *Pure and Applied Chemistry*, 71(4).

Fornasiero, P., Balducci, G., Kašpar, J., Meriani, S., di Monte, R. and Graziani, M. (1996) 'Metal-loaded CeO2-ZrO2 solid solutions as innovative catalysts for automotive catalytic converters', *Catalysis Today*, 29(1-4), pp. 47–52.

Fornasiero, P., Kaspar, J., Sergo, V. and Graziani, M. (1999) 'Redox behavior of high-surface-area Rh-, Pt-, and Pd-Loaded Ce0.5Zr0.5O2Mixed oxide', *Journal of Catalysis*, 182(1), pp. 56–69.

Galema, S.A. (1997) 'Microwave chemistry', *Chemical Society Reviews*, 26(3), pp. 233–238.

Glugla, P. (1989) 'Activated formation of a Hz.and;CO complex on Ni/Al2O3 catalysts', *Journal of Catalysis*, 115(1), pp. 24–33.

Glugla, P.G., Bailey, K.M. and Falconer, J.L. (1988) 'Isotopic identification of surface site transfer on nickel/alumina catalysts', *The Journal of Physical Chemistry*, 92(15), pp. 4474–4478.

Goez, M. (1995) ‘Chemical generation and reception of radio- and microwaves. Von A. L. Buchachenko undE. L. Frankevich. VCH Verlagsgesellschaft, Weinheim/VCH publishers, New York, 1994. 107(8), pp. 1020–1021.

Grundas, S. (2011) *Advances in induction and microwave heating of mineral and organic materials*. (Chapter 31 Vols). Rijeka, Croatia: Intech Open Access Publisher.

Hamilton, E. (1991) ‘Introduction to microwave sample preparation edited by H.M. Kingston and L.B. Jassie, American chemical society professional reference book, American chemical society, Washington, DC, 1988, pp 263.

Hagen J., (2006) ‘ Industrial catalysis: a practical approach’, Wiley-VCH Verlag GmbH & Co. KGaA.

Harris I.R., Caga I.T. , Tata A.Y. and Winterbottom J.M., (1993) Studies of Surface Science Catalysis., 75, 2801.

Hoang , M. Hughes A.E. and Turney T.W., (1993) Applied Surface Science., , 72, 55.

Huizinga, T. and Prins, R. (1981) ‘Behavior of titanium(3+) centers in the low- and high-temperature reduction of platinum/titanium dioxide, studied by ESR’, *The Journal of Physical Chemistry*, 85(15), pp. 2156–2158.

Iglesia, E. (1993) ‘Bimetallic synergy in cobalt ruthenium Fischer-Tropsch synthesis catalysts’, *Journal of Catalysis*, 143(2), pp. 345–368.

Jen, H., Graham, G.W., Chun, W., McCabe, R.W., Cuif, J.., Deutsch, S.E. and Touret, O. (1999) ‘Characterization of model automotive exhaust catalysts: Pd on ceria and ceria–zirconia supports’, *Catalysis Today*, 50(2), pp. 309–328.

Kang, Z.C. and Eyring, L. (1997) ‘A compositional and structural rationalization of the higher oxides of Ce, pr, and Tb’, *Journal of Alloys and Compounds*, 249(1-2), pp. 206–212.

Khangale, P.R., 2016. *Fischer-Tropsch reaction over alumina-supported cobalt catalyst: activation using H2 and CO* (Doctoral dissertation, University of Johannesburg).

Kester, K. (1984) ‘CO methanation on low-weight loading Ni/Al_2O_3: Multiple reaction sites’, *Journal of Catalysis*, 89(2), pp. 380–391.

Khoobiar, S. (1964) ‘Particle to particle migration of hydrogen atoms on Platinum—Alumina catalysts from particle to neighboring particles’, *The Journal of Physical Chemistry*, 68(2), pp. 411–412.

Kogelbauer A., Goodwin J.G. and Oukaci R., (1996) Journal of. Catalysis., 160, 125.

Kuriacose, J. (1957) *Industrial Journal of Chemistry*, 2, p. 159.

Lapidus A.L., Krylova A.Y., Kapur M.P., Leongardt E.V., Fasman A.B. and Mikhailenko S.D., Bull. Russ. Acad. Sci.-Div. Chem. Sci., 1992, 41, 45.

Lenz, D. (1987) 'Hydrogen spillover on silica: Ethylene hydrogenation and H_2-D_2 exchange', *Journal of Catalysis*, 104(2), pp. 288–298.

Levy, R. (1974) 'The kinetics and mechanism of spillover', *Journal of Catalysis*, 32(2), pp. 304–314.

Lewis, E.A., Le, D., Jewell, A.D., Murphy, C.J., Rahman, T.S. and Sykes, E.C.H. (2013) 'Visualization of compression and spillover in a Coadsorbed system: Syngas on cobalt Nanoparticles', *ACS Nano*, 7(5), pp. 4384–4392.

Linganiso, L. (2010) *Microwave induced solid-state interactions for the synthesis of Fischer-Tropsch catalysts* Phd thesis. University of the Witwatersrand.

Majetich, G. and Hicks, R. (1995) 'Applications of microwave-accelerated organic synthesis', *Radiation Physics and Chemistry*, 45(4), pp. 567–579.

Marin, R.P., Kondrat, S.A., Gallagher, J.R., Enache, D.I., Smith, P., Boldrin, P., Davies, T.E., Bartley, J.K., Combes, G.B., Williams, P.B. and Taylor, S.H., 2013. Preparation of Fischer–Tropsch Supported Cobalt Catalysts Using a New Gas Anti-Solvent Process. *Acs Catalysis*, *3*(4), pp.764-772.

Mingos, D.M.P. and Baghurst, D.R. (1991) 'Tilden lecture. Applications of microwave dielectric heating effects to synthetic problems in chemistry', *Chemical Society Reviews*, 20(1), p. 1.

Mirodatos,C. (1987) 'Deactivation of nickel-based catalysts during CO methanation and disproportionation', *Journal of Catalysis*, 107(2), pp. 275–287.

Morales F and B.M. Weckhuysen,., (2006) Promotion Effects in Co-based Fischer Tropsch Catalysts, Catalysis vol 19.

Nabaho, D. (2015) *The roles of platinum and gold as promoters for cobalt-based catalysts*. Phd thesis. University of Cape Town.

Neas, E.D. and Coolins, M.J. (1998) *Introduction to Microwave Sample Preparation*. (Chapter 2). Washington DC: ACS Professional Reference Book.

Ojeda, J., Escalona, N., Baeza, P., Escudey, M. and Gil-Llambías, F.J. (2003) 'Synergy between mo/SiO 2 and Co/SiO 2 beds in HDS: A remote control effect?', *Chem. Commun.*, (13), pp. 1608–1609.

Okabe K., Li X.H., Matsuzaki T., Toba M., Arakawa H. and Fujimoto K., (1999) Journal of Japanese

Oppermann, R.H. (1940) ‘Twelfth report of the committee on Catalysis, national research council’, *Journal of the Franklin Institute*, 230(4), pp. 527–528.

Pajonk, G.M., Teichner, S.J. and Germain, J.E. (1983) *Spillover of Adsorbed species*. Edited by G. M Pajonk, S. J. Teichner, and J. E. Germain. 17th edn. Amsterdam: Elsevier Science Publishers B.V.

Palazov, A. (1982) ‘Infrared spectroscopic study of the interaction between carbon monoxide and hydrogen on supported palladium’,*Journal of Catalysis*, 74(1), pp. 44–54.

Prins, R. (2012) ‘Hydrogen spillover. Facts and fiction’, *Chemical Reviews*, 112(5), pp. 2714–2738.

Reuel, R.C. & Bartholomew, C.H. 1985, “Effects of support and dispersion on the CO hydrogenation activity/selectivity properties of cobalt”, Journal of Catalysis, vol. 85 pp. 78- 88

Reubroycharoen, P., Vitidsant, T., Liu, Y., Yang, G. and Tsubaki, N. (2007) ‘Highly active Fischer–Tropsch synthesis Co/SiO_2 catalysts prepared from microwave irradiation’, *Catalysis Communications*, 8(3), pp. 375–378.

Robbins, J.L. and Marucchi-Soos, E. (1989) ‘“Evidence for multiple CO hydrogenation pathways on Pt/Al2O3”’, *Journal of Physical Chemistry*, 93(8), pp. 2885–2888.

Roland, U., Winkler, H. and Steinberg, K.H. (eds.) (1989) ‘Second Conference on Spillover’, Karl-Marx-Universitat Leipzig: K.H. Steinberg. p. 63.

Rozanov, V.V. and Krylov, O.V. (1997) ‘Hydrogen spillover in heterogeneous catalysis’, *Russian Chemical Reviews*, 66(2), pp. 107–119.

Schulz, H. and J. Cronje: (1977), 'Kohle, Fischer-Tropsch Synthese'. In: 14 (ed.): Ullmanns Enzyklopadie der technischen Chemie. Weinheim: Verlag Chemie, 4 edition, pp. 329- 350.

Schulz, H. and M. Claeys: (1999b), 'Reactions of a-Olefins of different Chain Length added during Fischer-Tropsch Synthesis on a Cobalt Catalyst in a Slurry Reactor'. Applied Catalysis. A: Gen. 186(1-2), 71-90.

Schulz, G., (1930), 'Highly polymerized Compounds. CXXII The Relation between Reaction Rate and Composition of the Reaction Product in Macropolymerization Processes'. Z. Physik. Chem. B30, 379-98.

Sen, B. (1990) ‘Dependence of temperature-programmed methanation on H2 pressure’, *Journal of Catalysis*, 125(1), pp. 35–44. doi: 10.1016/0021-9517(90)90075-u.
Sermon, P.A. and Bond, G.C. (1974) ‘Hydrogen spillover’, *Catalysis Reviews*, 8(1), pp. 211–239.

Sharma, V., Crozier, P.A., Sharma, R. and Adams, J.B. (2012) ‘Direct observation of hydrogen spillover in Ni-loaded pr-doped ceria’,*Catalysis Today*, 180(1), pp. 2–8.

Shell press release on March 9, 2004 (http://www.shell.com)

Sinfelt, J.M. and Lucchessi, P.J. (1963) *Journal of American Society*, 85, p. 3365.
Taylor, H.S. (1961) *Actes Congress International Catalysis*, 2, p. 159.

Teichner, S.J. (1990) 'Recent studies in hydrogen and oxygen spillover and their impact on catalysis', *Applied Catalysis*, 62(1), pp. 1–10.

Water/Hydrogen Mixtures'. Journal of Physical. Chernistry. B 109(8), 3575-3577.

van Steen, E. and H. Schulz: (1999), 'Polymerization Kinetics of the Fischer-Tropsch CO Hydrogenation using Iron and Cobalt based Catalysts'. Appl. Catal. A: Gen. 186(1-2), 309-320

van Steen, E., M. Claeys, M. Dry, J. van de Loosdrecht, E. Viljoen, and J. Visagie: (2005), 'Stability of Nanocrystals: Thermodynamic Analysis of Oxidation and Re-reduction of Cobalt in Water/Hydrogen Mixtures'. Journal of Physical. Chernistry. B 109(8), 3575-3577

Valdevenito, F., García, R., Escalona, N., Gil-Llambias, F.J., Rasmussen, S.B. and López-Agudo, A. (2010) 'Ni//mo synergism via hydrogen spillover, in pyridine hydrodenitrogenation', *Catalysis Communications*, 11(14), pp. 1154–1156.

Villarroel, M., Baeza, P., Escalona, N., Ojeda, J., Delmon, B. and Gil-Llambías, F.J. (2008a) 'MD//mo and MD//W [MD=Mn, Fe, Co, Ni, cu and Zn] promotion via spillover hydrogen in hydrodesulfurization',*Applied Catalysis A: General*, 345(2), pp. 152–157.

Villarroel, M., Baeza, P., Gracia, F., Escalona, N., Avila, P. and Gil-Llambías, F.J. (2009) 'Phosphorus effect on Co//mo and Ni//mo synergism in hydrodesulphurization catalysts', *Applied Catalysis A: General*, 364(1-2), pp. 75–79.

Vlaic, G., Fornasiero, P., Martra, G., Fonda, E., Kašpar, J., Marchese, L., Tomat, E., Coluccia, S. and Graziani, M. (2000) 'Morphology of Rhodium particles in ex-chloride Rh/Ce0.5Zr0.5O2 catalyst', *Journal of Catalysis*, 190(1), pp. 182–190.

Zagli, A. (1979) 'Methanation on supported nickel catalysts using temperature programmed heating', *Journal of Catalysis*, 56(3), pp. 453–467.

Zhang, X. and Hayward, D.O. (2006) 'Applications of microwave dielectric heating in environment-related heterogeneous gas-phase catalytic systems', *Inorganica Chimica Acta*, 359(11), pp. 3421–3433

http://www.fe.doe.gov/aboutus/history/syntheticfuels_history.html

CHAPTER 3

EXPERIMENTAL METHODS

3.1 Introduction

In this chapter the catalysts and equipment used to conduct this study are thoroughly explained. For the synthesis of carbon spheres, the vertical chemical vapour deposition method (CVD) was used (Moyo, 2012). Procedures used to prepare the catalysts and the characterization techniques used (Brunauer-Emmett-Teller, Raman spectroscopy, Transmission Electron Microscopy, Thermogravimetric Analysis (TGA), Temperature Programmed Reduction(TPR) are described. The Fischer Tropsch Synthesis setup for catalyst evaluation is also described in detail in this chapter.

3.2 Preparation of Carbon Spheres

3.2.1Materials

All chemicals used, including $RuCl_3.xH_2O$, $Co(NO_3)_2.6H_2O$, Degussa P25 titania, and ethylene glycol in this research project were purchased from Merck or Sigma Aldrich, and were used without further purification. The water used was deionized and was supplied by the School of Chemistry.

3.2.2 Gases

All the gases used such as argon and acetylene for this research study were purchased from African Oxygen (AFROX), each gas cylinder arrived with certificate of analysis which included an expiry date. For FT synthesis Ultra high purity (UHP) grade Hydrogen gas (99.997% purity) was used for catalyst reduction and syngas cylinders containing a mixture of H2/CO/Ar mixtures (0.60/0.30/0.1 vol; Purity: 99.99%) were used for the

reactant gas stream

3.2.3 Method for the preparation of carbon spheres

Carbon spheres (CS) were synthesized by a chemical vapour deposition method (CVD), which required no catalyst (Moyo, 2012). Acetylene gas was used as a carbon source, and decomposed at 900 ºC to synthesize the CSs. The experimental setup is shown as a schematic diagram in Figure 3.1. Ar gas was allowed to flow through the quartz tubular reactor at a flow rate of 800 mL/min while the furnace heated up to 900 ºC at a heating rate of 10 ºC/min. When the furnace had reached 900 ºC, the Ar gas was switched off and the acetylene was switched on and allowed to flow through the quartz tubular reactor at a flow rate of 300 mL/min for 3 h (Moyo, 2012). After 3 h the acetylene gas was switched off and argon gas was flowed through the reactor at 800 mL/min until the furnace had cooled down to room temperature. The CS soot was collected from the round bottom flask connected to the bottom of the quartz tubular reactor. The product was then weighed (6.3 g) and characterized by BET, TEM, TGA and Raman spectroscopy.

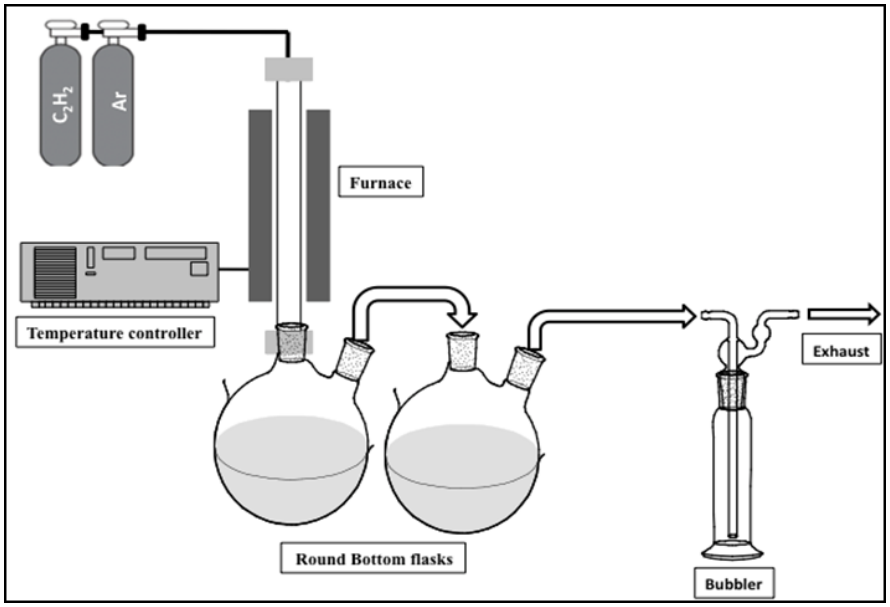

Figure 3.1: Vertical CVD setup for the synthesis of carbon spheres

The as-grown carbon spheres were washed with toluene using the soxhlet apparatus (see Figure 3.2). The as-grown CSs were washed with toluene to remove the waxy layer of non-polar molecules such as polycyclic aromatic hydrocarbons which were formed in the reaction. The purified CSs were then dried in an oven for 12 h at 120 °C (Moyo, 2012).

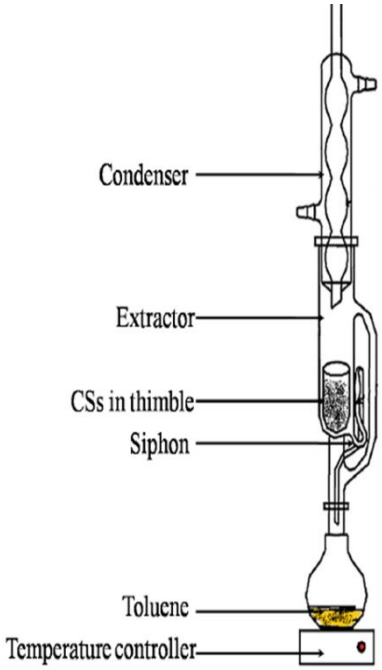

Figure 3.2: Soxhlet apparatus for the purification of as-grown carbon spheres

The CSs were functionalized using 55% HNO_3 at a temperature of 83˚C, to introduce acidic functional groups on the hydrophobic CS surface to allow for cation exchange properties. The CSs were functionalized in 55% HNO_3 for 12 h. The CSs were then slurried, filtered and washed with deionized water until the filtrate reached a pH of 7. The functionalized CSs (denoted F-CS) were dried in an oven for 12 h at 120 °C.

3.3 Catalyst preparation

Carbon and titania supported cobalt and ruthenium catalysts were synthesized in this study. The methodology used to prepare each catalyst is discussed below. For the hydrogen

spillover study the methods used to prepare the catalysts were the deposition precipitation and the incipient wetness methods. For the conventional and microwave heating method studies, the catalysts used were prepared using incipient wetness (from the hydrogen spillover study) and the Polyol methods.

3.3.1 Deposition precipitation-urea (DPU) method

In DPU method, calculated amount of metal precursor ($Co(NO_3)_2.6H_2O$ or $RuCl_3.3H_2O$) and urea were dissolved in de-ionized water (100 mL), then added dropwise to the functionalized carbon spheres (CSs) or titania support while stirring, depending on which catalyst was being prepared. The cobalt catalysts were calculated to give 10 % cobalt loading on CSs or titania supports. The ruthenium catalysts were calculated to give a 3% ruthenium loading on both supports. Each sample was then heated at 90 °C for 2 h to hydrolyze the urea, which allowed for the release of ammonia *in-situ*, while stirring under reflux. Each sample was left in an oil bath at 90 °C overnight to evaporate the water, while stirring. The left over water was then further removed by drying under vacuum at 90 °C for 40 minutes leaving slurry. The slurry was washed with deionized water four times. The slurry was then dried for 12 h in air at 120 °C in a static oven. The formed catalysts were then calcined at 250 °C under N_2 for 2.5 h for the CS supported catalysts and at 400 °C in air for 4 h for the Titania supported catalysts (Moyo, 2012; Kemball, C et al., 1981; Xiong et al., 2010).

3.3.2 Incipient wetness impregnation (IWI) method (conventional)

The IWI method is the traditional way of preparing a catalyst. The pore volume of each support was used to calculate the amount of deionized water required to fill the pores of the support. Calculated amounts of both metal precursors ($Co(NO_3)_2.6H_2O$ or $RuCl_3.3H_2O$) were dissolved in the calculated amount of deionized water and the resulting solution was added dropwise to fill the pores of the support. The resulting catalysts were then dried in a static oven for 12 h and further calcined as described in section 3.3.1 (Mgcima, 2012).

3.3.3 Incipient wetness impregnation (IWI) method (microwave)

The IWI method was also used to prepare catalysts using microwave irradiation as the heating method. The pore volume of each support, determined from BET results, was used to calculate the amount of deionized water required to fill the pores of the support. Calculated amounts of both metal precursors ($Co(NO_3)_2.6H_2O$ or $RuCl_3.3H_2O$) were dissolved in the calculated amount of deionized water and the resulting solution was added dropwise to fill the pores of the support. The resulting catalysts were irradiated using the Anton Paar Multiwave 3000 SOLV microwave at 500 W, a pressure rate 2.0 bar/s, with maximum pressure of 60 bar, infrared temperature of 240 °C, while stirring for approximately 30 min (Mgcima, 2012; Linganiso, 2008).

3.3.4 Polyol method (conventional)

In polyol method, calculated amount of the metal salt was added to 50 mL of ethylene glycol (EG) in a beaker, and 1 g of carbon spheres was added to EG in a separate beaker and both beakers were sonicated for 30 min. Each solution in the beaker was then stirred for 3 h. The metal precursor and ethylene glycol solution was then added dropwise to the support and ethylene glycol solution while stirring. The combined solution was refluxed at 195 °C for 3 h while stirring. The metal support mixture was then washed four times with deionized water then filtered and dried in a static oven for 12 h at 120 °C. The catalysts were then calcined under N_2 for 2.5 h at 250 ˚C (Fievet et al., 1989; Chieng and Loo, 2012).

3.3.5 Polyol method (microwave)

A calculated amount of the metal salt was added to 50 mL of ethylene glycol (EG) in a beaker, and 1 g of carbon spheres was added to EG in a separate beaker and both beakers were sonicated for 30 min. Each solution was stirred for 3 h, and then the metal precursor was added dropwise to the support and the ethylene glycol solution while stirring. The metal+support+EG solution was heated using the Anton PaarMultiwave 3000 SOLV microwave at 500 W, a pressure rate 2.0 bar/s, with maximum pressure of 60 bar, infrared temperature of 240 °C, while stirring for approximately 30 min. The resulting catalyst was

centrifuged, washed four times with deionized water, and then dried in a static oven for 12 h at 120 °C. The catalysts were then calcined under N_2 for 2.5 h at 250 ˚C (Tuval and Gedanken, 2007).

3.4 Catalyst characterization instruments

3.4.1 Thermal Gravimetric Analysis

Thermal Gravimetric Analysis (TGA) is a technique which is used to determine the thermal stability of a sample. The determination of thermal stability requires monitoring of the weight loss that occurs during heating at different temperatures. Metal loading onto to the carbon spheres was also confirmed using TGA. The TGA used to analyze samples for this research, was the Perkin Elmer Thermo-gravimetric Analyzer (TGA 4000), Figure 3.3. Approximately 0.01 g of sample was loaded onto a ceramic pan and analysis was done in air. Samples were analyzed in the temperature range from room temperature to 950 ˚C, at a heating rate of 10 ˚C/ min and a gas flow rate of 20 mL/min.

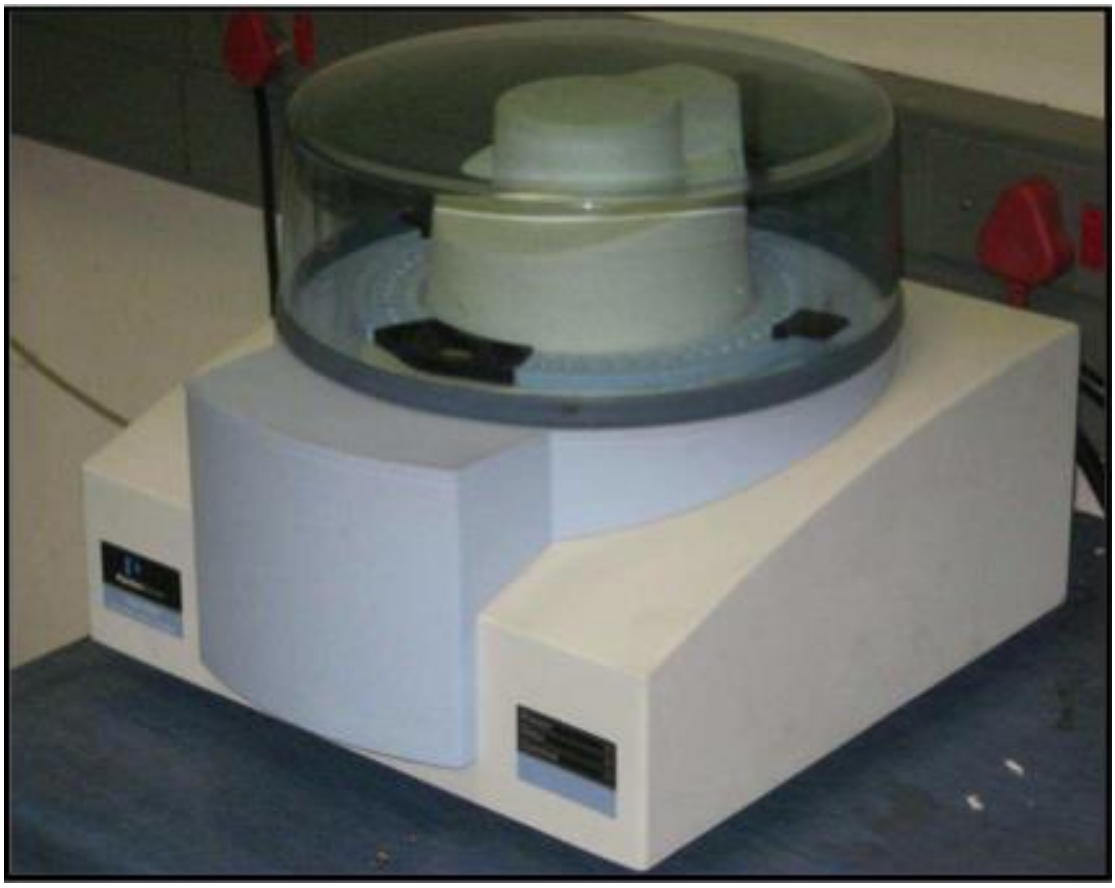

Figure 3.3: Image of Perkin Elmer thermo-gravimetric Analyzer 4000

3.4.2 Transmission electron microscope (TEM)

The FEI G^2 Spirit (Figure 3.4) at 120 kV was used to determine the morphology, particle size and dispersion of all catalyst samples. A small amount of each sample was ultrasonically suspended in methanol and a small drop of the suspension was transferred onto a SPI-carbon copper grid and allowed to dry prior to analysis under the microscope.



Figure 3.4: Image of FEI G2 Spirit TEM instrument

3.4.3 Brunauer Emmett Teller (BET) analysis

The ASAP-2000 Tristar analyzer from Micromeritics (Figure 3.5) was used to determine the surface area, pore volume and average pore diameter of all the catalysts. Approximately 0.20 g of sample was degassed under N_2 at 90 ˚C for 2 h and for a further 12 h at 200 ˚C prior to analysis using the Micromeritics Flow Prep 060, sample degassing system.



Figure 14.5: ASAP-2000 Tristar analyser (BET)

3.4.4 Temperature programmed reduction (TPR)

The Temperature Programmed Reduction (TPR) was the main characterization technique used in this study. The Micromeritics Autochem II TPR instrument (Figure 3.6) was used to determine the reduction temperature of the catalysts prior to application in Fischer Tropsch Synthesis. Approximately 0.2 g of sample was degassed, analysis was done under 5 % H_2 gas at a flow rate of 50 mL/min at 1 bar pressure, while the temperature was raised from room temperature to 800 ˚C at a heating rate of 10 ˚C/min.



Figure 3.6: Image of Micromeritics Autochem II TPR instrument

3.4.5 Raman spectroscopy

The quality of the graphitic nature of the carbon spheres was determined using a Jobin-Yvon T64 000 Raman spectrometer. The as-synthesized and purified carbon spheres were analyzed using this technique.

3.4.6 Powder x-ray diffraction

The phase composition of the titania and carbon spheres, including catalysts were determined by means of XRD analysis on the Brüker D2 Phaser X-ray diffractometer; a bench top diffractometer. The Brüker D2 Phaser X-ray diffractometer (Figure 3.7) operated at 30 kV and 10 mA current, in Bragg Brentano geometry with a Lynxeye detector using Cu-K_α radiation. The scan range was $5^\circ < 2\theta < 90^\circ$ in 0.040 steps using a

standard speed with an equivalent counting time of 1 second per step. The EVA (V11.0, rev. 0, 2005) software package was used to analyze the diffraction peaks, which were compared with those of standard compounds reported in the $Diffrac_{plus}$ evaluation package.

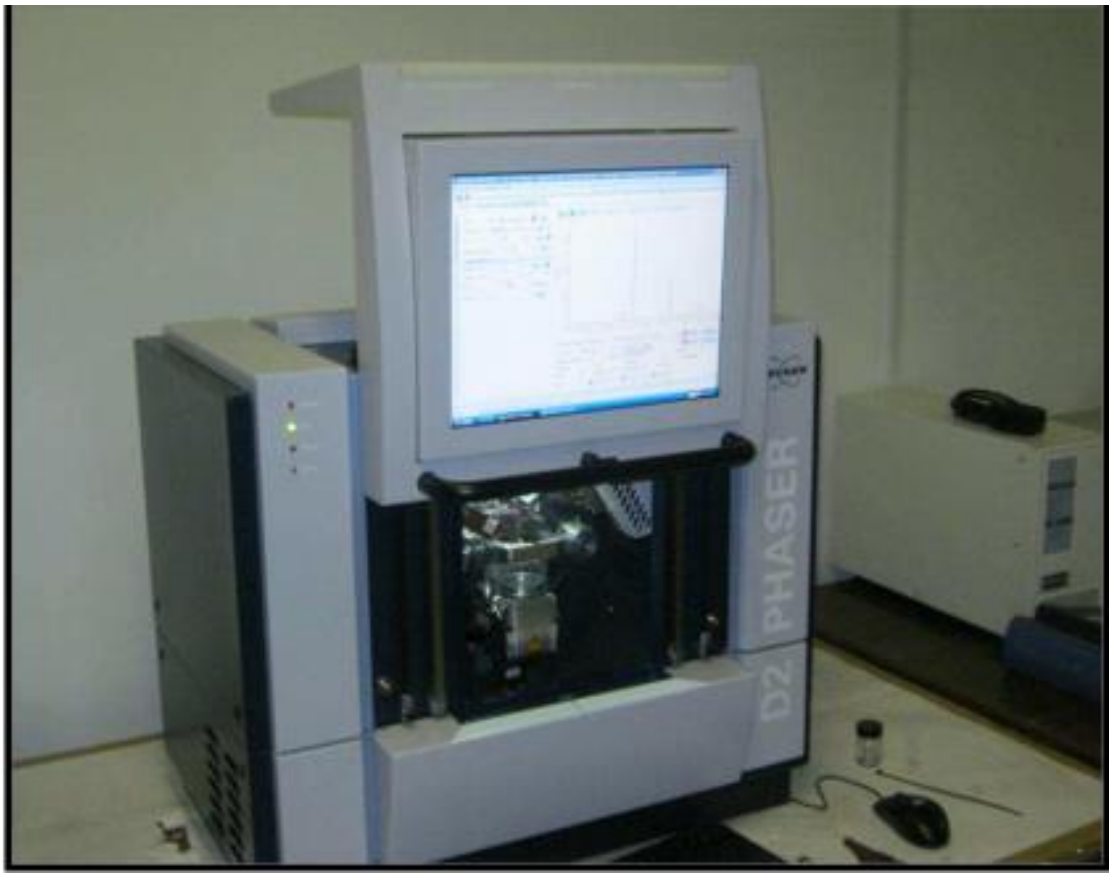

Figure 3.7: Brüker D2 Phaser X-ray diffractometer

3.5 Hydrogen spillover studies

Hydrogen spillover work was done using the TPR instrument, loading the catalyst beds into the TPR reactor is achieved as can be seen in Figure 3.8. The space was varied between the Co and Ru based catalyst beds to investigate the distance over which hydrogen spillover could occur, using different types of supports, but focusing on titania and carbon sphere supports.

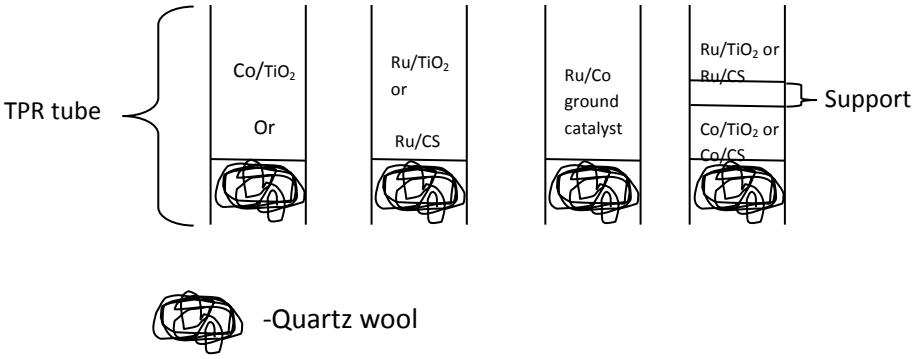

- Catalysts-10%Co/TiO_2,5%Co/CS, 3%Ru/TiO_2, 3%Ru/CS
- Ground catalyst-10%Co/$TiO_2$and 3%Ru/TiO_2, 5%Co/CS and 3%Ru/CScrushed using a pestle and mortar for 3 minutes and sieved at 150 µm
- Supports- TiO_2, Al_2O_3, CeO_2, ZnO and CS

Figure 3.8: Schematic diagram of the loading of stacked catalyst beds into the TPR sample holder

3.6 Reaction studies

All the prepared catalysts were evaluated in a fixed-bed micro reactor for the Fischer Tropsch Synthesis (FTS) reaction. FTS is a heterogeneous catalytic reaction that converts synthesis gas (Syngas), which is a mixture of CO and H_2, to predominantly hydrocarbons.

3.6.1 Gases

All the gases that were used for the Fischer Tropsch reactions were supplied by African Oxygen Limited (Afrox Ltd), the gas cylinders were accompanied by a certificate of analysis. For the reduction of the catalyst prior to FT synthesis, Ultra high purity (UHP) grade hydrogen gas (99.997%) was used and for the FT synthesis, syngas cylinders containing H_2/CO/N_2 mixtures (0.60/0.30/0.10 vol.; Purity 99.99%) were used as feed gas. Nitrogen gas was used as an internal standard to ensure accuracy in the mass balances and Ar gas was used as a carrier gas for the on-line gas chromatogram (GC).

3.7 Catalyst evaluation

3.7.1 Equipment setup

The setup of an FT rig consists of four major components: a fixed-bed micro reactor, the knockout pots, connecting lines and the GC's. Figure 3.9 shows the flow sheet diagram of the FT fixed-bed reactor system.

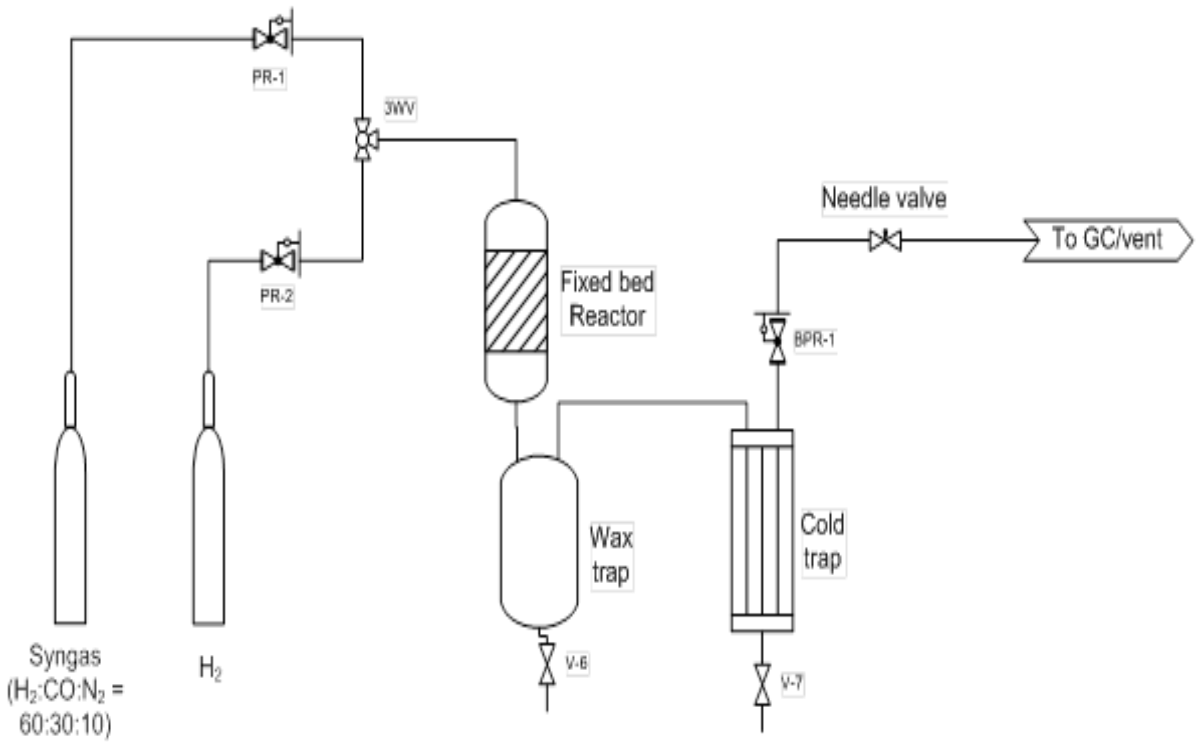

Figure 3.9: Flow sheet diagram of Fischer Tropsch rig set-up

Where: **PR-** Pressure regulator, **3WV-** Three way valves, **BPR**-Back pressure regulator, **V-6 and V-7**-Shut off valves.

The fixed bed reactor used was made out of stainless steel, which was connected to a thermocouple to control temperature in the reactor(in the catalyst chamber). Controlling of temperatures within the reactor, in the connection lines (temperatures kept at 100 °C) and the knockout pots were done using electronic temperature controllers and heating tape. The reactor was connected to the wax trap (also called the hot trap), which had its temperature set at 150 °C. The hot trap was connected in series with the cold trap, which was kept at ambient temperature; the cold trap was used to collect oil and water. The FT rig also included two gas chromatograms, connected in series. One used a Flame Ionization Detector (FID) and the other a Thermal Conductivity Detector (TCD), which analyzed the gaseous products.

In the Fischer Tropsch rig setup (Figure 3.9), the gas cylinders were connected to the fixed-bed reactor (FBR) using ⅛" stainless steel tubing and ¼" tubing, Swagelok Stainless steel fittings were connected from the reactor to the series knockout pots. The shut off valves used in the rig were SS Valco valves with Viton ® seals and the needle valves were Whitey valves. The pressure gauges were purchased from Wika. Data from both FI and TC detectors were captured using Clarity computer software. In Figure 3.10 a photograph of the FT rig used in this study is shown. A similar setup was used by Moyo (2012) and Motchelaho (2012).



Figure 3.10: Fischer Tropsch rig set-up with FID and TCD

3.7.2 Micro fixed bed reactor

The fixed bed micro-reactor (Figure 3.11) has three zones: 1) gas preheating zone, 2) catalyst chamber and 3) bottom of the reactor zone. In the gas-preheating zone, the syngas enters at 8 bars and is preheated. The catalyst chamber is where the catalyst is situated and the hydrocarbons produced. Lastly, the bottom of the reactor is where the hydrocarbons and unreacted gases collect and exit to the traps. Addition of steel balls above the catalyst, maintains a constant temperature within the reactor. The reactor is placed into a heating jacket, which is covered with fiberglass, to maintain a uniform temperature around the reactor. The heating of the reactor came from a heating element with a 700 W rating. The thermocouple is placed on the surface of the catalyst, to monitor the temperature of the catalyst as the reaction occurs.

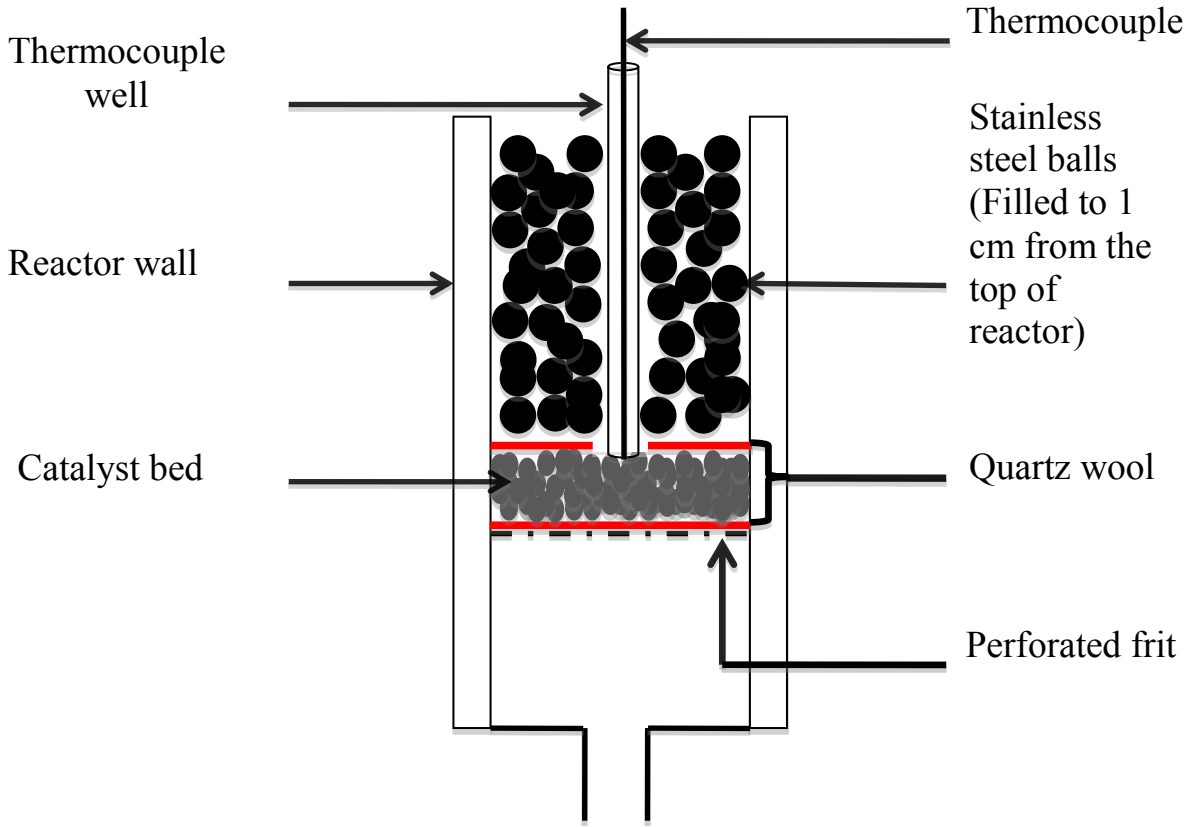

Figure 3.11: Schematic diagram of a Fischer Tropsch reactor

3.8 Experimental procedure for FT reactions

Catalysts supported on carbon, (0.5 g of catalyst) and supported on titania 1.0 g were used for FTS. All the catalysts were reduced using H_2 gas *in-situ* at a temperature of 350 °C and pressure of 2 bars for 16 h prior to reaction. The flow rate for the H_2 gas was maintained at 30 mL/min throughout the reduction step until the reactor had cooled to the reaction temperature.

The 3WV (Figure 3.9) was switched to allow H_2 to enter for the reduction step and after 16 h of reduction and cooling, the 3WV was switched to allow for syngas addition. The syngas pressure was set at 1 bar and analysis was done at room temperature so as to allow the determination of the composition of the syngas entering the reactor system. The

pressure of the syngas was then raised to 8 bar and the temperature was raised to 220 °C and maintained at that temperature throughout the FTS reaction. The flow rate of the syngas was dropped to 20 mL/min, to ensure a stable flow rate; while the flow rate of the tail gas was checked every morning and evening.

The gas pressure after the reactor was reduced to 1 bar, which was controlled by the back-pressure regulator BPR valve between the reactor and the GCs. All flow rates were measured using a stopwatch and a calibrated soap bubble flow meter. Each run was done for 120 h.

3.9 Gas chromatogram (GC) calibration

The GCs were calibrated using a specially prepared calibration gas mixture which was bought from AFROX Ltd. The composition of the gas was: CH_4 (2.5%), C_2H_4 (0.2%), C_2H_6 (0.5%), CO (10.0%), CO_2 (5.0%) and balance of Ar. A typical chromatograph is shown in Figure (3.11). After every FT run, the GCs were calibrated with syngas, which consists of H_2 (60%), N_2 (10%) and CO (30%), a typical syngas chromatograph is shown in Figure (3.12). The number of moles of that specific molecule passing through the detector was assumed to correspond to the peak area of each molecule detected by the detectors for the on-line analysis.

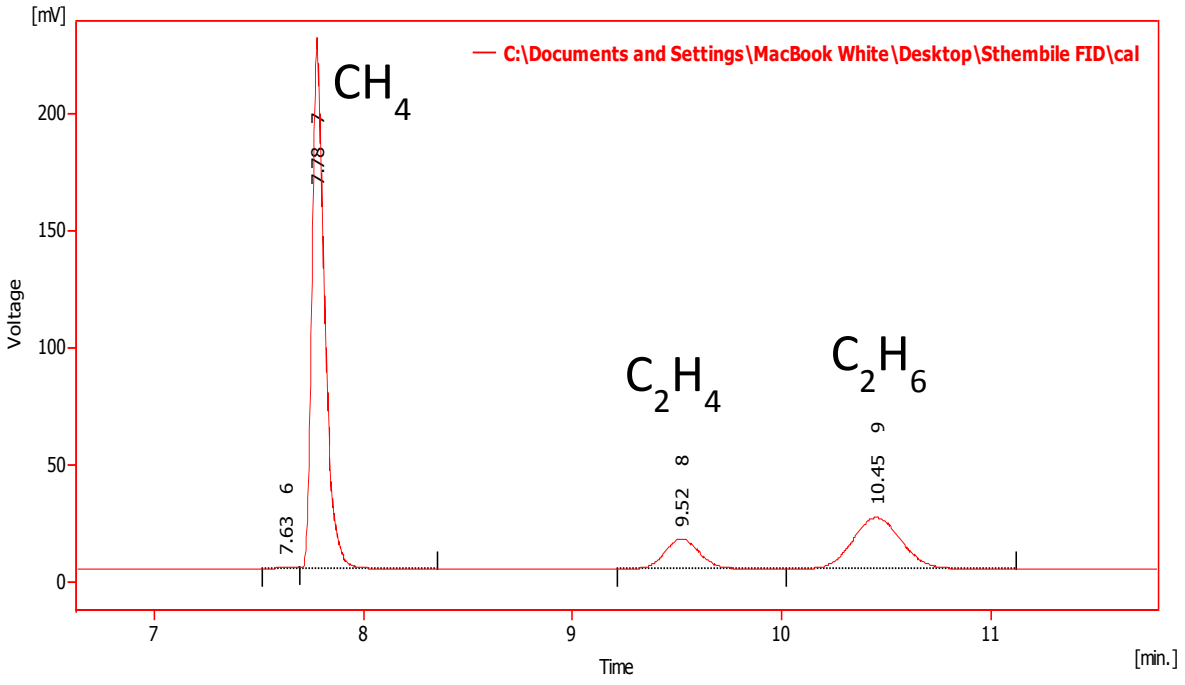

Figure 3.12: A chromatograph for the calibration gas using the GC-FID with nitrogen as the carrier gas

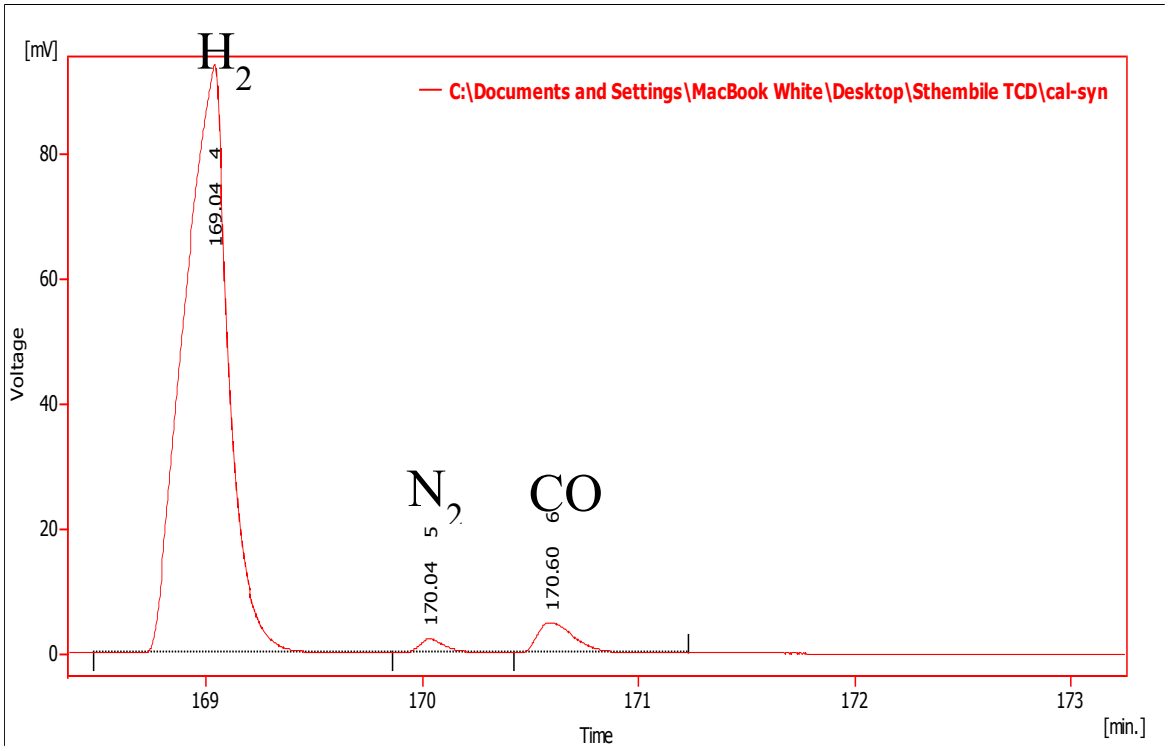

Figure 3.13: A chromatograph for the calibration gas using the GC-TCD with argon as the carrier gas

3.10 Product analysis

The analysis of the hydrocarbon spectrum was separated into two parts:

i. The online analysis comprises of two GCs with two detectors: the TCD and FID. These allowed for the analysis of the syngas, the N_2 internal standard, CO_2, methane, and the gaseous FT products. The GC-FID instrument was fitted with a Porapak Q packed column, while the GC-TCD instrument was fitted with a Carbosieve SII (1.50 m x 1/8 inch, stainless) packed column (Moyo, 2012).

ii. The offline analysis comprised of a GC-FID fitted with a capillary column, which was used for the analysis of the oil and wax FT products from the knockout traps.

3.11 Mass Balances

The mass balance calculations used in this work are similar to those used by Duvenhage (1994), Price (1994), and Mokoena (2005) , these calculations were performed on carbon and oxygen. The outlet flow rate was measured twice daily in the mornings and evenings using a soap flow meter at ambient pressure and temperature. The equation given below was used to calculate the feed flow rate (Duvenhage, 1994; Price, 1994).

$$F_{in} = \left[\frac{X_{N2,In}}{X_{N2,Out}}\right] \times F_{Out} \qquad (3.1)$$

where: -

F_{in} = the total feed flow rate in mol/s

F_{out} = the reactor exit stream flow rate in mol/s

$X_{N2,\,in}$= the mole fraction of N_2 in the feed (syngas)

$X_{N2,\,out}$= the mole fraction of the N_2 in the reactor exit stream

The number of moles of carbon in the feed stream in the total mass balance period was calculated by:

$$N_{c,in} = F_{in}.t.X_{co,in} \quad (3.2)$$

where: -

$N_{c,in}$ = the number of moles of carbon in the feed

F_{in} = the total feed flow rate in mol/s

t = the total mass balance time

$X_{CO,\ in}$ = the mole fraction of CO in the feed gas

A premixed gas of known composition consisting of: CH_4, C_2H_6, C_2H_4, CO, CO_2 and the balance Ar was used for their calibrations. The number of moles of each of the components present in the gas phase was calculated using the following equation:

$$N_{C,out} = \left[\frac{A_C}{A_{C,cal}}\right].X_{C,cal}.F_{out}.t \quad (3.3)$$

where: -

A_C = the integrated peak area for component c,

A_C, cal = the peak area for the component c in the calibration gas

$X_{C,\ cal}$ = the mole fraction of component c in the calibration gas

Hydrocarbon product areas were corrected for C_2H_4 (olefins) and C_2H_6 (paraffins) by using the response factors based on those presented by Dietz (1967) (see Table 3.1). The mole fractions of the hydrocarbons $X_{HC,i}$ were calculated using the following equation:

$$X_{HC,i} = \frac{RF_i.A_{HC,i}}{A_{C_2,cal}}.X_{C_2,cal} \quad (3.4)$$

where: -

RF_i = the response factor for carbon number *i*

$A_{HC,\,i}$ = the integrated peak are for a hydrocarbon with carbon number

$A_{C_2,}$ cal = the peak area of the C_2 in the calibration gas

X_{C_2}, cal = the mole fraction of the C_2 hydrocarbon in the calibration gas

Calculation of the mole fractions of the individual hydrocarbons with *i* number of carbons from the oil and wax were done in the same way and added to the gas fraction. Mass response factors of the carbon numbers greater than 15 were assumed to be 1.00. The mass fractions of the hydrocarbons with $i > 15$ were therefore determined directly from the GC integrated area using the equation below:

$$m_i = \frac{A_{HC,i}}{\sum A_{HC,i}} \qquad (3.5)$$

where: -

$A_{HC,\,i}$ = the integrated peaks area of hydrocarbon *i*

$\sum A_{HC,I}$ = the sum of the integrated peak area of all hydrocarbons analyzed in oil and wax fraction.

Table 3.1: Molar response factors for hydrocarbons(Dietz 1967)

Carbon Number	Olefin	Paraffin
1	-	1.00
2	1.00	1.00
3	0.70	0.74
4	0.78	0.55
5	0.47	0.47
6	0.40	0.40
7	0.35	0.35
8	0.32	0.32
9	0.28	0.28
10	0.24	0.24
11	0.21	0.21
12	0.19	0.19
13	0.18	0.18
14	0.17	0.17
15	0.15	0.15

The calculation for the % CO conversion was done as follows (Moyo, 2012; Linganiso, 2008; Duvenhage, 1994; Price, 1994; Mokoena, 2005)

$$\%CO_{conversion} = \frac{X_{CO,in} - X_{CO,out} \cdot \frac{X_{N_2,in}}{X_{N_2,out}}}{X_{CO,out}} \qquad (3.6)$$

where:

$X_{co,\ in}$ = CO molar fraction in the reactor feed

$X_{co,\ out}$ = CO molar fraction in the outlet gas

$\frac{X_{N_{2,co}}}{X_{N_{2,out}}}$= Gas contraction factor

Product selectivity for hydrocarbons S_i was calculated for component x_i as follows:

$$S_i = \left[\frac{X_i}{r_{CO.}t}\right] \times 100\% \quad (3.7)$$

X_i= moles of hydrocarbon containing *i* carbon atoms

r_{CO}= rate of conversion of CO

t = mass balance time

Rates of reaction for Fischer Tropsch synthesis and the water gas shift reaction were calculated as follows:

$$r_{WGS} = r_{CO_2} \quad (3.8)$$

$$r_{FTS} = r_{CO} - r_{CO_2} \quad (3.9)$$

where: -

r_{CO_2}= the rate of CO_2 formation

r_{CO} = the rate of CO conversion

Olefin to Paraffin ratio was calculated as follows:

$$\text{Olefin to paraffin } i = \frac{N_i^{=}}{N_i^{=} + N_i^{-}} \quad (4.0)$$

$N_i^{=}$= moles of olefin containing *i* carbon atoms

N_i^{-} = moles of paraffin containing *i* carbon atoms

Carbon and oxygen mass balances were determined using information obtained from the above calculations:

$$\%Mole\ balance = 100 \times \left[\frac{TotalC_{out}}{TotalC_{in}}\right] \quad (4.1)$$

where:

C_{in}= moles of carbon that enter reactor

C_{out}= moles of carbon that exit reactor

A mass balance data of ± 5 % error was accepted as adequate.

References

Chieng, B.W. and Loo, Y.Y., 2012. Synthesis of ZnO nanoparticles by modified polyol method. *Materials Letters*, *73*, pp.78-82.

Dietz, W.A. (1967) 'Response factors for gas chromatographic analyses', *Journal of Chromatographic Science*, Vol.5 Issue2, pp. 68–71.

Duvenhage, D.J., 1994. *The preparation, characterization and evaluation of titania supported Fe: Co bimetallic catalysts for the hydrogenation of CO* (Doctoral dissertation, PhD Thesis, University of the Witwatersrand, Johannesburg).

Fievet, F., Lagier, J.P., Blin, B., Beaudoin, B. and Figlarz, M., 1989. Homogeneous and heterogeneous nucleations in the polyol process for the preparation of micron and submicron size metal particles. *Solid State Ionics*, *32*, pp.198-205.

Kemball, C., Dowden, D.A., Acres, G.J.K., Bird, A.J., Jenkins, J.W. and King, F., 1981. The design and preparation of supported catalysts. In *Catalysis* (pp. 1-30).

Linganiso, L.Z., 2010. *Microwave induced solid-state interactions for the synthesis of Fischer-Tropsch catalysts* (Doctoral dissertation, University of the Witwatersrand, Johannesburg).

Mgcima, Z., 2012. *The purification of the polymer membrane fuel cell (PEMFC) reformate as by the methanation reaction with the use of platinum group metals (PGMs) on TiO2 support* (Doctoral dissertation, University of the Witwatersrand, Johannesburg).

Mokoena, E.M., 2006. *Synthesis and use of silica materials as supports for the Fischer-Tropsch reaction* (Doctoral dissertation, University of the Witwatersrand, Johannesburg).

Motchelaho, A.M.M., 2012. *Iron and cobalt catalysts supported on carbon nanotubes for use in the Fischer-Tropsch synthesis* (Doctoral dissertation, University of the Witwatersrand, Johannesburg).

Moyo, M., 2012. *Cobalt and iron supported on carbon spheres catalysts for Fischer Tropsch synthesis* (Doctoral dissertation, University of the Witwatersrand, Johannesburg).

Price, J.G., 1994. An investigation into novel bimetallic catalysts for use in the Fischer-Tropsch reaction. (Doctoral dissertation, University of the Witwatersrand, Johannesburg).

Tuval, T. and Gedanken, A. (2007) 'A microwave-assisted polyol method for the deposition of silver nanoparticles on silica spheres',*Nanotechnology*, 18(25), p. 255601.

Xiong, H., Moyo, M., Motchelaho, M.A.M., Jewell, L.L. and Coville, N.J. (2010) 'Fischer–Tropsch synthesis over model iron catalysts supported on carbon spheres: The effect of iron precursor, support pretreatment, catalyst preparation method and promoters', *Applied Catalysis A: General*, 388(1-2), pp. 168–178.

CHAPTER 4

EVALUATION OF COBALT AND RUTHENIUM SUPPORTED ON TITANIA AS CATALYSTS IN FISCHER TROPSCH SYNTHESIS

This chapter presents and discusses results obtained in Fischer Tropsch (FT) synthesis using cobalt (Co) and ruthenium (Ru) supported on titania. Characterization of the Co and Ru catalysts are presented first, and then the TPR study followed by catalyst testing under FT process conditions. The effect of the titania support in hydrogen spillover is also presented.

4.1 Characterization

4.1.1 Scanning electron microscopy and energy dispersive X-ray studies

The imaging studies of the catalysts were carried and the data are depicted in Figure 4.1. Figure 4.1a) shows a SEM image of the 10%Co/TiO_2catalyst which shows small particles of CoO (white spots) well dispersed on the big particles of titania. An EDX spectrum confirmed the presence of Co and titania in the sample. Quantification of the Co on the 10%Co/TiO_2 catalyst using EDX, showed that 11.27 wt% of cobalt was present in the sample and 88.73% titania. This confirms that ~10% loading of cobalt had been achieved. In Figure 4.1b) the SEM image of 3% Ru/TiO_2 shows small white particles on the rough surface of the titania support (dark grey). The RuO particles on the SEM proved to be difficult to detect quantitatively, due to the low loading of the Ru. However, EDX results confirmed the presence of Ru as well as titania in the sample.

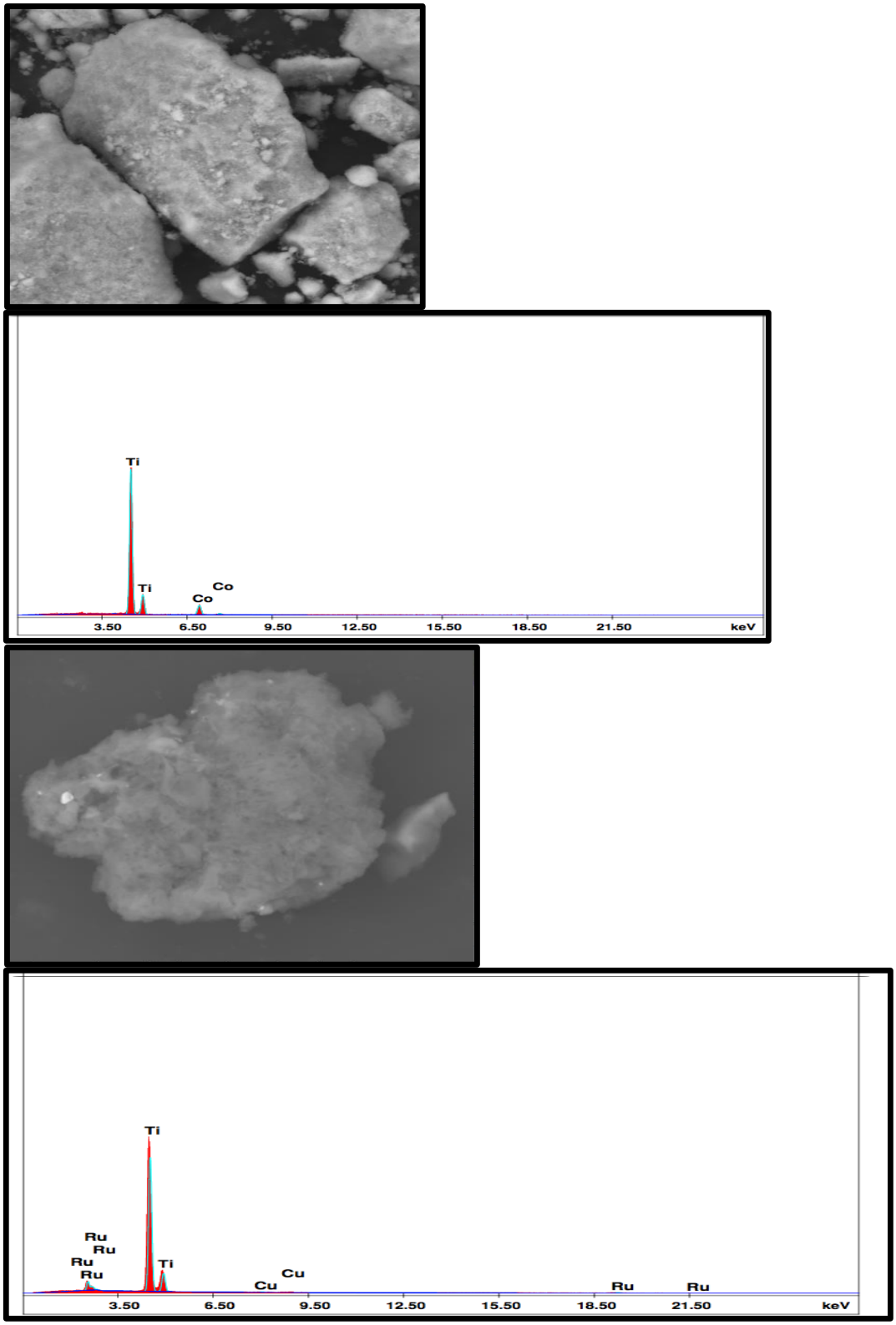

Figure 4.1: SEM images and EDX spectra of a) 10%Co/TiO2 and b) 3%Ru/TiO2 catalysts.

4.1.2 TEM and EDX

TEM images for both the Co and Ru catalysts supported on titania are shown Figure 4.2. Differentiating the titania and metal phase from both the ruthenium and cobalt proved to be difficult using low-resolution TEM. However, EDX that was recorded using the TEM images confirmed the presence of the metal phases on both catalysts, and the weight % for Co was found to be 11.5% and 3.4% for Ru.

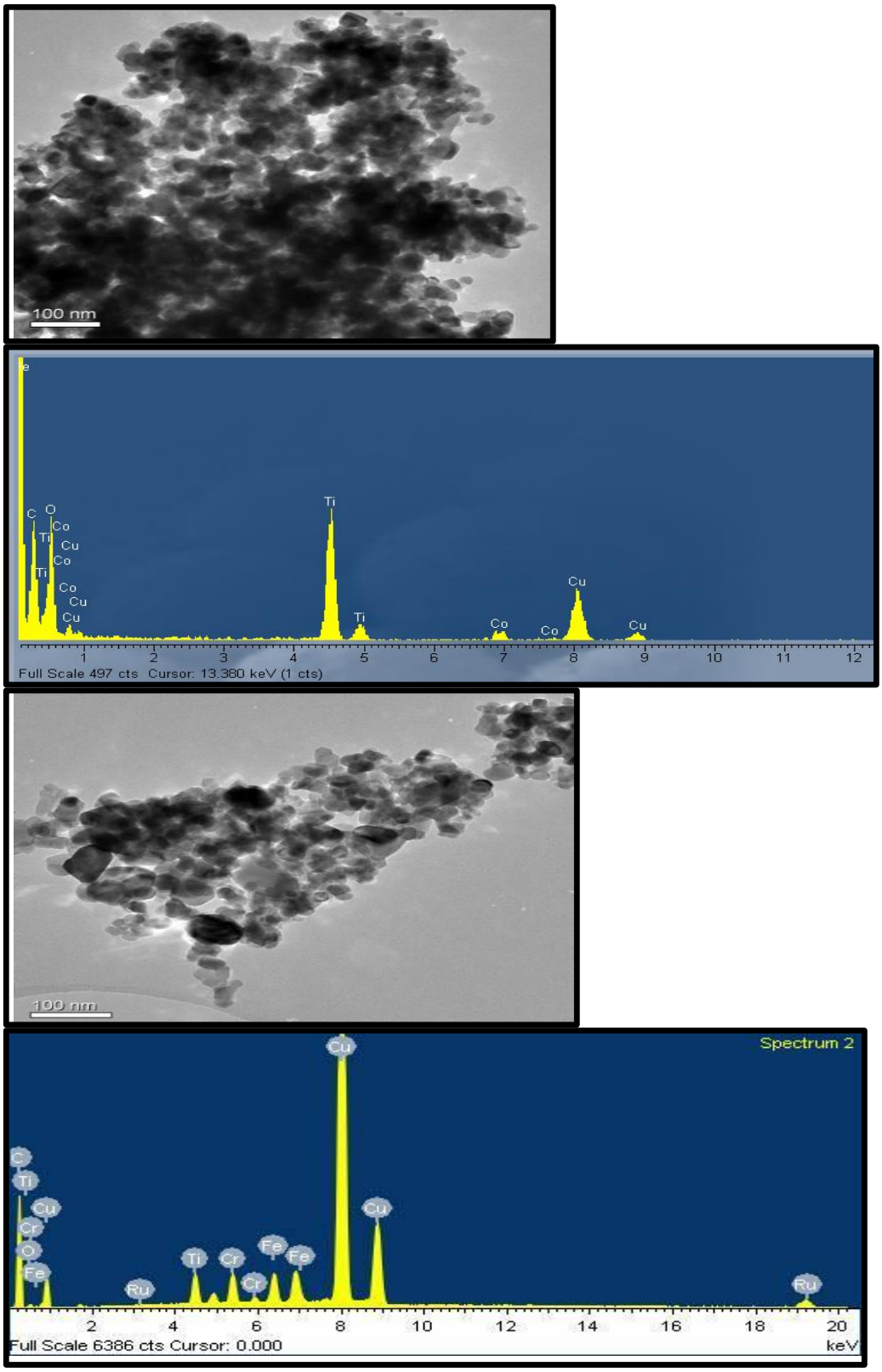

Figure 4.2: TEM images of a) 10%Co/TiO_2 and b) EDX of 10%Co/TiO_2 c) TEM image of 3%Ru/TiO_2, and d) EDX of 3% Ru/TiO_2.

4.1.3 XRD

The PXRD patterns for both 10%Co/TiO_2 and 3%Ru/TiO_2 are displayed in Figure 4.3. The PXRD pattern showed the presence of both the rutile and anatase phases of the titania. The rutile peaks are exhibited at 28°, 36° and 55°, whereas the anatase phase is seen at 26°, 56° and 70°. The cobalt oxide observed in the XRD pattern corresponded to Co_3O_4. The peaks for Co_3O_4 (*) were seen at 28°, 38° and 64°. The peaks for RuO_2 (#) were seen at 27°, and 36°. The RuO_2 peaks were indexed to be RuO_2 (110) and RuO_2 (101) planes (Mgcima, 2012). Due to the overlap of the RuO_2 and Co_3O_4 peaks, as well as the large relative size of the most intense peak, it proved to be difficult to measure the size of the particles of the oxides using the Scherrer equation.

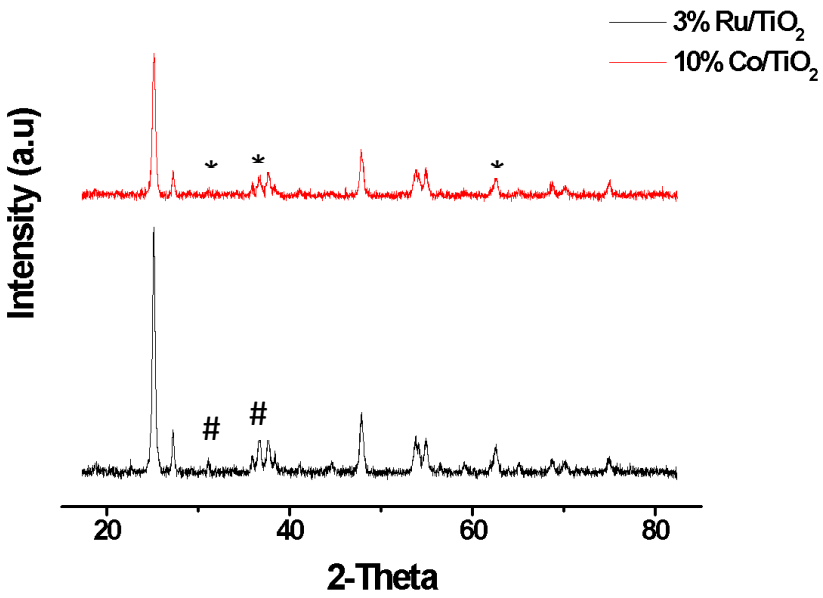

Figure 4.3: XRD pattern of 3% Ru/TiO_2 and 10% Co/TiO_2 (*-Co_3O_4 and #-RuO_2)

4.1.4 BET

The general trend for the surface area shows a decrease for both the ruthenium and cobalt catalysts relative to the pure support (Table 4.1). This decrease was expected, as the support was loaded with metal. As can be seen in Table 4.1, the pore volume of the

catalysts shows an increase in volume relative to titania because of the small pores of the titania are covered by the metal oxide.

Table 4.1: Porosity measurements of catalysts

Samples	Surface Area (m^2/g)	Pore Volume (m^3/g)
Titania (P-25 Degussa)	48.0	0.42
10%Co/TiO_2	46.3	0.21
3%Ru/TiO_2	44.0	0.31

4.1.5 H_2-TPR studies

TPR results revealed that in the 10% Co/TiO_2 catalyst, the first reduction step occurs at 325°C where Co_3O_4 is reduced to CoO, and the second peak occurs at 500°C, where CoO is reduced to metallic cobalt as seen on Figure 4.4. The 3% Ru/TiO_2 catalyst profile showed a sharp peak at 150°C, which was attributed to the reduction of RuO to metallic ruthenium. A small shoulder was observed at 200°C, this was explained to be due to the Ru forming a complex with TiO_2, known as strong metal support interaction (SMSI). This interaction was a result of the oxygen of titania forming a bond with the Ru. The TPR profile for the bimetallic catalyst of the 3% Ru and 10% Co supported on titania showed a shift to a lower temperature of 450°C at the peak where CoO is reduced to metallic cobalt. This was an indication that intimate interaction of Ru and Co resulted in the Co being reduced at lower temperatures. The Ru acts as electronic promoter, by changing the electronic environment of cobalt. Reduction of cobalt at 450 °C was also attributed to hydrogen spillover, because noble metals are known to be easily reduced to metallic state

at much lower temperatures then cobalt oxide. At their metallic state, the noble metal, Ru in this case facilitated the dissociation and activation of hydrogen and thus enhanced the whole cobalt reduction process.

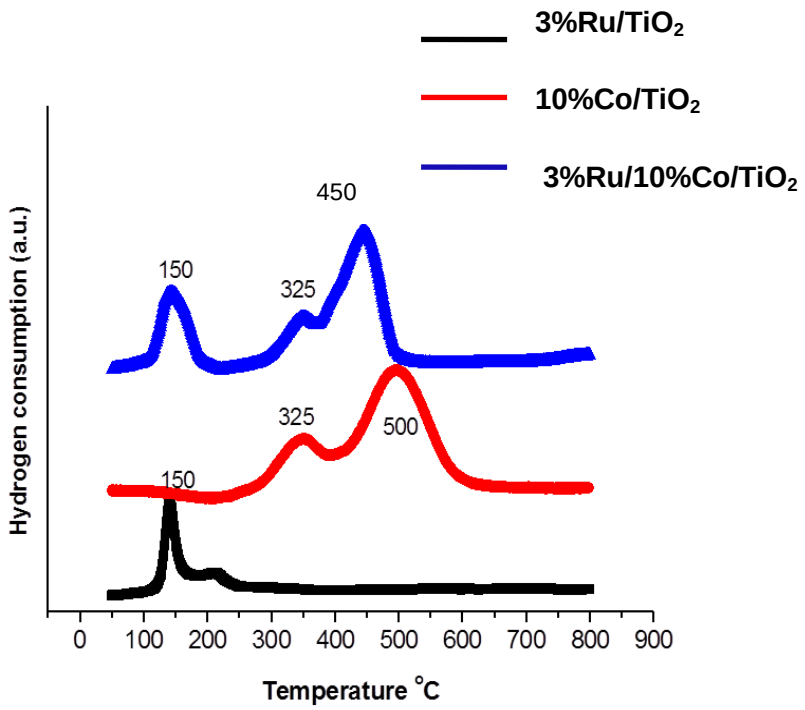

Figure 4.415: TPR profiles of black-3% Ru/TiO2; Red-10% Co/TiO2 and blue-bimetallic catalyst.

The TPR profile of the hybrid catalyst which was the ground mixture of the 3%Ru/TiO_2 and the 10%Co/TiO_2 shown in Figure 4.5, exhibits the reduction of Co_3O_4 to metallic cobalt, at 326 and 455 °C. The reduction of RuO_2 to Ru occurred at 156 °C. These reduction temperature results for both Co_3O_4 and RuO_2 are similar to those observed in Figure 4.3 above. This shows that in the hybrid catalyst, there was an intimate interaction between Co and Ru, resulting in the reduction of Co_3O_4 occurring at lower temperatures than the monometallic Co catalyst.

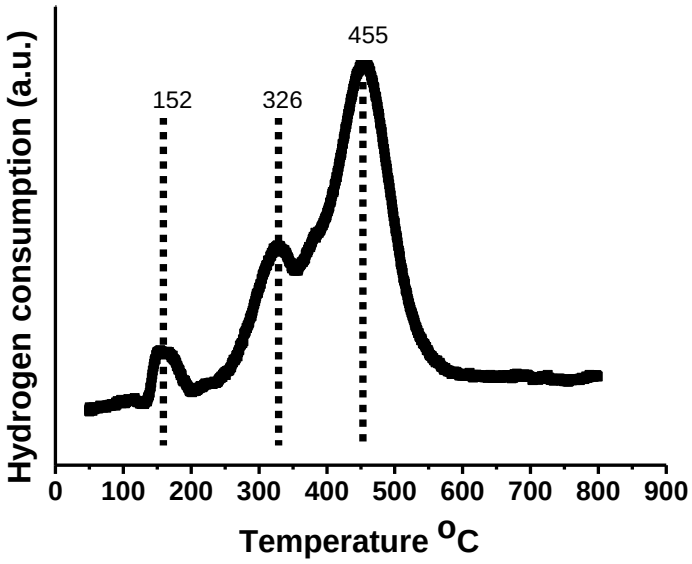

Figure 4.5: TPR profile of hybrid catalyst (Ground mixture).

The 10%Co/TiO_2 and 3%Ru/TiO_2catalysts were then loaded onto the TPR U-shaped reactor and separated by Degussa TiO_2.The TPR profiles were as follows:

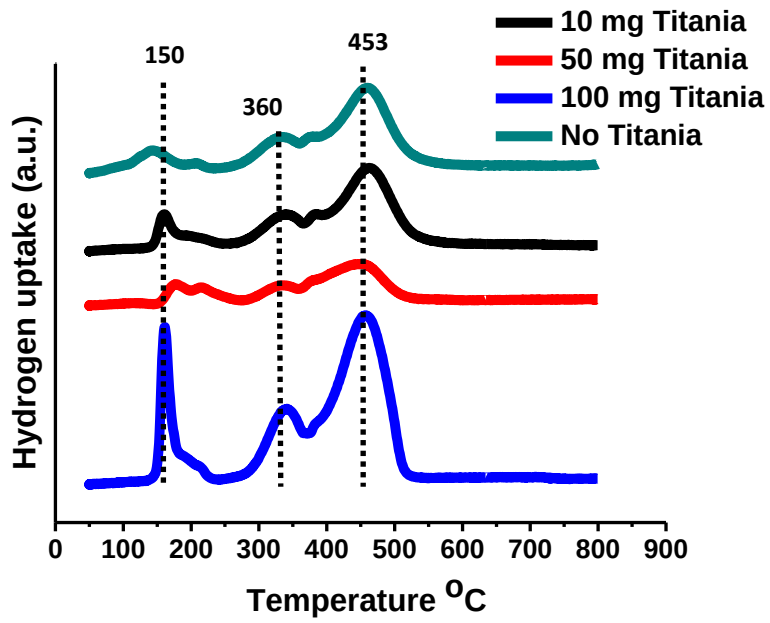

Figure 4.6: TPR profiles of 3% Ru/TiO2 and 10% Co/TiO2 separated by different amounts of Titania.

The TPR profiles in Figure 4.4 showed a reduction in temperature of the second cobalt peak which originally occurred at 500°C, where CoO is reduced to metallic cobalt to 453 °C. However, there was no shift in temperature for the first cobalt peak; at 325 °C for all profiles except the 5mm titania separated catalysts in Figure4.6 and Table 2. However a small peak was observed at 360 °Cthis could be due to some complex formation of cobalt and titania ($CoTiO_3$). Even though the distance was varied using TiO_2 as a separating bed, no difference was observed from 1 cm to 2 mm for the TiO_2 used with respect to shifting of peaks to lower temperatures when the distance between the two catalysts was reduced (1 cm to 2 mm). No titanates were observed at higher temperatures above 453 °C, as expected.

Table 4.2: Peak reduction temperatures from TPR profiles with TiO_2

Distance of separating bed /TiO_2	**Peak 1(°C)** **Ru^{2+} to Ru^0**	**Peak 2(°C)** **Co^{3+} to Co^{2+}**	**Peak 3(°C)** **Co^{2+} to Co^0.**
1 cm (100mg)	150	325	453
5mm (50 mg)	153	325	453
2 mm (10 mg)	150	325	453
0 mm	148	325	453

Other oxides were tested to see if they showed any greater improvement compared to titania incorporated triple bed systems. CeO_2, ZrO_2andAl_2O_3were chosen as separating beds to separate 10%Co/TiO_2 and 3%Ru/TiO_2. The results obtained are shown below:

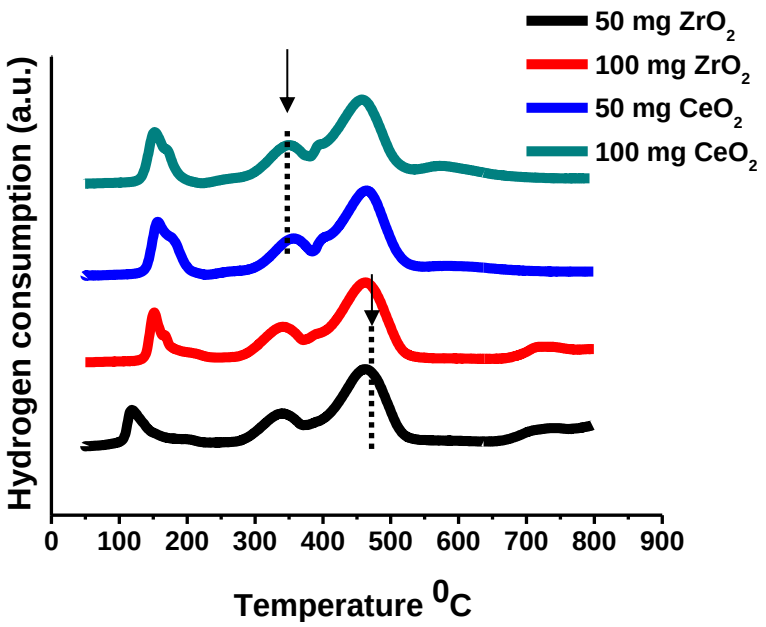

Figure 4.7: TPR profiles of 3% Ru/TiO2 and 10% Co/TiO2 separated by different amounts of oxides

The $Ru/TiO_2//CeO_2//Co/TiO_2$ system shows the Co and Ru peaks appear at the same temperature as found in the titania system. A new peak was observed at 569°C, this was ascribed to be the reduction of surface and bulk ceria crystallites.

For the system of $Ru/TiO_2//ZrO_2//Co/TiO_2$ beds, the Ru and Co peaks appear at the same temperature region as found for the CeO_2. However, an additional peak was observed at 720 °C. According to Hoang *et. al.* pure ZrO_2does not show any consumption of hydrogen in the TPR profile, however upon addition of noble metals supported on ZrO_2, a peak was observed at a higher temperature of 550 °C. The same explanation could be given to this system $Ru/TiO_2//ZrO_2//Co/TiO_2$, where a broad peak was observed at 720 °C. The peak must be connected to the presence of the cobalt or ruthenium, but the reduced cobalt and ruthenium can be ruled out as hydrogen consumers at this temperature. Therefore this peak

at 720 °C can be assigned to the hydrogen consumption of ZrO_2 mediated by the cobalt or ruthenium metals. Noble metals have shown to activate hydrogen, with spillover to the surface of the support, such as zirconium dioxide, at temperatures of 550 °C. We therefore assume that this peak is due to hydrogen spillover.

Table 4.3: Peak reduction temperatures from TPR profiles with CeO_2

Salt	**Distance of separating bed**	**Peak 1(°C)** Ru^{2+} **to** Ru^0	**Peak 2(°C)** Co^{3+} **to** Co^{2+}	**Peak 3(°C)** Co^{2+} **to** Co^0**.**	**Peak 4 (°C)** Ce^{2+} **to** Ce^0
CeO_2	100 mg	150	354	468	569
CeO_2	50 mg	151	355	469	564
ZrO_2	100 mg	125	353	469	725
ZrO_2	50 mg	150	353	469	725

The alumina system exhibited three peaks, as seen in Figure 4.8. The first was attributed to the reduction of RuO_2 to Ru, as found in the previous TPR profiles for cerium oxide, titania and zirconium dioxide. A broad shoulder peak was observed between 200 and 300 °C, and this was ascribed to be Ru forming a complex with TiO_2, as mentioned above. The other two peaks were due to the two step reduction of cobalt, as previously mentioned. However, the two reduction peaks for Co_3O_4 are shown to have shifted to higher temperatures of 360 and 590 °C respectively, this shift is ascribed to the interaction of cobalt with the alumina support, which results in both peaksoccurring at higher temperatures. Both H_2-TPR profiles after addition of 50 and 100 mg alumina to 10% Co/TiO_2 and the 3% Ru/TiO_2did not show any differences (see Table 3).

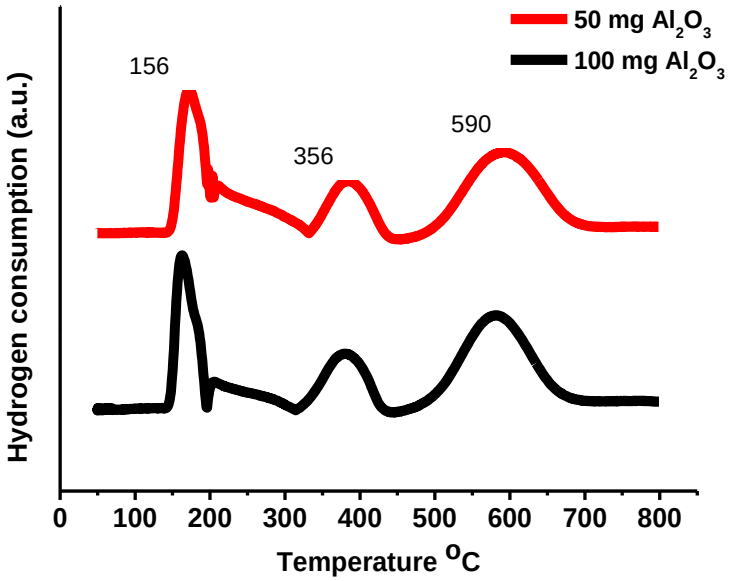

Figure 4.8: TPR profiles of 3% Ru/TiO2 and 10% Co/TiO2 separated by alumina.

Table 4.4: Peak reduction temperatures from TPR profiles with Al_2O_3

Distance of separating bed/Al_2O_3	**Peak 1(°C)** **Ru^{2+} to Ru^0**	**Peak 2(°C)** **Co^{3+} to Co^{2+}**	**Peak 3(°C)** **Co^{2+} to Co^0**
100 mg	156	356	590
50 mg	156	354	594

4.3 Catalyst testing

The percentage CO conversion was determined as a function of time on stream for 120 h of reaction. The results are shown in Figure 4.9 a) for 10% Co/TiO_2, b) for a ground mixture of 50/50 wt% of 3% Ru/TiO_2 and 10% Co/TiO_2 and **c**) for 3% Ru/TiO_2. Figure 4.9 shows that the 3% Ru/TiO_2 catalyst has the highest activity for CO conversion over 120 h; the conversion decreased slightly over this period. The Ru promoted catalyst gave the highest conversion of about 40%. However when 3% Ru/TiO_2 and 10% Co/TiO_2 were mixed

(Figure 4.9b), the activity dropped by 50%. After 50 h of time on stream, the CO conversion decreased further, to below the activity of 10% Co/TiO_2. The 10% loaded cobalt catalyst proved to be stable compared to the 3% Ru and the ground mixture. The hybrid (mixture of Ru and Co) was prone to deactivation at high conversion (25% to 12% in 50 h) and showed some stability at conversions around 10%. The 3% Ru/TiO_2 catalyst exhibited a high CO conversion activity compared to the un-promoted cobalt catalyst supported on titania. The results agree with previous findings (Iglesia, 1992; Ma et al., 2013).

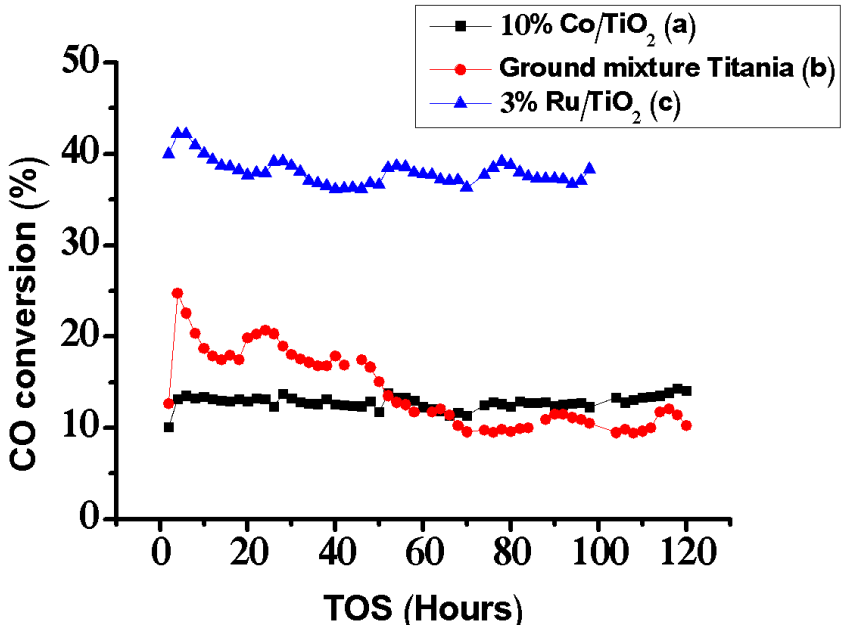

Figure 4.9: Conversion of the catalysts over 120 hours on stream a) 3% Ru/TiO_2 b) 10% Co/TiO_2 and c) Ground mixture of 3%Ru/TiO_2 and 10%Co/TiO_2

However, the ground mixture of the 10% Co/TiO_2 and the 3% Ru/TiO_2 led to an initial increase of the CO conversion relative to 10% Co/TiO_2, but this value dropped after 50 h. This decrease in the CO conversion could be due to a lack of synergism between the cobalt and ruthenium particles because the formed ground mixture was a "hybrid" catalyst, and not a bimetallic catalyst. The CO conversion for the 3% Ru/TiO_2 had the highest conversion (approximately 40 %) out of all three catalysts supported on titania, which is in agreement with work done by Carballo et al. (Carballo et al., 2011). Chloride is a known

poison Fischer Tropsch catalysis (Ma et al., 2013) and it was anticipated that the chloride ions weer removed from the FT catalyst prior to use. Indeed, in this study even though the 3% Ru/TiO_2 was prepared with a ruthenium chloride solution, the catalyst still showed the best CO conversion when compared to other catalysts (Co/TiO_2 and 3% Ru/TiO_2 and 10% Co/TiO_2).

4.4 Product selectivity

The selectivity to hydrocarbons was determined for the titania supported catalysts and plotted against the carbon number. The results are depicted in Figure 4.10 a) for 3% Ru/TiO_2, b) for 10% Co/TiO_2 and c) ground mixture (3% Ru/TiO_2 and 10% Co/TiO_2).

Figure 4.10 showed the selectivity of the three titania supported catalysts. The 3% Ru/TiO_2 catalyst gave a relatively high 20% methane selectivity, a low percentage of gaseous products and a selectivity to 70% C_{5+} hydrocarbons. The high methane selectivity could be ascribed to the small metal particles. The 10% Co/TiO_2 catalyst gave a slightly lower methane selectivity (<20%), while the selectivity for gaseous products was around 10%, but similar to that for 3% Ru/TiO_2. The C_{5+} selectivity was high (>0%). The FTS data for the ground mixture gave a very high methane selectivity (35%), and there was a drop in C_{5+} selectivity compared to the monometallic catalysts. There was an expectation that the C_{5+} selectivity would increase relative to the monometallic Co catalyst, and the methane selectivity would drop, but this was not case. The reason as to why this occurred is unknown. However, the decrease in the performance of this catalyst was suspected to be due to the presence of residual Cl^- ions from the Ru precursor used. According to Bartholomew et al. chloride is a severe poison and enhances methane production and FT synthesis when chloride ions are not all removed by calcination. The presence of chloride ions could thus interact with a large fraction of the reduced cobalt sites which would result in a reduction in FT activity (Bartholomew, 1991). Bakar et al. (2015) also mentioned that the presence of residual chloride ions formeds a partition between the support and metal, which resulted in the inhibition of both CO and hydrogen chemisorption phenomena on the catalyst surface (Bakar et al., 2015).

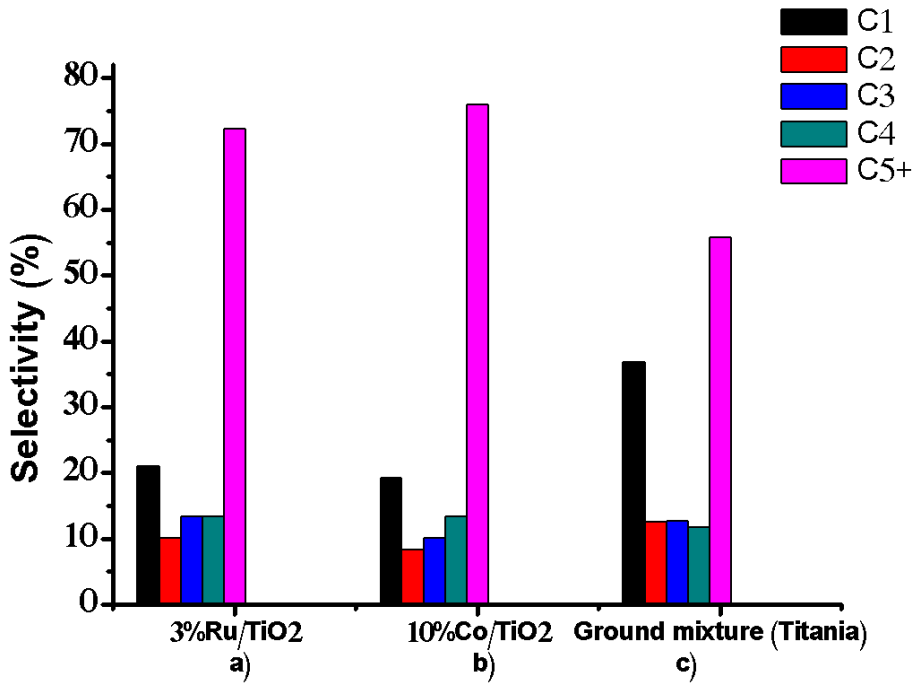

Figure 4.10: Selectivity of the catalysts over 120 hours on stream a) 3% Ru/TiO2, and b) 10% Co/TiO2 c) Ground mixture (3%Ru/TiO2 and 10%Co/TiO2)

4.5 Olefin to paraffin ratio

The olefin to paraffin ratio data was plotted against the light hydrocarbons (C_2 to C_5). Figure 4.6 shows the gas phase olefin to paraffin ratio of the titania supported catalysts. The cobalt catalyst with low FT activity, gave a higher olefin than paraffin ratio than the 3%Ru/TiO_2, which has a relatively high FT activity, but gives a low olefin content in the product. The same was observed for the ground mixture, and intermediate to low FT activity was seen in Figure 4.4. The olefin/paraffin ratio lay between that of the 3% Ru/TiO_2 and the 10% Co/TiO_2.

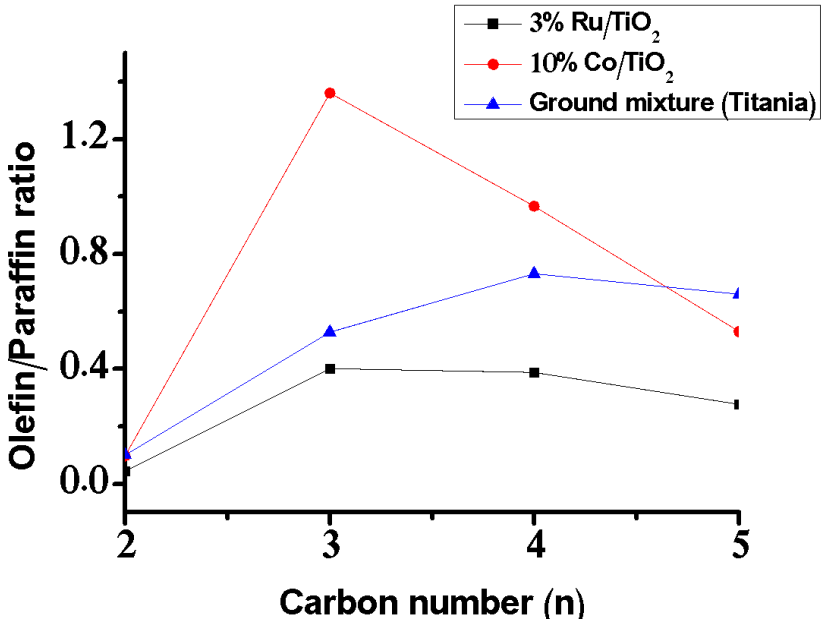

Figure 4.11: Olefin to paraffin ratio of Co catalysts supported on titania.

4.6 Conclusion

In this study, we have demonstrated the successful synthesis of cobalt and ruthenium titania supported catalysts. The characterization techniques such as TEM and SEM were used to obtain images of the catalysts. The presence of Co or Ru was proven by EDX analysis. XRD revealed the phase of the catalyst support.

In Figure 4.4 the activity of the titania supported catalysts were presented and it was concluded that 3%Ru/TiO_2 (Figure 4.4 b) gave higher CO conversion of 36.5%, compared to the other catalysts. This was expected; from the literature (Carballo et al., 2011) it is known that ruthenium is the most active metal for FTS. The ground mixture of the titania supported catalysts showed an initial increase in CO conversion but this dropped after 50 h. For the titania supported catalysts the ground mixture gave a very high methane selectivity (35%), and there was a drop in C_{5+} selectivity compared to the monometallic catalysts.

References

Bakar, W.A.W.A., Ali, R. and Mohammad, N.S., 2015. The effect of noble metals on catalytic methanation reaction over supported Mn/Ni oxide based catalysts. *Arabian Journal of Chemistry*, *8*(5), pp.632-643.

Baratti, R., Feckova, V., Morbidelli, M. and Varma, A., 1997. Optimal catalyst activity profiles in pellets. 11. the case of multiple-step distributions. *Industrial & engineering chemistry research*, *36*(8), pp.3416-3420.

Bartholomew, C.H., 1990. Recent technological developments in Fischer-Tropsch catalysis. *Catalysis Letters*, *7*(1-4), pp.303-315.

Beaumont, S.K. (2014) 'Recent developments in the application of nanomaterials to understanding molecular level processes in cobalt catalysed Fischer–Tropsch synthesis', *Physical Chemistry Chemical Physics*, 16(11), p. 5034.

Capek, I. (2004) 'Preparation of metal nanoparticles in water-in-oil (w/o) microemulsions', *Advances in Colloid and Interface Science*, 110(1-2), pp. 49–74.

Carballo, J.M.G., Yang, J., Holmen, A., García-Rodríguez, S., Rojas, S., Ojeda, M. and Fierro, J.L.G. (2011) 'Catalytic effects of ruthenium particle size on the Fischer–Tropsch synthesis', *Journal of Catalysis*, 284(1), pp. 102–108.

Carballo, J.M.G, Finocchio, E., García, S., Rojas, S., Ojeda, M., Busca, G. and Fierro, J.L.G. (2011) 'Support effects on the structure and performance of ruthenium catalysts for the Fischer–Tropsch synthesis', *Catalysis Science & Technology*, 1(6), p. 1013.

Iglesia, E., Soled, S.L. and Fiato, R.A., 1992. Fischer-Tropsch synthesis on cobalt and ruthenium. Metal dispersion and support effects on reaction rate and selectivity. *Journal of Catalysis*, *137*(1), pp.212-224.

Kaminsky, M.P., Winograd, N., Geoffroy, G.L. and Vannice, M.A., 1986. Direct SIMS observation of methylidyne, methylene, and methyl intermediates on a nickel (III) methanation catalyst. *Journal of the American Chemical Society*, *108*(6), pp.1315-1316.

Khassin, A.A., Yurieva, T.M., Kaichev, V.V., Bukhtiyarov, V.I., Budneva, A.A., Paukshtis, E.A. and Parmon, V.N. (2001) 'Metal–support interactions in cobalt-aluminum co-precipitated catalysts: XPS and CO adsorption studies', *Journal of Molecular Catalysis A: Chemical*, 175(1-2), pp. 189–204.

Kurhinen, M. and Pakkanen, T.A. (2000) 'Temperature-programmed decomposition, oxidation, and reduction studies of Co_2 $(CO)_8$ supported on alumina', *Langmuir*, 16(6), pp. 2658–2664.

Liu, X., Li, X. and Fujimoto, K., 2007. Effective control of carbon number distribution during Fischer–Tropsch synthesis over supported cobalt catalyst. *Catalysis Communications*, *8*(9), pp.1329-1335.

Ma, W., Jacobs, G., Kang, J., Sparks, D.E., Gnanamani, M.K., Pendyala, V.R.R., Shafer, W.D., Keogh, R.A., Graham, U.M., Thomas, G.A. and Davis, B.H. (2013) 'Fischer–Tropsch synthesis. Effect of alkali, bicarbonate and chloride addition on activity and selectivity',*Catalysis Today*, 215, pp. 73–79.

Ma, W., Jacobs, G., Keogh, R.A., Bukur, D.B. and Davis, B.H. (2012) 'Fischer–Tropsch synthesis: Effect of Pd, Pt, re, and Ru noble metal promoters on the activity and selectivity of a 25%Co/al2O3 catalyst',*Applied Catalysis A: General*, 437-438, pp. 1–9.

Mgcima, Z., 2012. *The purification of the polymer membrane fuel cell (PEMFC) reformate as by the methanation reaction with the use of platinum group metals (PGMs) on TiO2 support* (Doctoral dissertation, University of the Witwatersrand, Johannesburg).

Okabe, K., Li, X., Wei, M. and Arakawa, H. (2004) 'Fischer–Tropsch synthesis over Co–SiO2 catalysts prepared by the sol–gel method',*Catalysis Today*, 89(4), pp. 431–438.

Pérez-Cadenas, A.F., Zieverink, M.M., Kapteijn, F. and Moulijn, J.A., 2005. High performance monolithic catalysts for hydrogenation reactions. *Catalysis today*, *105*(3), pp.623-628.

Ralston, D.H. and Klabunde, K.J., 1982. Clustering of metal atoms in organic media: 10. Various arene solvated nickel atom systems employed in the preparation of nickel powder and nickel-alumina catalysts. Surface area, catalytic akd x-ray photoelectron spectroscopy studies. *Applied Catalysis*, *3*(1), pp.13-28.

Rautiainen, A., Lindblad, M., Backman, L.B. and Puurunen, R.L., 2002. Preparation of silica-supported cobalt catalysts through chemisorption of cobalt (II) and cobalt (III) acetylacetonate. *Physical Chemistry Chemical Physics*, *4*(11), pp.2466-2472.

Roucoux, A., Schulz, J. and Patin, H. (2002) 'Reduced transition metal Colloids: A novel family of reusable catalysts?', *Chemical Reviews*, 102(10), pp. 3757–3778.

Van Der Grift, C.J.G., Elberse, P.A., Mulder, A. and Geus, J.W. (1990) 'Preparation of silica-supported copper catalysts by means of deposition-precipitation', *Applied Catalysis*, 59(1), pp. 275–289.

CHAPTER 5

EVALUATION OF CARBON SUPPORTED CATALYSTS IN FISCHER-TROPSCH SYNTHESIS

This chapter presents and discusses results obtained using carbon supported catalysts in FTS in alignment with the objective(s) of this research study. Characterization of the Co and Ru catalysts are presented first, and then theTPR study followed by catalyst testing using FTS. The effect of the carbon spheres support for hydrogen spillover was investigated using conventional catalyst synthesis methods and a microwave procedure.

5.1 Characterization

5.1.1 TEM and particle size distribution

Figure 5.1 depicts a TEM image of the synthesized spherically shaped carbon spheres, with an average size of 200 nm. The carbon spheres form a necklace like structure due to the van der Waal's forces, which attract the CSs to each other (Moyo, 2012).

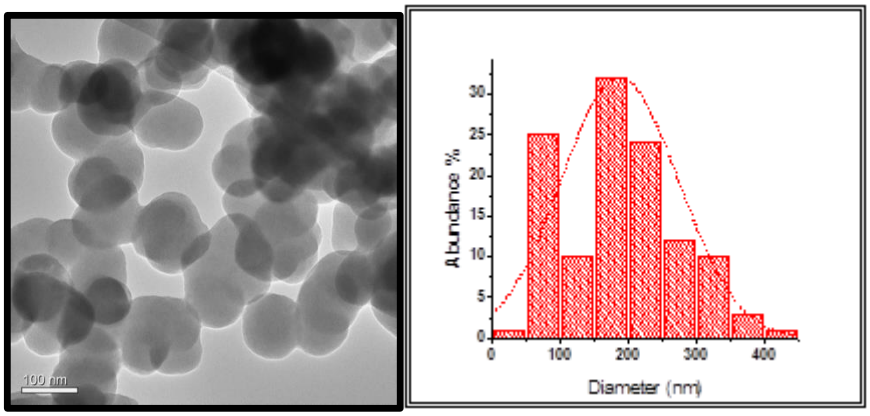

Figure 5.1: TEM image of as-synthesised carbon spheres and particle size distribution histogram (the superimposed dashed line represents a Gaussian distribution)

The TEM analysis of the conventionally and the microwave prepared catalysts, shown in Figure 5.2, was employed to determine if the metal particles were attached to the support, as well as to observe the dispersion of the particles. The conventionally prepared catalyst showed the small metal particles agglomerated on the side of the CSs, and some of the metal aggregates were not found on the CSs support. Poor dispersion was observed for the conventionally prepared catalyst, however for the microwave synthesised catalyst, good dispersion was observed, with no agglomeration and small metal particles were obtained. The poor dispersion was attributed to the HNO_3treatment which was used to functionalise the CSs, which led to the acid attacking the edges of the CSs, resulting in the metal particles attaching on the edge of the CSs (Moyo, 2012). The microwave synthesized catalyst in Figure 5.2(b) (good dispersion) was attributed to the effect of the microwave irradiation, similar to the explanation given by Reubroycharoen et al. (2007). This led to a uniform dispersion of the metal particles. The sizes of the metal particles were determined using Image J software, which showed that the metal particles for the conventionally prepared catalyst were in the range of 10-12 nm, and the microwave synthesised catalyst were in the range of 4-6 nm.

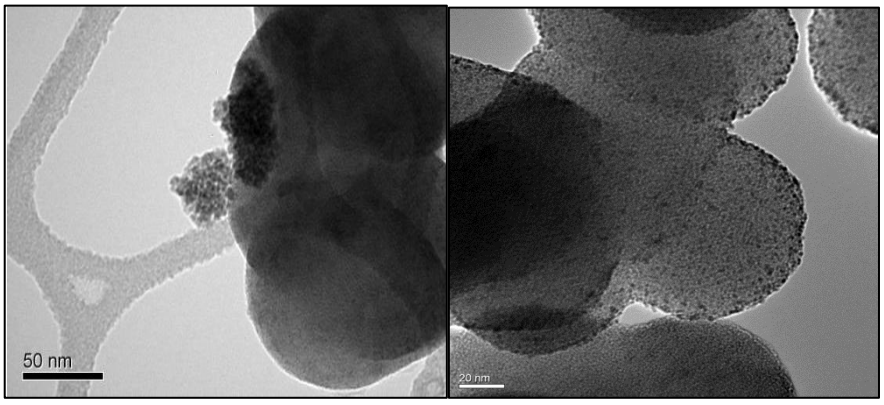

Figure 5.2: TEM images of 3% Ru/CSs catalyst prepared by incipient wetness a) using conventional heating and b) using microwave heating during the calcination step

TEM images shown in Figure 5.3 are images of catalysts prepared by the deposition precipitation method. A particle size determination was done using ImageJ software, which

found that the particle size range was between 6 and 10 nm for both the conventionally heated and the microwave heated catalysts, even though the heating methods used to synthesize the catalysts were different. Both catalysts showed good metal particle dispersion. However, the metal particles seem to be slightly more concentrated on the outer area of the carbon spheres. This could be explained as due to the functionalization of the carbon spheres using HNO_3, namely that the broken edges of the graphite sheets are attached to the oxygen based functionalities, which assist in anchoring of the metal particles (Moyo, 2012; Reubroycharoen. 2007).

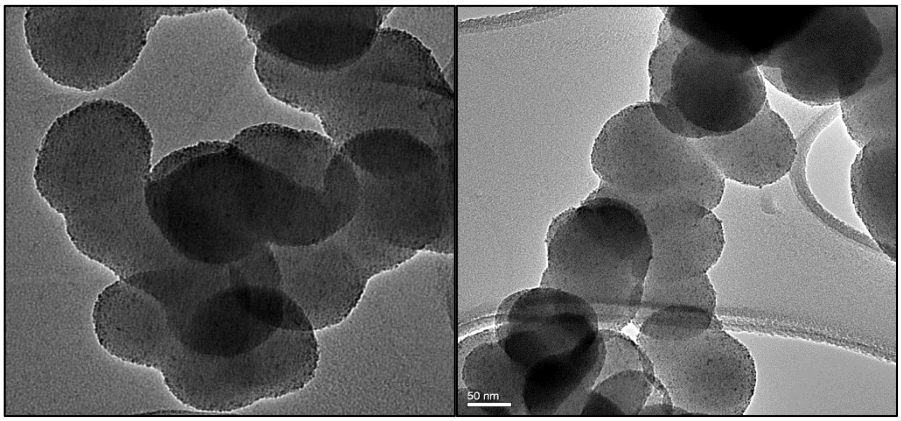

Figure 5.3: TEM images of 3% Ru/CSs catalyst prepared by deposition precipitation a) using conventional heating and b) microwave heating for the drying step

The carbon spheres supported catalysts prepared using the polyol method, are shown in Figure 5.4. Figure 5.4 (a) shows the agglomeration of metal particles on the edges of the CSs, but this was not observed for the microwave synthesized catalysts. This confirms that the microwave method in this case gave a better metal particle dispersion compared to the conventional heating method. The particle sizes for both catalysts were found to be in the range of 3 to 10 nm. Once again, the metal particles are seen to have gathered more on the edges of the CSs, as seen in Figure 5.1.

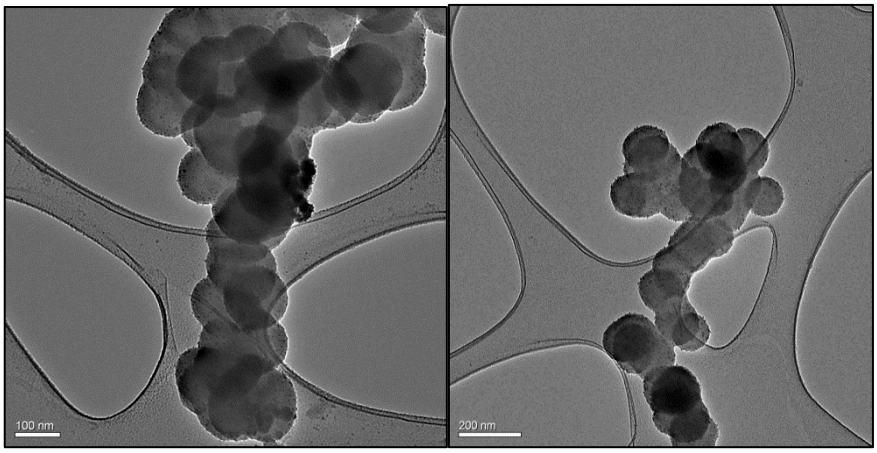

Figure 5.4: TEM images of 3% Ru/CSs catalyst prepared by polyol method a) using conventional and b) microwave heating for the drying step

.

5.1.2 Raman spectroscopy

The Raman spectra of as-synthesised carbon spheres (Figure 5.5), shows the presence of two broad peaks with the D-band at 1349 cm^{-1} and the G-band at 1584 cm^{-1} (Georgakilas et al, 2015). The D-band is due to the disorder characteristics present in the CSs, while the G-band is due to the ordered graphitic nature of the CSs. The I_D/I_G ratio of the CSs gives a value of 0.85, which suggest that the material has a high level of sp^3 hybridized carbon atoms (Georgakilas et al, 2015). A small band can be observed at ca. 2700 cm^{-1} which was can be due to a 2D band, because of the graphitic nature of carbon.

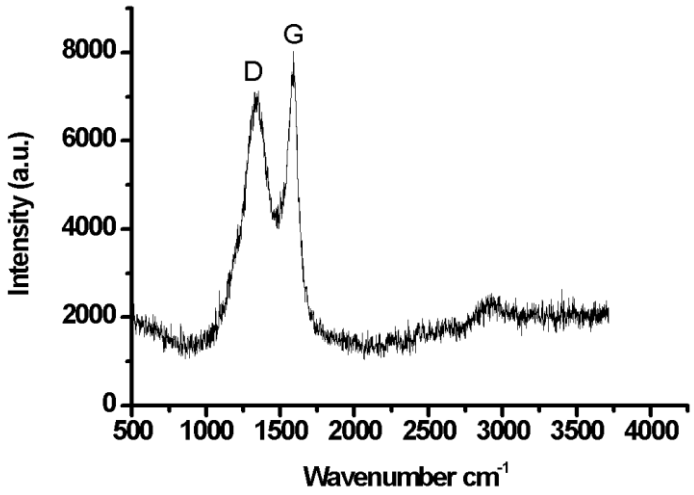

Figure 5.5: Raman spectra of as-synthesised CS

5.1.3 Brunauer Emmett Teller analysis

Table 5.1 shows BET results of the as synthesized (as-CSs) and functionalized (F-CSs) CSs, which show no difference in the surface area, and have very low values as expected. The addition of oxygen functionalities did not improve the surface area of the CSs.

Table 5.1: BET results of the functionalised and un-functionalised carbon spheres

Sample	Surface Area (m^2/g)	Pore Volume (cm^3/g)	Pore Size (nm)
As-CSs	**2.2**	**0.20**	**17.5**
F-CSs	**2.0**	**0.01**	**23.7**

Upon the addition of metals, there was an increase in the surface area as seen in Table 5.2 (Parlayici et al., 2015). The surface areas of the microwave synthesized catalysts are higher i.e. sample IWI-M, DPU-M and Polyol-M. This increase in surface area shows that microwave irradiation plays a role in improving the surface area; good dispersion was also seen in the TEM images for these samples. Not unexpectedly, the pore volumes for all catalysts were found to be similar, as well as the pore sizes.

Table 5.2: BET results of the catalysts prepared by different synthesis and heating methods

Sample	Surface area (m^2/g)	Pore volume (c m^3/g)
IWI-C	**8.0**	**0.20**
IWI-M	**29**	**0.10**
DPU-C	**6.0**	**0.12**
DPU-M	**36**	**0.10**
Polyol-C	**7.0**	**0.13**
Polyol-M	**37**	**0.11**

5.1.4 Thermogravimetric Analysis

The residual Ru metal loading (2.7%) was confirmed using TGA data which was run in air (Figure 5.6) (Moyo, 2012; Sreethawong 2006). Smooth curves can be observed in figure 5.6(a). The catalysts with metal particles loaded showed a decrease in oxidation

temperature of the CSs from 800 °C for the F-CSs to 600 °C. This was expected due to the presence of the ruthenium metal particles which catalyse the oxidation of the CSs. Figure 5.6(b) shows that the TGA profiles of samples which were loaded with metals. The profiles show two regions as also seen in work done by Moyo (2012). The two regions were explained to be due firstly to the presence of carbon in close proximity to metal, which is Ru in this case. The ruthenium speeds up the oxidation of carbon to carbon dioxide. The second region was due to the non-catalysed oxidation of carbon. The functionalised carbon spheres oxidized at 630 °C, and the catalysts with metals showed a reduced temperature to 430 °C. The microwave (Figure 5.6 b) synthesised catalysts showed a further decrease in the oxidation temperature compared to the conventionally prepared catalyst (Figure 5.6(a)), The presence of Ru sped up the oxidation therefore leading to oxidation temperature decreasing.

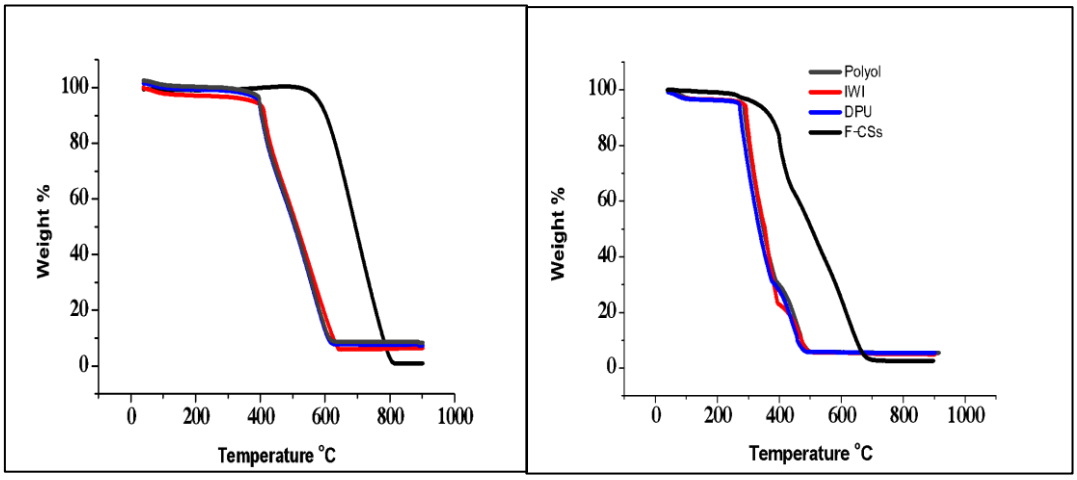

Figure 5.6: TGA profiles run on air of 3% Ru/CSs catalyst prepared by polyol method a) using conventional heating and b) microwave heating for the drying step

5.1.5 X-Ray Diffraction data analysis

The XRD diffraction patterns shown in Figure 5.7 show the pronounced broad peak at 2θ values at 25° and a small one at 43° of the carbon spheres. However, due to the small size of the RuO_2 particles, determining the presence of the RuO_2 proved to be difficult. The same XRD pattern was observed for the microwave synthesised catalysts. According to literature the RuO_2 phases which have been indexed to RuO_2(101) could not be detected at

2θ values of 28° and 43° (Okal, 2007), and due to the small size of the particles the phases could not be determined.

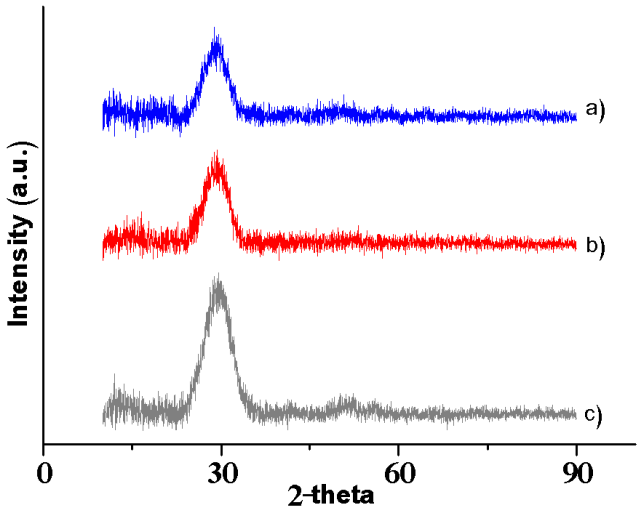

Figure 5.7: XRD patterns for catalysts heated conventional using the a) Polyol b) DPU c) IWI preparation method

5.1.6 H_2-TPR studies

Carbon supported catalysts were also synthesized, to understand the effect of this type of support on hydrogen spillover. The use of carbon based materials as support for heterogeneous catalysis has numerous advantages that include: high chemical inertness, cheap production, easy recovery of metal phase and thermal stability at high temperatures. TPR was used to understand the reduction of Co and Ru when supported on carbon.

The TPR profiles of the catalysts supported on carbon spheres are shown in Figure 5.8 below. There are two peaks which can be observed for the Ru/CSs catalyst. The first peak occurred at 250 and the second at 522 °C. The first was attributed to the reduction of RuO_2

to Ru, but the reduction occurred at slightly high temperature than expected. This could be explained by an interaction between the CSs support and the Ru. The TPR profile for the 10%Co/CSs showed only one peak for the reduction of cobalt oxide, and this could be due to the cobalt oxide species residing on the surface of the support, which allowed for easy reduction. This peak was assumed to be due to the reduction of cobalt oxide, directly to metallic cobalt. When the two catalysts were ground together, the TPR profile produced can be seen in Figure 5.8. The peak at 90°C was due to the conversion of RuO_2 to Ru. This shift from 250 °C to 90 °C was explained to be due to the easy access of the $RuO_2$to H_2on the surface of the support. The Co_3O_4 reduction peaks, shifted from 550 to 460 °C because of a Co-Ru interaction. The last peaks for all three profiles were due to the methanation of the carbon support. Methanation of carbon occurs in the presence of hydrogen at temperatures above 430° C.

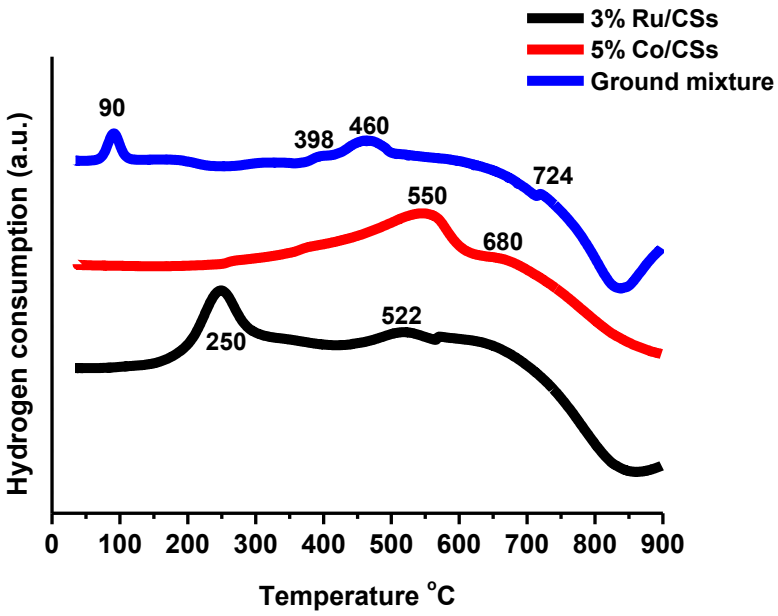

Figure 5.8: TPR profiles of black-3% Ru/CSs; Red-10% Co/CSs and blue-ground mixed catalysts.

Figure 5.8above shows the TPR profile of 3%Ru/CS//F-CSs//10%Co/CS system. The RuO_2 to Ru peak was observed at 220°C, but this peak overlapped with the Co_3O_4 peak.

This was suggested to be because of an interaction of Co-Ru, which caused the delayed reduction of RuO_2. The second peak was due to the reduction of Co(III) to Co(II), at 350 °C. A shoulder peak was observed next to the 350 °C, this was attributed to the remnants of nitrates from the cobalt precursor. The third peak was due to the reduction of Co(II) to metallic cobalt.No shift in temperature was observed when compared to the titania supported catalysts. The last peak at 650 °C was due to the methanation of the carbon spheres.

5.3 Catalytic activity

The CO conversion percentage was determined as a function of time on stream for 120 h. The results are shown in Figure 5.9(a) for 5% Co/CS, (b) for the ground mixture of 3% Ru/CSand 5% Co/CS and (c) for 3% Ru/CS. The CO conversion for the catalyst (Figure 5.9 (a)) was initially low and then increased significantly, then remained constant for 19-50 h, then dropped after 50 h until the end of the experiment. The drop in conversion was attributed to sintering of the metal particles, because the carbon spheres did not have a strong metal-support interaction with the metal particles.

From Figure 5.9, it can be seen that the Ru+Co/CSs (ground mixture catalyst) revealed the highest initial increase in the CO conversion most likely due to CO hydrogenation. The increase in CO hydrogenation is attributed to the increase in both extents of Co reduction and Co dispersion with the addition of Ru (Ma et al., 2012). The ground catalyst (Figure 5.9) initially increased considerably in the first 20 h, but the CO conversion dropped and stabilized between 20 h until the end of the run. The CO conversion shown in Figure 5.9(b) was 15% when the run was stable, this was higher than observed for the two monometallic catalysts, and the reason could be the intimate contact between the Co and the Ru metal particles, which results in a higher conversion. Figure 5.9(c) shows a very low CO conversion of 9%; this was attributed to the very small metal particles on the CSs support.

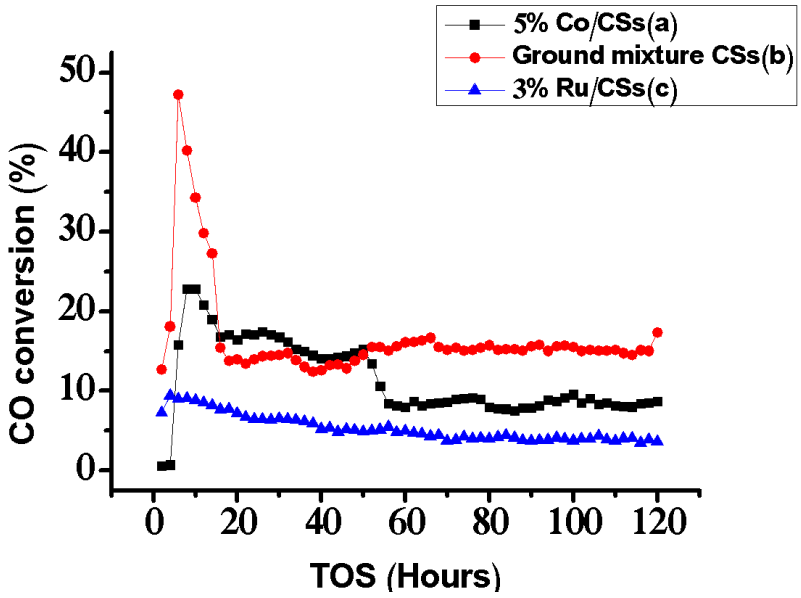

Figure 5.9: Conversion of the catalysts over 120 hours on stream a) 10% Co/CSs, b) for the ground mixture of 3% Ru/CS and 10% Co/CS and c) 3% Ru/CSs.

5.4 Product selectivity

The selectivity to the hydrocarbons was determined for the carbon supported catalysts and plotted against the carbon number. The results are depicted in Figure 5.10 (a) for 3% Ru/CSfor 10% Co/CS and **c**) ground mixture (Ru+Co/CS). The selectivity to the hydrocarbons was also measured for the CS supported catalysts and plotted against the carbon number. The results are depicted in Figure 5.10 a) for 3% Ru/CSs, b) for 10% Co/CSs and c) for the ground mixture of 3% Ru/CSand 10% Co/CS.

High methane selectivity characterizes the carbon spheres supported catalysts. The selectivity for Ru/CSs shown in Figure 5.10 was low for methane (>25%) and very high for C_{5+} (65%). The small particle size of the Co metal particles resulted in a high methane selectivity (Moyo, 2012; Phadi, 2012). However, an increase of the gaseous products (<15%) was observed for the 5%Co/CSs and the low selectivity towards the C_{5+} products was ascribed to the increase in C_1 to C_4 products. The ground mixture/hybrid catalyst FTS data showed an increase in the C_{5+} hydrocarbons, and a high selectivity towards C_{5+}

products (>70%), these results were ascribed to the intimate contact between the Co and Ru in the hybrid catalyst resulting in a slightly increased CO conversion and high C_{5+} selectivity. The improved activity and selectivity arose from the Ru cleansing the Co surface ensemble during FTS (Moyo, 2012, Iglesia, 1993; Iglesia, 1992, González Carballo., 2011; Kogelbauer, Goodwin, Jr., and Oukaci, 1996).

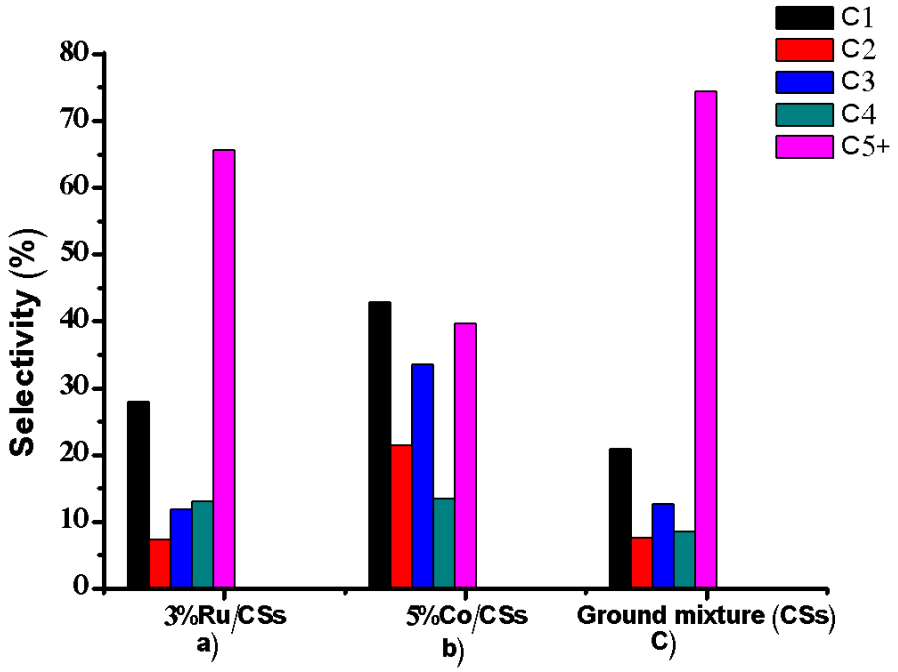

Figure 5.10: Selectivity of the catalysts over 120 hours on stream a) 5% Co/CSs, b) for the ground mixture of 3% Ru/CS and 10% Co/CS and c) 3% Ru/CSs

5.5 Olefin to paraffin ratio

The olefin to paraffin ratio data was plotted against the light hydrocarbons (C2 to C5). Figure 5.11 shows the gas phase olefin to paraffin ratio of the carbon spheres supported catalysts. The Co and Ru catalysts appear to follow a similar trend, which showed that more olefins than paraffins are produced. However, the ground mixture (Figure 5.11) gave

different results, there was no variation in terms of the olefin to paraffin ratio for C3 to C5, even though the FT activity was higher for the mono-metallic catalysts of Co and Ru.

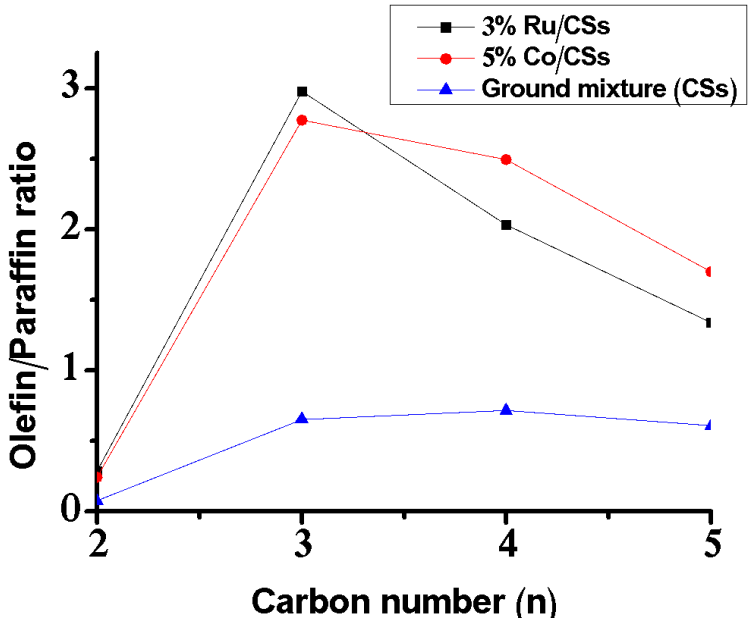

Figure 5.11: Olefin to paraffin ratio of Co catalysts supported on carbon spheres.

5.6 Conclusion

The synthesised carbon spheres gave an average size of 200 nm and formed a necklace like structure as expected (Moyo, 2012). The TEM images in Figure 5.3 showed that when catalysts were prepared using the incipient wetness method, the microwave synthesized catalyst gave a better dispersion and smaller particles. Similar behavior was observed for the catalysts prepared using the polyol method (Figure 5.4), where the conventionally prepared catalyst metal particles agglomerated and the microwave synthesized catalysts showed good dispersion. The surface area of the microwave synthesized catalysts gave higher surface area in comparison to the conventionally prepared catalysts. The TGA data, showed that in Figure 5.6b), the presence of metal particles for the microwave synthesized catalysts showed a larger decrease in temperature from 630°C to 430°C. This is probably due to the better dispersion of the metal on the CS support for the microwave heated catalyst, which in turn means better contact between the metal and the carbon and thus

oxidation of the carbon surface at lower temperatures. Thus the microwave radiation played a role.

The Ru/CS catalyst (Figure 5.9 (c)) gave a very low CO conversion of 9%, which was attributed to the very small metal particles on the CSs support. In Figure 5.9, it was shown that for the ground mixture (Figure 5.9 b) the CO conversion shot up in the first 20 h, but dropped and became stable at 15 %, this was relatively higher than the monometallic catalysts supported on the CSs. This is due to more intimate contact between the Co and Ru in this ground mixture. For the CSs supported catalysts the ground mixture had a very high methane selectivity (ca. 20%), and there was an increase in the C_{5+} selectivity compared to the monometallic catalysts. The ground mixture/hybrid catalyst (Figure 5.10 (c)) showed a decrease in the C_4 hydrocarbons, and a high selectivity towards C_{5+} products. These results were discussed as due to the intimate contact between the Co and Ru in the hybrid catalyst resulting in a slightly increased CO conversion and high C_{5+} selectivity.

References

Auer, E., Freund, A., Pietsch, J. and Tacke, T. (1998) 'Carbons as supports for industrial precious metal catalysts', *Applied Catalysis A: General*, 173(2), pp. 259–271.

Balint, I., Miyazaki, A. and Aika, K. (2002) 'Methane reaction with NO over alumina-supported Ru Nanoparticles', *Journal of Catalysis*, 207(1), pp. 66–75.

Bertole, C. (2004) 'Support and rhenium effects on the intrinsic site activity and methane selectivity of cobalt Fischer–Tropsch catalysts',*Journal of Catalysis*, 221(1), pp. 191–203.

Campidelli, S., Klumpp, C., Bianco, A., Guldi, D.M. and Prato, M. (2006) 'Functionalization of CNT: Synthesis and applications in photovoltaics and biology', *Journal of Physical Organic Chemistry*, 19(8-9), pp. 531–539.

De la Osa, A.R., De Lucas, A., Romero, A., Valverde, J.L. and Sánchez, P., 2011. Influence of the catalytic support on the industrial Fischer–Tropsch synthetic diesel production. *Catalysis today*, *176*(1), pp.298-302.

Donnet, J.B., 1968. The chemical reactivity of carbons. *Carbon*, *6*(2), pp.161-176.

Fulcheri, L. and Schwob, Y., 1995. From methane to hydrogen, carbon black and water. *International journal of hydrogen energy*, *20*(3), pp.197-202.

Flahaut, E., Peigney, A., Laurent, C., Marlière, C., Chastel, F. and Rousset, A. (2000) 'Carbon nanotube–metal–oxide nanocomposites: Microstructure, electrical conductivity and mechanical properties',*Acta Materialia*, 48(14), pp. 3803–3812.

Georgakilas, V., Perman, J.A., Tucek, J. and Zboril, R., 2015. Broad family of carbon nanoallotropes: classification, chemistry, and applications of fullerenes, carbon dots, nanotubes, graphene, nanodiamonds, and combined superstructures. *Chemical reviews*, *115*(11), pp.4744-4822.

González Carballo, J.M., Finocchio, E., García, S., Rojas, S., Ojeda, M., Busca, G. and Fierro, J.L.G. (2011) 'Support effects on the structure and performance of ruthenium catalysts for the Fischer–Tropsch synthesis', *Catalysis Science & Technology*, 1(6)

Iglesia, E., Soled, S.L. and Fiato, R.A., 1992. Fischer-Tropsch synthesis on cobalt and ruthenium. Metal dispersion and support effects on reaction rate and selectivity. *Journal of Catalysis*, *137*(1), pp.212-224.

Iglesia, E., Soled, S.L., Fiato, R.A. and Via, G.H., 1993. Bimetallic synergy in cobalt ruthenium Fischer-Tropsch synthesis catalysts. *Journal of Catalysis*, *143*(2), pp.345-368.

Jacobs, G., Das, T.K., Zhang, Y., Li, J., Racoillet, G. and Davis, B.H. (2002) 'Fischer–Tropsch synthesis: Support, loading, and promoter effects on the reducibility of cobalt catalysts', *Applied Catalysis A: General*, 233(1-2), pp. 263–281.

Khodakov, A.Y. (2009) 'Fischer-Tropsch synthesis: Relations between structure of cobalt catalysts and their catalytic performance',*Catalysis Today*, 144(3-4), pp. 251–257.

Kogelbauer, A., Goodwin Jr, J.G. and Oukaci, R., 1996. Ruthenium Promotion of Co/Al2O3Fischer–Tropsch Catalysts. *Journal of Catalysis*, *160*(1), pp.125-133.

Kohls, D.J. and Beaucage, G., 2002. Rational design of reinforced rubber. *Current Opinion in Solid State and Materials Science*, *6*(3), pp.183-194.

Kraum, M. and Baerns, M. (1999) 'Fischer–Tropsch synthesis: The influence of various cobalt compounds applied in the preparation of supported cobalt catalysts on their performance', *Applied Catalysis A: General*, 186(1-2), pp. 189–200.

Lahaye, J., 1992. Particulate carbon from the gas phase. *Carbon*, *30*(3), pp.309-314.

Leblanc, J.L. (1997) 'A molecular explanation for the origin of bound rubber in carbon black filled rubber compounds', *Journal of Applied Polymer Science*, 66(12), pp. 2257–2268.

Lu, X., 2012. *Fischer-Tropsch Synthesis: Towards understanding* (Doctoral dissertation).

Ma, W., Jacobs, G., Keogh, R.A., Bukur, D.B. and Davis, B.H. (2012) 'Fischer–Tropsch synthesis: Effect of Pd, Pt, Re, and Ru noble metal promoters on the activity and selectivity of a 25%Co/Al_2O_3 catalyst',*Applied Catalysis A: General*, 437-438, pp. 1–9.

Mhlanga, S.D., Coville, N.J., Iyuke, S.E., Afolabi, A.S., Abdulkareem, A.S. and Kunjuzwa, N. (2010) 'Controlled syntheses of carbon spheres in a swirled floating catalytic chemical vapour deposition vertical reactor', *Journal of Experimental Nanoscience*, 5(1), pp. 40–51.

Mhlanga, S., Mondal, K.C., Naidoo, N., Kunjuzwa, N., Witcomb, M.J. and Coville, N.J. (2009) 'Synthesis and study of carbon microspheres for use as catalyst support for cobalt', *South African Journal of Science*, 105, pp. 304–308.

Miyazaki, A., Balint, I., Aika, K. and Nakano, Y. (2001) 'Preparation of Ru Nanoparticles supported on γ-Al_2O_3 and its novel catalytic activity for ammonia synthesis', *Journal of Catalysis*, 204(2), pp. 364–371.

Moyo, M., 2012. *Cobalt and iron supported on carbon spheres catalysts for Fischer Tropsch synthesis* (Doctoral dissertation).

Okal, J., Zawadzki, M., Kępiński, L., Krajczyk, L. and Tylus, W., 2007. The use of hydrogen chemisorption for the determination of Ru dispersion in Ru/γ-alumina catalysts. *Applied Catalysis A: General*, *319*, pp.202-209.

Parlayici, S., Eskizeybek, V., Avcı, A. and Pehlivan, E., 2015. Removal of chromium (VI) using activated carbon-supported-functionalized carbon nanotubes. *Journal of Nanostructure in Chemistry*, *5*(3), pp.255-263.

Phadi, T.T., 2013. *Titanium dioxide-carbon spheres composites for use as supports in cobalt Fischer-Tropsch synthesis* (Doctoral dissertation).

Reubroycharoen, P., Vitidsant, T., Liu, Y., Yang, G. and Tsubaki, N., 2007. Highly active Fischer–Tropsch synthesis Co/SiO 2 catalysts prepared from microwave irradiation. *Catalysis Communications*, *8*(3), pp.375-378.

Scully, D.B. and Davies, R.A., 1965. Carbon formation from aromatic hydrocarbons. *Combustion and Flame*, *9*(2), pp.185-191.

Sreethawong, T., Yamada, Y., Kobayashi, T. and Yoshikawa, S., 2006. Optimization of reaction conditions for cyclohexene epoxidation with H_2O_2 over nanocrystalline mesoporous TiO_2 loaded with RuO_2. *Journal of Molecular Catalysis A: Chemical*, *248*(1), pp.226-232.

Van der Laan. G.P. (1999), *Kinetics, selectivity and scale up of the Fischer-Tropsch Synthesis*. PhD thesis. University of Groningen, Groningen.

Van der Laan, G.P. and Beenackers, A.A.C.M. (1999) 'Kinetics and selectivity of the Fischer–Tropsch synthesis: A literature review',*Catalysis Reviews*, 41(3-4), pp. 255–318.

Wissler, M. (2006) 'Graphite and carbon powders for electrochemical applications', *Journal of Power Sources*, 156(2), pp. 142–150.

Zhu, X., Lu, X., Liu, X., Hildebrandt, D. and Glasser, D., 2014. Heat transfer study with and without Fischer-Tropsch reaction in a fixed bed reactor with TiO_2, SiO_2, and SiC supported cobalt catalysts. *Chemical Engineering Journal*, *247*, pp.75-84.

CHAPTER 6

CONCLUSIONS AND RECOMMENDATIONS

6.1 Conclusions

This study sought to understand the role of the support in hydrogen spillover using Ru catalysts to initiate the reduction Co in the chosen catalysts. Carbon spheres, and titania were the chosen supports. The ground mixed catalysts for the CS and the titania supported catalysts were used to observe the effect of hydrogen spillover in Fischer-Tropsch Synthesis.

The intimate contact between Co and Ru in the ground mixtures of the supported catalysts, confirmed that the reduction temperature of Co decreased from 500 °C to 450 °C, as seen in Figure 6.2(c). The synergy between the catalyst components of the Co and Ru based catalysts could be clearly shown for systems, where both were in immediate contact. Varying the distance between Ru/TiO_2 and Co/TiO_2, by using a separating bed of four different oxides was successfully done. The stacking of the catalyst beds was used to study hydrogen spillover using TPR. The $Ru/TiO_2//TiO_2//Co/TiO_2$ system showed pronounced changes which confirmed the occurrence of hydrogen spillover. However, varying the amount of TiO_2 between the Ru/TiO_2 and Co/TiO_2 had no significant effect on the shift of the temperature. For the CS supported Ru and Co catalysts the reduction temperature of cobalt oxide increased from 325 °C to 398°C for the $Co_3O_4 \rightarrow CoO$ reaction, and decreased from 550 °C to 460 °C for $CoO \rightarrow Co$ reaction when comparing the mono-metallic Co/CS catalyst, with the hybrid ground mixture catalyst (CS supported). Upon separating the monometallic Co and Ru catalysts with a bed of F-CSs there was a shift in reduction temperature of the ground catalyst compared to the Co/CS of CoO.

In this study, we have successfully demonstrated the synthesis of cobalt and ruthenium carbon and titania supported catalysts. The characterisation techniques such as TEM and

SEM were used to obtain images of the catalysts. The presence of Co or Ru was proven by EDX analysis. X-ray diffraction patterns indicate the presence of crystalline phase in the samples.The FTS results showed that the titania supported catalysts of the ground mixture gave high conversions towards methane (35%), and there was a drop in C_{5+} selectivity compared to the monometallic catalysts. Whereas for the ground mixture of the CSs supported catalysts, very high methane selectivity (ca. 20%) was observed, and there was an increase in the C_{5+} selectivity compared to the monometallic catalysts

The carbon spheres gave an average size of 200 nm and formed a necklace like structure. The TEM images showed that when catalysts were prepared using the incipient wetness method, the microwave synthesised catalyst gave better dispersion and smaller particles. The same was observed for the catalysts prepared using the polyol method where the conventionally prepared catalyst metal particles agglomerated and the microwave synthesised catalysts showed good dispersion. The surface area of the microwave synthesised catalysts gave a higher surface area in comparison to the conventionally prepared catalysts.

6.2 Recommendations

The following recommendations will be necessary for future studies:

- Monitor the effect of reversing the stacking of the catalysts, where the acceptor phase (Co catalysts) is placed at the top and the donor phase (Ru catalyst) at the bottom.

- Use of carbon spheres as separator bed in the Ru/TiO_2 and Co/TiO_2(and also for Ru/CSand Co/CS), and study the effect of CS size.

- XPS studies should be conducted for elemental surface analysis and to understand the environment of the cobalt phase.

- The use of the in-situ TPR-XRD would be vital for further identification of the species associated with the reduction of the cobalt oxide.